

Characterization of the OXPHOS system in plant mitochondria

Von der Naturwissenschaftlichen Fakultät
der Gottfried Wilhelm Leibniz Universität Hannover
zur Erlangung des Grades
Doktorin der Naturwissenschaften
Dr. rer. nat.

genehmigte Dissertation
von
M.Sc. Katrin Peters
geboren am 16. März 1982 in Uelzen

Referent: Prof. Dr. Hans-Peter Braun

Korreferent: Prof. Dr. Christoph Peterhänsel

Tag der Promotion: 22. Dezember 2011

Abstract

This thesis aims to provide a deeper understanding of structure and function of the oxidative phosphorylation (OXPHOS) system in plant mitochondria. Thanks to improvements in electron microscopy (EM), a high number of structural details were obtained in the last years. Besides the already known stable interactions of OXPHOS complexes, termed supercomplexes, even higher-ordered oligomers are formed by those (section 2.2). Evidence is adduced for a row-like organization of complexes I, III and IV, termed ‘respiratory string’. Furthermore, ATP-synthase (complex V) forms long rows of dimers located at locally curved cristae membranes, which are supposed to induce the bending of the inner mitochondrial membrane (IMM). New details about the structure of complex I and the I+III₂ supercomplex in *Zea mays* are outlined in section 2.1. The typical L-shaped complex I structure resembles the one from *Arabidopsis thaliana* and also in maize, a member of the group of C₄ species, the plant specific carbonic anhydrase (CA) domain could be detected. Comparing this domain with the X-ray structure of homotrimeric γ -CA from the archaeobacterium *Methanosarcina thermophila*, it is suggested that the CA domain in maize most likely represents a trimer, too. Additionally, single-particle EM of complex I from maize reveals structural heterogeneity in complex I, which is not known for other plant species so far. Different physiological roles for these two complex I forms have to be discussed. Moreover, the I+III₂ supercomplex seems to be more stable in maize than in *Arabidopsis*. In section 2.4 an immunoblot based quantification approach is presented, revealing the ratio of OXPHOS complexes in different plant tissues. Drastic differences in complex I to complex II ratio of individual plant tissues of *Arabidopsis thaliana* are displayed. This leads to the suggestion of additional tissue dependent functions of these respiratory chain complexes in plants besides electron transfer. Due to the results obtained by this study, light-dependent side functions of complex I are discussed. Beyond these approaches on the characterization of the OXPHOS system, a new application based on blue native polyacrylamide gel electrophoresis (BN-PAGE), which is the method of choice for analyses of membrane protein complexes, was established in this thesis (section 2.3). Different protein samples are labelled with distinct fluorescent dyes, pooled and resolved in one single gel (blue native difference gel electrophoresis, BN-DIGE). This technique allows systematic and quantitative comparisons of protein complexes of related protein fractions, structural investigations of protein complexes as well as assignments of protein complexes to subcellular fractions like organelles.

Keywords: OXPHOS system, plant mitochondria, respiratory chain complexes

Zusammenfassung

Ziel dieser Arbeit ist es zur Aufklärung von Struktur und Funktion des oxidativen Phosphorylierungs (OXPHOS) -Systems in pflanzlichen Mitochondrien beizutragen. Mit Hilfe der Elektronenmikroskopie (EM) konnten neue strukturelle Erkenntnisse gewonnen werden. Neben den bereits bekannten Interaktionen von OXPHOS Komplexen, sogenannten Superkomplexen, lassen sich auch höher organisierte Strukturen bestehend aus diesen nachweisen (Abschnitt 2.2). Bisher konnte eine Abfolge der Komplexe I, III und IV („respiratory string“) sowie eine Aneinanderreihung von ATP-Synthase (Komplex V) Dimeren gezeigt werden. Letztere sind vermutlich für die Krümmung der inneren Mitochondrienmembran (IMM), den sogenannten Cristae, verantwortlich. Neue strukturelle Details des Komplex I sowie des I+III₂ Superkomplex aus *Zea mays* werden in Abschnitt 2.1 vorgestellt. Die typische L-förmige Struktur von Komplex I ist ähnlich der aus *Arabidopsis thaliana* und auch die pflanzenspezifische Carboanhydrase (CA) Domäne konnte in Mais, als einem Vertreter der C₄ Spezies, detektiert werden. Ein Vergleich mit der Röntgenstruktur der homotrimeren γ -CA Domäne des Archaeobakteriums *Methanosarcina thermophila* deutet darauf hin, dass die CA Domäne in Mais ebenfalls als Trimer vorliegt. Zusätzlich konnte durch „single-particle“ EM eine bisher unbekannte strukturelle Heterogenität des Komplex I gezeigt werden, weshalb unterschiedliche physiologische Rollen dieser zwei Formen diskutiert werden. Des Weiteren konnten in dieser Arbeit zum ersten Mal die OXPHOS Komplexe in verschiedenen pflanzlichen Geweben mittels eines immunologischen Ansatzes quantifiziert werden (Abschnitt 2.4). Es werden deutliche Unterschiede im Verhältnis von Komplex I zu Komplex II aus einzelnen Geweben von *Arabidopsis thaliana* gezeigt. Die Ergebnisse lassen vermuten, dass die Atmungskettenkomplexe in Pflanzen neben dem Elektronentransport noch zusätzliche, gewebespezifische Funktionen besitzen. Darüber hinaus werden lichtabhängige Nebenfunktionen des Komplex I diskutiert. Neben der Charakterisierung des pflanzlichen OXPHOS Systems wurde im Rahmen dieser Arbeit eine neue Methode etabliert (Abschnitt 2.3), welche auf der blau nativen Polyacrylamid-Gelelektrophorese (BN-PAGE) basiert. Hierzu werden Proteinproben mit unterschiedlichen Fluoreszenz-Farbstoffen markiert, vereint und anschließend in einem einzigen Gel aufgetrennt. Diese Technik (blau native differentielle Gelelektrophorese, BN-DIGE) ermöglicht einen systematischen und quantitativen Vergleich von ähnlichen Proteinfractionen, eine strukturelle Untersuchung von Proteinkomplexen sowie eine Zuordnung von Proteinkomplexen zu subzellulären Fraktionen wie zum Beispiel Organellen.

Schlagworte: OXPHOS System, pflanzliche Mitochondrien, Atmungsketten-Komplexe

Contents

Abbreviations		1
Chapter 1	General Introduction	3
	1.1 Mitochondria: structure and evolution	
	1.2 The respiratory chain of mitochondria and its role in oxidative phosphorylation	
	1.3 Supramolecular organization of the OXPHOS system	
	1.4 Characteristic features of the OXPHOS system in plants	
	1.5 Approaches used for the investigation of the OXPHOS system	
	1.6 Objective of the thesis	
Chapter 2	Publications and Manuscripts	16
	2.1 A structural investigation of complex I and I+III ₂ supercomplex from <i>Zea mays</i> at 11-13 Å resolution: assignment of the carbonic anhydrase domain and evidence for structural heterogeneity within complex I. <i>Biochim. Biophys. Acta 1777: 84-93.</i>	
	2.2 Structure and function of mitochondrial supercomplexes. <i>Biochim. Biophys. Acta 1797: 664-670.</i>	
	2.3 Comparative analyses of protein complexes by blue native DIGE. <i>Methods Mol. Biol. In press.</i>	
	2.4 Complex I - complex II ratio strongly differs in various organs of <i>Arabidopsis thaliana</i> . <i>In preparation.</i>	
Chapter 3	Supplementary Discussion and Outlook	75
	3.1 The highly branched electron transport chain of plant mitochondria	
	3.2 Outlook	
References		83
Affix	Curriculum vitae Publications Danksagung Eidesstattliche Erklärung	91

Abbreviations

1D	one-dimensional
2D	two-dimensional
3D	three-dimensional
AOX	alternative oxidase
ADP	adenosine diphosphate
ATP	adenosine triphosphate
BN	blue native
CA	carbonic anhydrase
γ CA	gamma-type carbonic anhydrase
γ CAL	gamma-type carbonic anhydrase like
CAM	carbonic anhydrase of <i>Methanosarcina thermophila</i>
CCM	CO ₂ concentrating mechanism
CMS	cytoplasmic male sterility
Complex I	NADH dehydrogenase
Complex II	succinate dehydrogenase
Complex III	cytochrome c reductase
Complex IV	cytochrome c oxidase
Complex V	ATP synthase
COX	cytochrome c oxidase
DDM	dodecyl maltoside
DIGE	difference gel electrophoresis
DNA	deoxyribonucleic acid
e ⁻	electron
EM	electron microscopy
ET	electron tomography
(m)ETC	(mitochondrial) electron transfer chain
ETFQ-OR	electron transfer flavoprotein:quinone oxidoreductase
F ₀	F ₀ part of complex V
F ₁	F ₁ part of complex V
FADH ₂	flavin adenine dinucleotide; reduced form
FMN	flavin mononucleotide
G3P	glycerol-3-phosphate
GLDH	L-galactono-1,4-lactone dehydrogenase
H ⁺	proton
HSP70	heat shock protein 70
IEF	isoelectric focusing
IMM	inner mitochondrial membrane
IMS	inter membrane space
kDa	kilo Dalton
MDa	mega Dalton
MPP	mitochondrial processing peptidase
MS	mass spectrometry
NAD(P) ⁺	nicotine amid dinucleotid (phosphate); oxidized form
NAD(P)H	nicotine amid dinucleotid (phosphate); reduced form
OMM	outer mitochondrial membrane
OXPPOS	oxidative phosphorylation
PAGE	polyacrylamide gel electrophoresis
P _i	phosphate

Abbreviations

PMF	proton motive force
RNA	ribonucleic acid
ROS	reactive oxygen species
SDS	sodium dodecyl sulphate
TIM	translocases of the inner mitochondrial membrane
TOM	translocases of the outer mitochondrial membrane
UQ	ubiquinone
UQH ₂	ubiquinol
VDAC	voltage-dependent anion channel
WT	wild type

Chapter 1

1 General introduction

This chapter aims to provide an overview of the oxidative phosphorylation (OXPHOS) system in general and the plant specific features of cellular respiration in particular. It will also present the recent progress in this field of research.

1.1 Mitochondria: structure and evolution

The word mitochondrion comes from the Greek and is composed of the words ‘μίτος’ (or ‘mitos’) meaning thread and ‘χονδρίον’ (or ‘chondrion’) for granule. Mitochondria are double-membrane bound organelles with a size of 1 to 3 μm and an abundance of 1 to 1000 per cell. Their shape varies from tubular or reticulated (when mitochondria are attached to the cytoskeleton) to ellipsoidal or spherical (isolated mitochondria in suspension) (Mannella 2006). In most species, mitochondria are maternally inherited and propagate by division. They contain their own small genome, often in a circular form, as well as a fully functional apparatus for protein synthesis. Mitochondrial DNA encodes for some mitochondrial proteins, but the majority of proteins are encoded by nuclear genes synthesized in the cytosol and imported into the organelle. Two specific transport complexes in the outer and the inner mitochondrial membrane, termed translocases of the outer/inner mitochondrial membrane (TOM and TIM), as well as the matrix protein complex HSP70 (heat shock protein 70) are involved in the protein import process (Braun and Schmitz 1999, Carrie et al. 2010).

According to the endosymbiotic hypothesis, the ancestor of mitochondria was an aerobe prokaryote, taken up by a eukaryotic cell via endocytosis (Sagan 1967 and references therein). It is assumed that this event happened only once in the evolution of the eukaryotic cell. Today, the closest living relatives to this incorporated prokaryote are the α -proteobacteria (reviewed in Gray et al. 2001). Mitochondria contain two membranes: inner and outer mitochondrial membrane (IMM, OMM) (Fig. 1A). These two membranes enclose the inter membrane space (IMS). The OMM separates the IMS from the cytosol and is permeable for proteins below 5000 Dalton due to voltage-dependent anion channels (VDAC) (Vander Heiden 2001) and due to pores, formed by transmembrane proteins (porines), which allow the movement of solutes up to 1000 Dalton (Mannella and Tedeschi 1987). The IMM encloses the dense, protein-rich mitochondrial matrix and is heavily folded, forming the so-called ‘cristae’, which results in an enormous enlargement of the membrane surface (Mannella 2006). The origins of the foldings, called ‘crista junctions’, are constricted (Fig 1B) and therefore cristae can be regarded as additional compartments (Mannella et al. 1997). The permeability for molecules across the

IMM is restricted and only small, uncharged molecules like O_2 and CO_2 are able to pass the lipid-bilayer by diffusion. The IMM is rich in the phospholipid cardiolipin which, compared to other lipids, contains four fatty acids instead of two. It was originally discovered in beef hearts (Pangborn 1942) and is common for mitochondrial and bacterial membranes. Cardiolipin was found in mammalian cells as well as in plant cells and is essential for stabilization and optimal function of numerous enzymes involved in mitochondrial metabolism, like the protein complexes of the OXPHOS system (Schlame et al. 2000, Schägger 2002). Due to the impermeability of the IMM, ions and other charged, hydrophilic and/or big molecules have to be transported by channels or specialized translocases across the IMM.

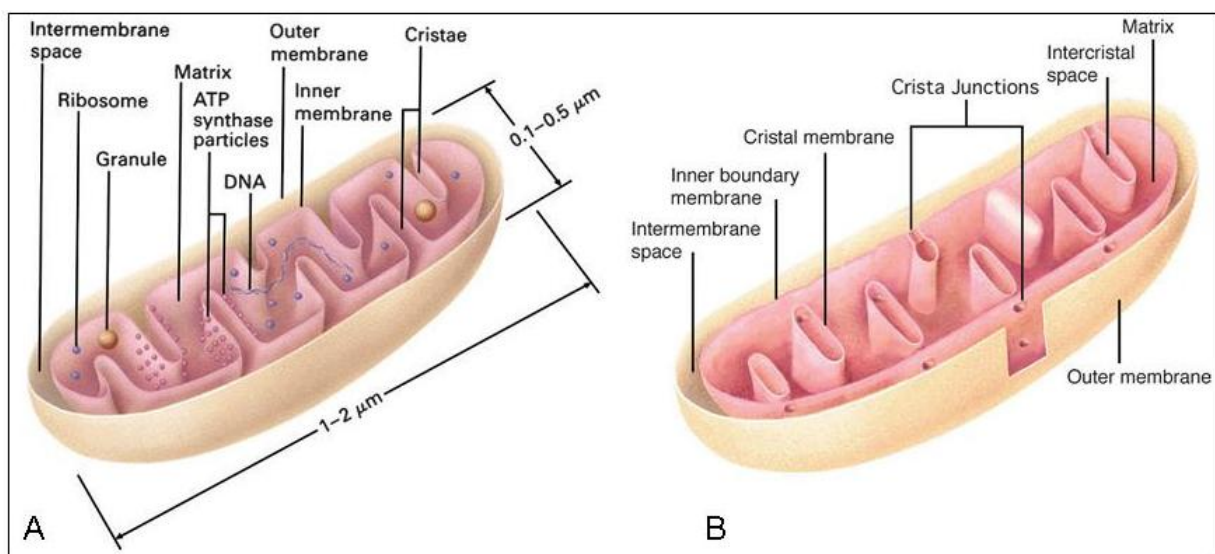


Figure 1: Mitochondrial membrane structures. A: Model of mitochondria with typical cristae structure, which is often found in textbooks also known as infolding or 'baffle' model. B: Crista junction model of the mitochondrion displaying the internal compartments formed by invagination of the IMM and the very constricted origins of the foldings known as crista junctions. Image is taken from Logan (2006).

1.2 The respiratory chain of mitochondria and its role in oxidative phosphorylation

All organisms need energy for maintenance, growth and reproduction. Most of the energy is provided in form of adenosin triphosphate (ATP). This molecule can be split into adenosine diphosphate (ADP) and phosphate (P_i). By splitting the phosphoanhydride bond between both parts of the molecule the energy invested in creating this bond becomes available. ATP regeneration is achieved by phosphorylation of ADP. The energy required for this process is taken from diverse energy sources like inorganic and organic compounds, as well as light (only in some organisms). ATP in plant cells is generated in part by substrate-chain-phosphorylation

in the cytosol and in the mitochondrial matrix, but mainly by oxidative phosphorylation in mitochondria or by photophosphorylation in chloroplasts.

During the photophosphorylation process in chloroplasts large amounts of ATP are produced, but these are used directly in the plastids and therefore are not available to meet the energy demands of the cell. The supply of ATP to the whole cell is mainly provided by oxidative phosphorylation. This process takes place in the inner mitochondrial membrane and involves the respiratory chain and the ATP-synthase complex. The respiratory chain, also termed electron transport chain (ETC), transfers electrons from reduced nicotinamide adenine dinucleotide (NADH) or flavin adenine dinucleotide (FADH₂), generated by the action of the citric acid cycle, via four different multi protein complexes and two mobile electron transporters (ubiquinone and cytochrome c) onto molecular oxygen (O₂) which is reduced to water (H₂O) (Fig. 2). Since this process is exergonic, the stepwise transfer of electrons allows translocation of protons from the matrix to the intermembrane space resulting in a proton gradient. Controlled reflux of these protons into the matrix drives the ATP-synthase complex in the IMM which phosphorylates ADP to yield ATP (Mitchell 1961).

In total, the OXPHOS system consists of five integral multi protein complexes in the IMM (Fig 2): NADH dehydrogenase (complex I), succinate dehydrogenase (complex II), cytochrome c reductase (complex III), cytochrome c oxidase (complex IV) and ATP-synthase (complex V) (Hatefi 1985).

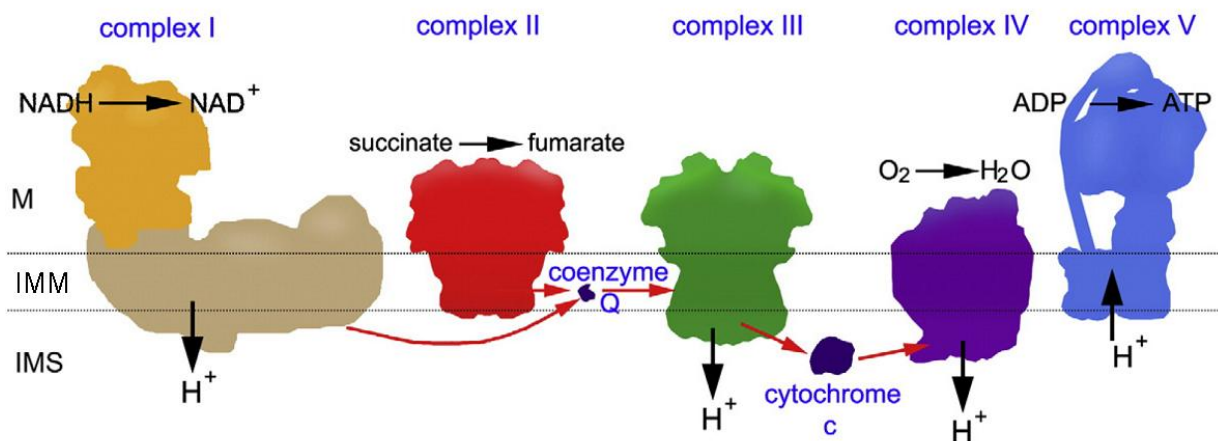


Figure 2: Schematic representation of the OXPHOS system showing its individual components but ignoring their structural interactions. Complex III is a functional dimer, in contrast to complex IV, although a high-resolution dimeric structure of the latter has been solved by X-ray crystallography. The scheme also depicts the two mobile electron carrier ubiquinone (also known as coenzyme Q) and cytochrome c. The position of the matrix (M), the intermembrane space (IMS) and the inner mitochondrial membrane (IMM) has been indicated. Image is taken from Dudkina et al. (2010a); slightly modified.

Complex I (NADH dehydrogenase) is the largest of the OXPHOS complexes and the main entrance point of electrons into the respiratory chain. It has two elongated domains that, together, form the typical L-shaped structure of this complex. The IMM located domain (membrane arm) is involved in proton translocation across the membrane, whereas the domain protruding into the mitochondrial matrix (peripheral arm) is responsible for the oxidation of NADH. The number of protein subunits depends on the type of organism. Bacterial complex I only comprises 14 subunits and has a size of 550 kDa (Yagi et al. 1998). It is also referred as 'minimal form' of complex I. Homologies can be found in other organisms and therefore these 14 subunits are also called 'central' subunits (Brandt 2006). Eukaryotic complex I has about 30 so called 'additional' subunits, ending up with over 40 subunits and a size of about 1 MDa. The 14 'central' subunits carry the redox centres, the flavin mononucleotide (FMN) and up to nine iron-sulfur-clusters (Brandt 2006 and references therein). Two electrons are transferred from each NADH (matrix side) to ubiquinone (UQ), also known as coenzyme Q (located in the IMM). Oxidation of one molecule NADH is coupled to the translocation of four protons from the matrix to the intermembrane space.

Complex II (succinate dehydrogenase) represents a second entrance point of electrons into the respiratory chain. It is the smallest of the OXPHOS complexes and the only one that does not comprise any mitochondrial encoded subunits (Scheffler 1998). The succinate dehydrogenase is not only part of the mitochondrial respiratory chain, but also forms part of the citric acid cycle located in the mitochondrial matrix. This protein complex consists of two IMM-integral subunits and two hydrophilic subunits which are attached to the hydrophobic proteins and protrude into the matrix (Yankovskaya et al. 2003). Several plant species exhibit up to four additional subunits with so far unknown functions (Eubel et al. 2003, Millar et al. 2004). Therefore, this complex has a molecular mass of 180 kDa in plants (Huang et al. 2010), whereas its mass in animals is only about 124 kDa (Sun et al. 2005). Complex II catalyzes the oxidation of succinate to fumarate. Simultaneously, electrons are transferred from FADH₂ to the mobile electron transporter ubiquinone, which is reduced to ubiquinol (UQH₂). Since this enzyme complex does not translocate protons across the IMM, it is not directly involved in the generation of the proton gradient.

Complex III (cytochrome c reductase) exists as a functional dimer and has a molecular mass of about 500 kDa. It consists of two times 10 to 11 subunits (Dudkina et al. 2006a). Only a minor part of the cytochrome c reductase protrudes into the intermembrane space, the bulk of the complex is matrix exposed. On complex III, electrons are transferred from ubiquinol to cytochrome c. A special feature of complex III is the Q-cycle. When UQH₂ binds to the

complex, the two electrons take different pathways. One electron is transferred to the mobile electron transporter cytochrome c via a Rieske iron-sulfur centre, whereas the other electron is transferred back to an UQ (bound to a second UQ-binding site) which is reduced to ubiquinol. The UQH₂ releases the remaining two protons to the intermembrane space. Now being oxidized again, the UQ enters the ubiquinone-pool. A second UQH₂ then binds to the complex and again the electrons are transferred as mentioned above. However, this time the ubiquinol, still bound on the second binding site, gets fully reduced and takes up two protons from the matrix, leaving complex III as UQH₂. By this, altogether two electrons are transferred from UQH₂ to cytochrome c thereby two protons are taken from the matrix and four protons are released to the intermembrane space (reviewed in Berry et al. 2000). Thus, complex III plays an important role in building up the proton gradient between the mitochondrial matrix and the IMS.

Complex IV (cytochrome c oxidase) is the last enzyme complex of the mitochondrial respiratory chain. This complex consists of 12 to 13 subunits with an overall size of about 220 kDa (Tsukihara et al. 1996). The cytochrome c oxidase (COX) catalyzes the sequential transfer of four electrons, one at a time from four reduced cytochrome c molecules, to molecular oxygen, thereby generating water. Coupled to electron transfer, four protons are pumped across the IMM (Welchen et al. 2011 and references therein).

Complex V (ATP-synthase complex) comprises 15 distinct subunits. Some of these are present in multiple copies in the holo-enzyme. The molecular mass of the complex is between 500 and 600 kDa (Dudkina et al. 2006a). The ATP-synthase complex consists of two parts: The F₀-part anchors the complex to the inner mitochondrial membrane, whereas the F₁ headpiece protrudes into the mitochondrial matrix (Stock et al. 2000). Both parts of the complex are connected by a central stalk. The ATP-synthase complex is driven by the proton motive force (PMF) of the proton gradient across the IMM. Protons are flowing back through complex V from the IMS to the matrix. The energy, gained by this reflux of protons, leads to a rotation of the F₀-part and the central stalk, whereas the F₁-part is fixed by an additional peripheral stalk and thereby prevented from rotation. Due to the rotation, ADP and phosphate are getting in a close proximity to each other building up the basis for phosphorylation.

1.3 Supramolecular organization of the OXPHOS system

The multi protein complexes of the respiratory chain were first described in the early 1960s (reviewed in Hatefi 1985), when OXPHOS complexes were subfractionated from mitochondrial membranes from beef. In some cases defined combinations of respiratory chain

complexes were reported, e.g. an active supercomplex of the complexes I and III as well as several other supercomplexes containing stoichiometric associations of OXPHOS complexes (Fowler and Hatefi 1961, Hatefi et al. 1961, Hatefi et al. 1962). Due to these findings, the structure of the respiratory chain was firstly described by the ‘solid-state model’ (Fig. 3b). Based on this model, the ETC complexes stably interact with each other forming supercomplexes. This model was questioned by Fowler and Richardson (1963) regarding the necessity of an association of complexes for the transfer of electrons. Later on, the ‘solid-state model’ again was challenged. The five complexes could be purified and were found to be stable particles, since they were easily separable from each other upon membrane solubilization. Thus, their separate existence under *in vivo* conditions was suggested. This hypothesis was supported by activity measurements of the OXPHOS complexes in inner membrane vesicles during lipid dilution experiments (Hackenbrock et al. 1986). Based on this new model, termed ‘fluid-state model’, respiratory chain complexes are separated in the inner mitochondrial membrane and electron transfer takes place by random collisions of the components (Fig. 3a). Accordingly, this model is also referred to as the ‘random collision model’ (Hackenbrock et al. 1986), which became widely accepted. However, recent experimental data, such as co-purification of defined respiratory chain complexes, high electron transfer activities of defined combinations of respiratory complexes and results of noninvasive flux control measurements, led to the suggestion of an alternative ‘solid-state model’ (see Welchen et al. 2011 and references therein). This model received support by native gel electrophoresis and single-particle electron microscopy (EM). Using different experimental setups, the following supercomplexes were detected: I+III₂, III₂+IV₁₋₂, I+III₂+IV₁₋₄ and V₂ (Dudkina et al. 2010a). Thereby, subscripted numbers indicate the number of individual complexes within the supercomplex. It is proposed that not all respiratory chain complexes are part of supramolecular structures at any time but co-exist with supercomplexes (Fig. 3c), which are dynamically assembled and degraded depending on the physiological state of the cell (Welchen et al. 2011). Recently, even higher organizational levels of respiratory supercomplexes were detected. One of these structures is a row-like association of complexes I, III and IV, termed ‘respiratory string’ (Bultema et al. 2009). Another higher organization of supercomplexes is represented by formation of dimeric ATP-synthase complexes. This supercomplex is assumed to participate in forming the cristae of the IMM (Strauss et al. 2008, Davies et al. 2011).

Sections 2.1 and 2.2 of this thesis will present further details on structure and function of mitochondrial supercomplexes.

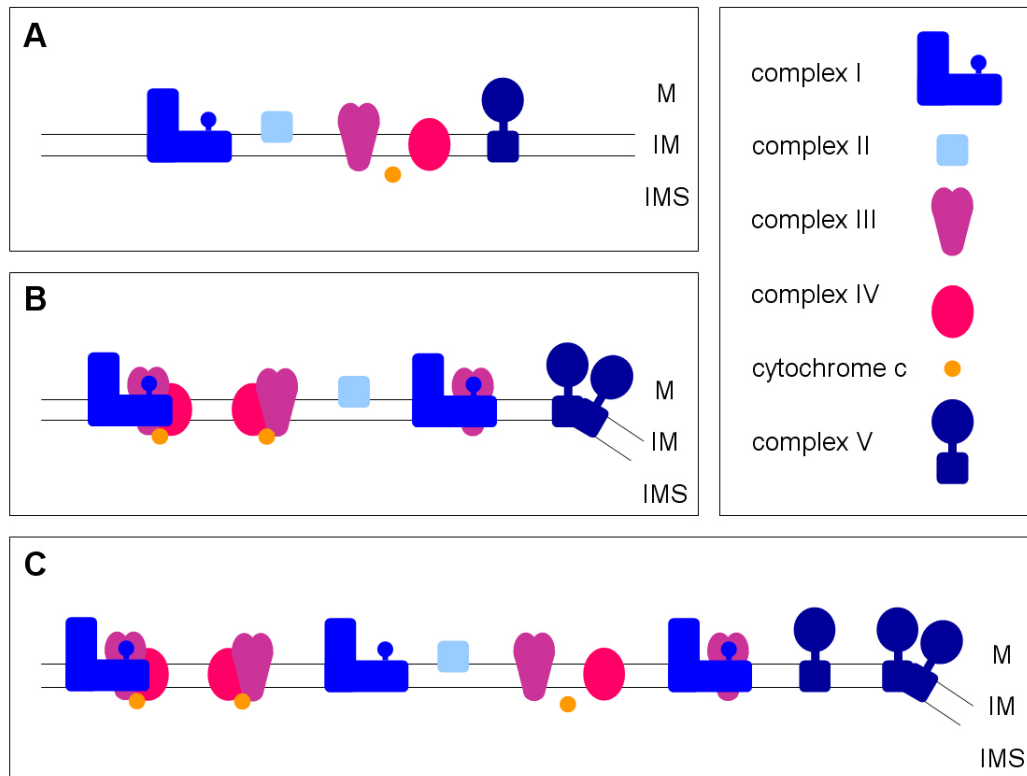


Figure 3: Schematic model of the mitochondrial OXPHOS system. A: 'Fluid-state model'. The respiratory chain complexes exist separately and electron transfer takes place by random collisions of the involved components. B: 'Solid-state model'. OXPHOS complexes stably interact forming supercomplexes. C: Integrated model of the OXPHOS system. Singular OXPHOS complexes and supercomplexes co-exist. Supercomplexes are dynamically formed and degraded. IM, inner mitochondrial membrane; IMS, intermembrane space; M, matrix. Image is taken from Welchen et al. (2011).

1.4 Characteristic features of the OXPHOS system in plants

The OXPHOS system in plants differs in many aspects from that found in mammals. One major difference is the highly branched plant mitochondrial ETC, which contains additional 'alternative' electron transport components. Enzymes catalyzing these alternative pathways are type II NAD(P)H dehydrogenases and the alternative oxidase (AOX). The former ones are bypassing complex I by reducing ubiquinone, whereas AOX bypasses complex III and IV by oxidizing ubiquinol (Fig. 4) (Rasmusson et al. 2008). Mitochondrial type II NAD(P)H dehydrogenases are encoded by three gene families. In the model plant *Arabidopsis thaliana*, they are encoded by seven nuclear genes (*AtNDA1*, *AtNDA2*, *AtNDB1-AtNDB4*, *AtNDC1*) and all proteins are targeted for mitochondria. *AtNDA1*, *AtNDA2* and *AtNDC1* are internal matrix-oriented NAD(P)H dehydrogenases, whereas the *AtNDBs* are external NAD(P)H dehydrogenases (Rasmusson and Wallström 2010). AOX is encoded by five genes in *Arabidopsis*, named *AOX1a* – *AOX1d* and *AOX2* (Thirkettle-Watts 2003). Functional differences between these homologues are not known.

The transport of electrons via these alternative pathways is not coupled to proton translocation across the inner mitochondrial membrane and hence does not contribute towards respiratory ATP production. Activity of the alternative electron pathway enzymes therefore results in lower ATP production and thus leads to decreased respiratory energy conservation (Rasmusson and Wallström 2010).

The internal and external alternative dehydrogenases enable the mitochondrial ETC to regulate the reduction levels of mitochondrial and cytosolic NADH (Rasmusson and Wallström 2010). It was already reported before, that NAD(P)H dehydrogenases are co-expressed with AOX (Clifton et al. 2006, Ho et al. 2007, Rasmusson et al. 2009) and that these genes are light-dependent (Michalecka et al. 2003, Svensson and Rasmusson 2001). These findings indicate a function of these enzymes in stabilizing the matrix NADH reduction level during photorespiration, when there is an excess of NADH in the mitochondrial matrix, derived from oxidation of photorespiratory glycine. Thus, the alternative respiratory pathways function as overflow mechanisms for the OXPHOS system by preventing the production of reactive oxygen species (ROS), which can occur due to an over-reduction of the ETC (Maxwell et al. 1999).

Regulation of the type II NAD(P)H dehydrogenases is not fully understood so far. In 2008, Rasmusson et al. reviewed the knowledge of the regulation of the alternative dehydrogenases: (i) Partitioning of complex I and alternative NADH dehydrogenase is supposed to be regulated kinetically. Complex I therefore oxidises NADH only under high matrix NADH concentration, which for example occurs during photorespiration. (ii) Partitioning could also be modified by the regulation of complex I activity, for example by phosphorylation. (iii) The electrochemical proton gradient also might play a role in regulation. This assumption is connected to consequences for other reactions, which are involved in reduction of UQ pool and substrate channelling for restricting proton motive force (for details see Rasmusson et al. 2008 and references therein).

Apart from the function as bypasses, NAD(P)H dehydrogenases also represent a broad spectrum of entry points for electrons into the ETC. Additionally, there are few other enzymes like electron transfer flavoprotein:quinone oxidoreductase (ETFQ-OR), L-galactono-1,4-lactone dehydrogenase (GLDH) and glycerol-3-phosphate (G3P) dehydrogenase which supply the ETC with electrons. All together, the bypasses via alternative NAD(P)H dehydrogenases and AOX as well as the existence of several electron entry points besides complex I and II result in a highly branched respiratory chain in plants (Rasmusson et al. 2008).

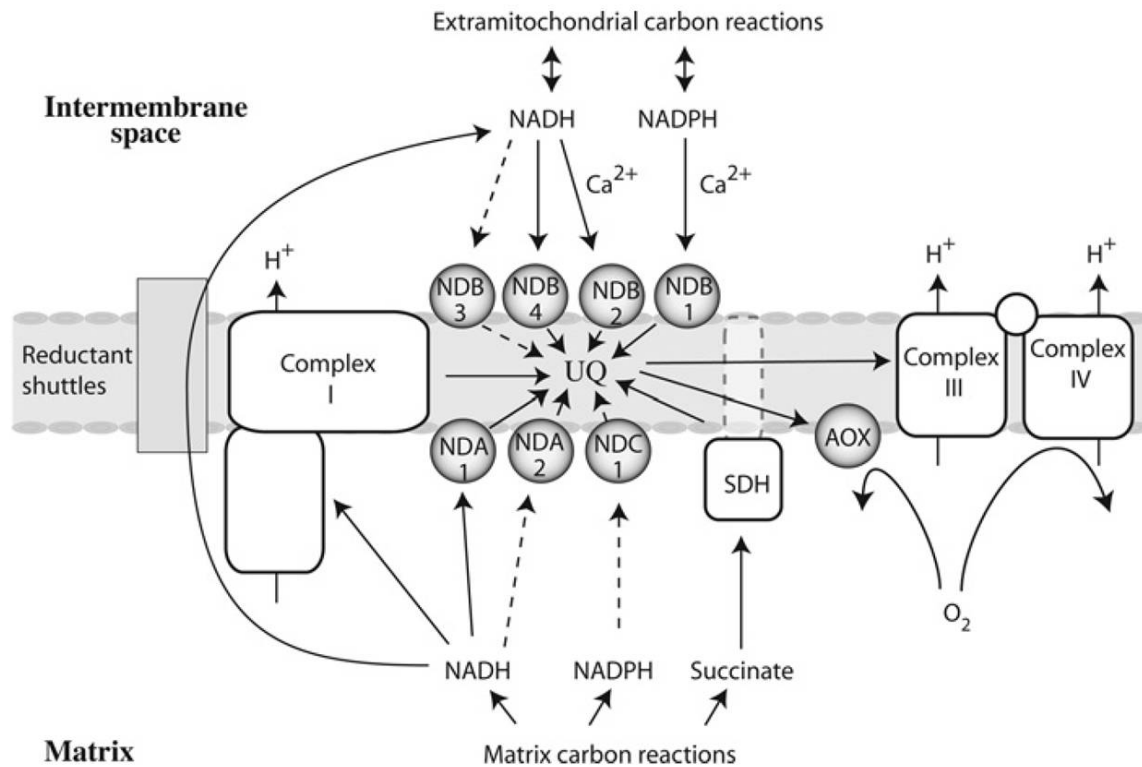


Figure 4: Respiratory chain complexes and alternative respiratory enzymes in plant mitochondria. The standard complexes are depicted in white, type II NAD(P)H dehydrogenases and AOX are shown in grey. Broken lines represent unclear enzymatic properties. SDH, succinate dehydrogenase (complex II). Image is taken from Rasmusson and Wallström (2010).

Another remarkable difference in the OXPHOS systems of plants and mammals is the presence of additional protein subunits in respiratory complexes in plants, which introduce side activities to these complexes.

For example, complex I consists of 14 core subunits in all organisms but contains about 30 extra subunits in eukaryotes (Klodmann and Braun 2011). As reported in Klodmann et al. (2010), complex I from *Arabidopsis thaliana* has 13 plant specific subunits. One of these additional subunits is the GLDH. This enzyme catalyzes the final step of the ascorbate synthesis pathway and is associated with a smaller version of complex I (Heazlewood et al. 2003, Millar et al. 2003). Pineau et al. (2008) assumed GLDH to be a bifunctional protein which is not only involved in ascorbate synthesis, but also in the assembly of complex I.

Another group of plant specific subunits in complex I is composed of five structurally related 30 kDa proteins, which show sequence similarity to gamma-type carbonic anhydrases (γ CA) of the archaeobacterium *Methanosarcina thermophila* (also referred to as CAM). Single particle electron microscopy of complex I from *Arabidopsis thaliana*, *Zea mays* and the green alga *Polytomella* indicates a plant specific extra domain composed of γ CAs that is attached to the central part of the membrane arm of the complex, protruding into the matrix (Sunderhaus et al.

2006, Peters et al. 2008). The five carbonic anhydrase proteins are named CA1, CA2, CA3 and carbonic anhydrases like proteins 1 and 2 (CAL1, CAL2). These two CAL proteins differ from the γ CA of the archaeobacteria to a greater extent than CA1 – CA3 (Braun and Zabaleta 2007). Carbonic anhydrases are zinc containing metallo-enzymes, catalyzing very rapidly the inter-conversion of CO_2 and HCO_3^- . So far such an activity could not be demonstrated for the γ CAs in plants.

Therefore, the physiological role of the CA extra domain in plant complex I is not completely understood. Several lines of evidence indeed support a model in which CAs and CALs are involved in $\text{CO}_2/\text{HCO}_3^-$ metabolism (reviewed in Klodmann and Braun 2011). Additionally, a physiological role of the plant specific CA-domain in photorespiration was postulated by Braun and Zabaleta (2007). In plants, CO_2 is an essential substrate for photosynthesis, which becomes limiting under certain conditions such as closed stomata due to arid environmental conditions. This rapidly results in low concentration of CO_2 in chloroplasts, whereas mitochondria at the same time produce large amounts of CO_2 due to photorespiration. Braun and Zabaleta (2007) suggested an active CO_2 transport system between mitochondria and chloroplasts, which is based on the $\text{CO}_2/\text{HCO}_3^-$ conversion at complex I. Bicarbonate is then transported across the mitochondrial and chloroplast membranes and is again re-converted into CO_2 by CAs in the chloroplast. An analogous mechanism for CO_2 concentration is well characterized for cyanobacteria, termed CO_2 concentrating mechanism (CMM) (Price et al. 2008).

As previously reported, also the succinate dehydrogenase (complex II) of *Arabidopsis thaliana* consists of four extra plant specific subunits (Eubel et al. 2003, Millar et al. 2004), termed SDH 5 – SDH 8. Huang et al. (2010) reported that 7 of the 8 subunits found in *Arabidopsis* have homologues in rice, while SDH 8 is missing. This study reveals that also rice complex II contains at least three plant specific subunits. In all other organisms, complex II consists of only four subunits. The functions of the ‘core’-subunits are well established (section 1.2), but until today the functions of the plant specific subunits are still unknown and none of these proteins show homology to known functional proteins in any database. Hence, it is not clear if the extra subunits of complex II in plants also introduce side activities to the complex as it could be shown for complex I in plants.

Another complex, for which specific side activities in plants were detected, is the cytochrome c reductase. As reported by Braun et al. (1992), two core subunits of complex III display mitochondrial processing peptidase (MPP) activity. The major MPP activity, which leads to a cleavage of the presequences from imported precursor proteins, normally can be found in the

soluble fraction of fungal and mammalian mitochondria. In plants, this activity is located to complex III in the inner mitochondrial membrane.

1.5 Approaches used for the investigation of the OXPHOS system

The aim of investigations of the OXPHOS system is to further characterize the physiological functions and the structures of the complexes and supercomplexes. One important technique for the investigation of protein complexes is blue native polyacrylamide gel electrophoresis (BN-PAGE), which is also used extensively in this thesis (for details see section 2.3) (Schägger and von Jagow 1991). This method allows separation of OXPHOS complexes and stable supercomplexes on polyacrylamide gels under native conditions. In a first step, mitochondrial membranes are solubilised by the use of a mild, non-ionic detergent. In most cases this is dodecyl maltoside (DDM), Triton X100 or digitonin. Working with *Arabidopsis* and other plant mitochondria, e.g. from maize, digitonin is the detergent of choice, because it is best suited to retain complexes with high molecular masses like plant complex I or the I-III₂ supercomplex. After solubilization, proteins are mixed with the anionic dye Coomassie blue. This water-soluble dye has a high affinity to hydrophilic and hydrophobic proteins and introduces negative charges to the proteins without denaturing them. Since all proteins are now negatively charged in a uniform fashion, they migrate towards the anode, thereby getting resolved according to size and not to charge. Coomassie blue addition also prevents protein aggregation, since all proteins carry negative charges. The separation capacity of BN-PAGE is best if the gradient of the polyacrylamide gel is chosen according to sample properties, because proteins get stuck in the gel when they reach their size dependent specific pore-size limit (Wittig et al. 2006). The size of pores is depending on concentration of acrylamide and amounts of cross-linkers (e.g. bisacrylamide). An increase in acrylamide concentration results in a decrease of pore-size and *vice versa* (Rüchel et al. 1978). Therefore, separation of proteins with low molecular weights would require high acrylamide concentrations resulting in smaller pore-sizes.

BN-PAGE is often the first step in various approaches. The most common one is the combination with sodium dodecyl sulfate polyacrylamide gel electrophoresis (SDS-PAGE). For this, the protein complexes separated by BN-PAGE are first denatured by β -mercaptoethanol and SDS. Afterwards, protein complex subunits are resolved in a second gel dimension according to molecular weight. By this procedure, known as two-dimensional (2D) BN/SDS-PAGE, the subunit composition of protein complexes and supercomplexes can be visualized (Wittig et al. 2006).

Other methods often used in combination with BN-PAGE are: (i) in-gel activity stains (sections 2.1 and 2.4), (ii) native immunoblotting (supplementary material of section 2.4), (iii) electroelution with subsequent analyses by isoelectric focusing (IEF), sometimes also followed by SDS-PAGE as a third-dimension (3D BN/IEF/SDS-PAGE) and (iv) a second BN-PAGE (2D BN/BN-PAGE) (Wittig et al. 2006).

When it becomes necessary to compare the protein complex or subunit composition of different samples, e.g. mutant lines, blue native difference gel electrophoresis (BN-DIGE) is the method of choice. For this, the protein fractions of interest are labelled with different fluorescent dyes, pooled and then separated on a single gel, thereby minimizing gel-to-gel variations. However, the BN-DIGE technique can be combined with a second dimension SDS-PAGE. Section 2.3 will describe this method in detail.

Besides all these techniques, mainly based on electrophoresis, other methods are available which enable investigations of the OXPHOS complexes. One powerful technique is single-particle EM, which is also used in this thesis (sections 2.1 and 2.2). For this procedure individual protein complexes and supercomplexes are purified, mostly by the use of sucrose density gradients, and investigated by negative stain or cryo-EM. Thousands of images are taken, classified and averaged electronically, resulting in an image of the structure of a complex. Cryo-EM allows depicting internal details of the object whereas the negative stain reflects the shape of a protein complex. Single-particle EM is able to generate detailed images of structures and determine the orientation of singular complexes as well as the contact sites of complexes in supramolecular structures.

Furthermore, cryo-electron tomography (cryo-ET) is used for 3D reconstruction of a sample from tilted 2D images taken by a CCD-sensor at cryogenic temperatures. This method generates structural information of complex cellular organizations at subnanometer resolution without changes due to chemical treatments, staining procedures or microsectioning. In this thesis cryo-electron tomography is used to investigate the arrangement of supercomplexes within intact mitochondria (section 2.2).

1.6 Objective of the thesis

The objective of this thesis is the extended characterization of the OXPHOS system in plant mitochondria. This includes structural and functional analyses of supercomplexes, single protein complexes and plant specific subunits. Furthermore, a method for comparative analyses of protein complexes was established.

In the following chapter four investigations on the plant OXPHOS system are presented:

In section 2.1, a structural characterization of complex I and the I+III₂ supercomplex in *Zea mays*, which emphasises on the carbonic anhydrase domain, will be presented. In this study, carbonic anhydrases are explored for the first time in a C₄ plant. Additionally, not reported so far for any plant species, a structural heterogeneity within complex I is displayed.

The supramolecular structure and function of the mitochondrial OXPHOS system in general is reviewed in section 2.2.

A new approach for the comparative analysis of protein complexes by BN-DIGE is described in detail in section 2.3. This method is an excellent tool for comparative investigations of the OXPHOS system.

For the first time, the ratios of OXPHOS complexes in different plant tissues were analyzed and results will be discussed in section 2.4. So far, only mammalian OXPHOS complexes were investigated in such an approach and the knowledge related to plants is limited. In this section, the quantity of the five OXPHOS complexes from different tissues of *Arabidopsis thaliana* is defined. This study reveals strong differences in complex abundances, especially with respect to complexes I and II. Furthermore, it leads to new insights into physiological functions of complex I.

Supplementary discussions of the thesis as well as an outlook are given in chapter 3.

Chapter 2

2 Publications and manuscripts

This thesis comprises four manuscripts. The first manuscript ‘A structural investigation of complex I and I+III₂ supercomplex from *Zea mays* at 11-13 Å resolution: assignment of the carbonic anhydrase domain and evidence for structural heterogeneity within complex I’ was published in the scientific journal ‘Biochimica et Biophysica Acta’ (1777, 84-93) in 2008. I performed the isolation of the maize mitochondria, the gel electrophoresis procedures (1D BN-PAGE, 2D BN/SDS-PAGE) and the spot picking for protein analyses by mass spectrometry as well as the purification of complex I and I+III₂ supercomplex by sucrose gradient ultracentrifugation. All figures concerning these parts were designed by myself. Mass spectrometry was carried out by Prof. Dr. L. Jansch and single-particle electron microscopy was done by Dr. N.V. Dudkina. The bulk of the protocol was written by Dr. N.V. Dudkina, I added the main part of the materials and methods section and was involved in proof reading. The manuscript was corrected by Prof. Dr. H.-P. Braun and Prof. Dr. E.J. Boekema.

The second manuscript, a review on the ‘Structure and function of mitochondrial supercomplexes’ was published in the scientific journal ‘Biochimica et Biophysica Acta’ (1797, 664-670) in 2010. Together with Prof. Dr. H.-P. Braun, I was responsible for the literature research for this review. In cooperation with the co-authors we wrote the manuscript. Figures in this manuscript concerning single-particle EM and electron tomography were prepared by Dr. N.V. Dudkina and Dr. R. Kouril.

The third manuscript ‘Comparative analyses of protein complexes by blue native DIGE’ is a protocol for fluorophore labelling of native protein fractions for separation by blue native PAGE. I wrote the manuscript, which was subsequently corrected by Prof. Dr. H.-P. Braun. This manuscript is in press and will be published soon in the book ‘Differential Gel Electrophoresis’, part of the series ‘Methods in Molecular Biology’ published by Humana Press.

In the fourth manuscript ‘Complex I - complex II ratio strongly differs in various organs of *Arabidopsis thaliana*’ approximately 90% of the research was performed by myself. All experiments and figures in this manuscript were made by me, with support of the co-authors in some parts. The complete manuscript was written by myself and subsequent correction were done by Prof. Dr. H.-P. Braun. At this stage the manuscript is still in preparation.



A structural investigation of complex I and I+III₂ supercomplex from *Zea mays* at 11–13 Å resolution: Assignment of the carbonic anhydrase domain and evidence for structural heterogeneity within complex I

Katrin Peters^a, Natalya V. Dudkina^b, Lothar Jänsch^c, Hans-Peter Braun^{a,*}, Egbert J. Boekema^b

^a Institute for Plant Genetics, Faculty of Natural Sciences, Leibniz Universität Hannover, Herrenhäuser Str. 2, D-30419 Hannover, Germany

^b Groningen Biomolecular Sciences and Biotechnology Institute, University of Groningen, Nijenborgh 4, 9747 AG Groningen, The Netherlands

^c Proteome Research Group, Division of Cell and Immune Biology, Helmholtz Centre for Infection Research, Inhoffenstraße 7, D-38124 Braunschweig, Germany

Received 21 August 2007; received in revised form 18 October 2007; accepted 19 October 2007

Available online 4 November 2007

Abstract

The projection structures of complex I and the I+III₂ supercomplex from the C₄ plant *Zea mays* were determined by electron microscopy and single particle image analysis to a resolution of up to 11 Å. Maize complex I has a typical L-shape. Additionally, it has a large hydrophilic extra-domain attached to the centre of the membrane arm on its matrix-exposed side, which previously was described for *Arabidopsis* and which was reported to include carbonic anhydrase subunits. A comparison with the X-ray structure of homotrimeric γ -carbonic anhydrase from the archaeobacterium *Methanosarcina thermophila* indicates that this domain is also composed of a trimer. Mass spectrometry analyses allowed to identify two different carbonic anhydrase isoforms, suggesting that the γ -carbonic anhydrase domain of maize complex I most likely is a heterotrimer. Statistical analysis indicates that the maize complex I structure is heterogeneous: a less-abundant “type II” particle has a 15 Å shorter membrane arm and an additional small protrusion on the intermembrane-side of the membrane arm if compared to the more abundant “type I” particle. The I+III₂ supercomplex was found to be a rigid structure which did not break down into subcomplexes at the interface between the hydrophilic and the hydrophobic arms of complex I. The complex I moiety of the supercomplex appears to be only of “type I”. This would mean that the “type II” particles are not involved in the supercomplex formation and, hence, could have a different physiological role.

© 2007 Elsevier B.V. All rights reserved.

Keywords: Complex I; Cytochrome *c* reductase; Carbonic anhydrase; Supercomplex; Electron microscopy, *Zea mays*

1. Introduction

Complex I is the major entrance point of electrons to the respiratory chain. It catalyses the transfer of two electrons from NADH to quinone, which is coupled to the translocation of four protons across the inner mitochondrial membrane [1–3]. The subunit composition of complex I is highly variable depending on the type of organism. Bovine and human complex I are composed of about 46 different subunits and have a molecular weight of about 1 MDa. Complex I of prokaryotes and chloroplasts are substantially smaller and composed mostly of 14 subunits that are homologues of a “core” complex of mitochondrial complex I. They have been defined as the “minimal” enzyme. The remaining

subunits are so-called “accessory” subunits [3]. Complex I consists of a hydrophobic membrane arm and a hydrophilic peripheral arm, which protrudes into the matrix. Together they give complex I an unique L-shape, as has been revealed at low-resolution by three-dimensional electron microscopy [4–6]. The crystal structure of the peripheral arm of complex I from *Thermus thermophilus* has been solved [7]. The positions of eight subunits and all redox centres of the enzyme were determined, including nine iron–sulfur centres.

The main known function of the membrane arm is proton translocation [8], but the precise functions of the membrane domain are not well understood because of a lack of high-resolution structural data. However, a medium-resolution projection map at 8 Å of complex I from *E. coli* was recently obtained by electron microscopy [9]. It indicates the presence of about 60 transmembrane α -helices, both perpendicular to the

* Corresponding author. Tel.: +49 511 7622674; fax: +49 511 7623608.
E-mail address: braun@genetik.uni-hannover.de (H.-P. Braun).

membrane plane and tilted, which is consistent with secondary structure predictions. A possible binding site and access channel for quinone is found at the interface with the peripheral arm. Tentative assignment of individual subunits to the features of the map has been made. The NuoL and NuoM subunits, which were proposed to be responsible for proton translocation, are localized at the tip of the membrane arm of complex I. Since this tip is at a substantial distance to the redox centres of the peripheral arm of complex I, conformational changes most likely play a role in the coupling between electron transfer and proton pumping.

Complex I can form stable associations with complex III of the respiratory chain [10,11]. This interaction is especially stable in plants. An investigation by EM and single particle analysis revealed a lateral association of dimeric complex III to the tip of the membrane part of complex I in *Arabidopsis* [12]. The functional role of the I+III₂ supercomplex so far is unknown.

Complex I of plant mitochondria resembles complex I of other multicellular organisms but includes some extra subunits [13–15]. As a consequence, its overall molecular mass is slightly larger than that of complex I of beef [16]. Some of the extra subunits introduce side-activities into plant complex I. In probably all higher eukaryotes, the “acyl carrier protein” of the mitochondrial fatty acid biosynthesis pathway is integrated into complex I [17,18]. However, occurrence of this protein in complex I of plants recently has been disputed [19]. Additionally, L-galactono-1,4-lactone dehydrogenase (GalLDH), the terminal enzyme of the mitochondrial ascorbate biosynthesis pathway, forms part of complex I in plants [20]. Furthermore, plant mitochondria include a group of five structurally similar 30 kDa proteins which resemble a γ -type carbonic anhydrase of the archaeobacterium *Methanosarcina thermophila*. A structural characterization by single particle electron microscopy of complex I from *Arabidopsis* and the green alga *Polytomella* indicated a plant-specific spherical extra-domain of about 60 Å in diameter, which is attached to the central part of the membrane arm of complex I on its matrix face [15]. This spherical domain is proposed to be composed of the γ -carbonic anhydrase subunits. Although the inner features of the domain could not be resolved it is probably arranged as a trimer of three subunits, because γ -carbonic anhydrase of *Methanosarcina thermophila* is known to have a trimeric structure [21,22].

The functional role of the complex I integrated carbonic anhydrases in plants is not quite understood. It was speculated that they form part of an active CO₂ transport system between mitochondria and chloroplasts for efficient CO₂ fixation during photosynthesis [23]. CO₂, one of the main substrates of photosynthesis, is often growth limiting in plants. The CO₂ concentration within chloroplasts especially declines if plants are grown in the presence of high-light conditions, enabling high rates of CO₂ fixation. Furthermore, the CO₂ concentration declines at high temperature due to Ribulose-1,5-bisphosphate Carboxylase/Oxygenase (RubisCO) kinetics and water solubility of oxygen and CO₂. As a consequence, the Oxygenase side-activity of RubisCO increases dramatically, giving rise to the formation of phosphoglycolate. This compound cannot be used for the Calvin cycle and is recycled by the so-called “photorespiration” pathway. Finally, during photorespiration, large amounts of CO₂ are liberated in the mitochondria.

In summary, CO₂ concentration in the chloroplasts of plant cells often is low. At the same time, the mitochondria produce large amounts of CO₂. Rapid conversion of mitochondrial CO₂ into bicarbonate by carbonic anhydrases is speculated to form the basis of an active indirect CO₂ transport mechanism between mitochondria and chloroplasts. Indeed, genes encoding the complex I integrated carbonic anhydrases are down-regulated in *Arabidopsis*, if plants are cultivated in the presence of elevated CO₂ concentration [22]. An analogous role of complex I was reported in the context of a cyanobacterial CO₂ concentrating mechanism [24].

A characterization of maize (*Zea mays*) complex I was initiated to further investigate the physiological role of the mitochondrial carbonic anhydrases in plants. In contrast to the “C₃” plant *Arabidopsis*, maize is a so-called “C₄” plant that uses phosphoenolpyruvate (PEP) for pre-fixation of CO₂ in the form of a four-carbon (C₄) compound. Pre-fixation is carried out in specialized cells termed mesophyll cells, which also carry out the photosynthetic light reactions and water splitting. The final CO₂ fixation by RubisCO takes place in so-called bundle sheath cells, which do not carry out photosynthetic water splitting. C₄ metabolism is based on the transfer of C₄-compounds from mesophyll to bundle sheath cells and liberation of CO₂ in bundle sheath cells. As a consequence, the final CO₂ fixation by RubisCO is very efficient and photorespiration is avoided. Therefore, the functional role of the mitochondrial carbonic anhydrases might differ between *Arabidopsis* and maize. However, in certain subtypes of C₄ metabolism, which use a mitochondrial enzyme for CO₂ release in bundle sheath cells, the presence of carbonic anhydrases in mitochondria might be especially important.

Here, we describe a structural analysis by single particle electron microscopy of maize complex I. It has the same L-shaped form like *Arabidopsis* complex I, including the extra carbonic anhydrase domain. This domain is, as well as other features, much better resolved in the current projection maps, and comparison to the high-resolution X-ray structure of the γ -carbonic anhydrase now shows it to be a trimer. Mass spectrometry was performed to evaluate the composition of the carbonic anhydrase trimer. In addition, the structure of the respiratory I+III₂ supercomplex was analyzed. This supercomplex has a horse-shoe structure, identical to the one found in *Arabidopsis*. It appears to be a very stable, rigid structure that allowed the determination of projection maps at 12 Å resolution. New insights into the complex I–complex III interaction are presented.

2. Materials and methods

2.1. Cultivation of maize seedlings

Green maize seedlings (*Zea mays* convar *saccharata* L. “Tasty Sweet” F1) were cultivated in a greenhouse under long-day conditions (16 h light, 8 h dark) at 22 °C for 9 days. Etiolated maize seedlings were cultivated in growth chambers in the absence of light at 22 °C for the same time period.

2.2. Isolation of maize mitochondria

Starting material for organelle preparations were 100 g of green and etiolated tissue. The material was suspended each in 500 ml of ice-cold “grinding buffer” (0.4 M mannitol, 1.0 mM EGTA, 25.0 mM MOPS, 0.1% [w/v] bovine serum

albumin [BSA], 15 mM β -mercaptoethanol, and 0.05 mM phenylmethylsulfonyl fluoride [PMSF]/KOH, pH 7.8). The cells were disrupted by homogenization for three periods of 10 s using a Waring blender and then filtered through two layers of muslin. Mitochondria were isolated by differential centrifugation and Percoll density gradient centrifugation as described by Braun et al. [25]. The three-step Percoll gradients for density gradient centrifugation contained 14%, 26%, and 45% Percoll in 0.8 M mannitol, 2.0 mM EGTA, 20.0 mM KH_2PO_4 /KOH, pH 7.2. After gradient centrifugation (45 min at $70,000 \times g$), mitochondria were isolated from the 26%/45% interphase. To remove the Percoll the purified mitochondria were centrifuged three times in “resuspension buffer” (0.4 M mannitol, 1.0 mM EGTA, 10.0 mM KH_2PO_4 , 0.2 mM PMSF/KOH, pH 7.2) for 10 min at $14,500 \times g$.

Purities of our organelle preparations were investigated by analyses of protein complex compositions using 2D Blue-native/SDS-PAGE (see below) [26]. Mitochondrial fractions included all the known protein complexes of the OXPHOS system but were devoid of plastidic complexes, e.g. the photosystems, the b_6f complex and the plastidic ATP synthase complex. The latter two complexes are also formed in etioplasts but were absent in mitochondrial fractions isolated from maize seedlings cultivated in the dark (data not shown). Furthermore, the subunit completeness of all OXPHOS complexes was very good indicating that the purified organelles were isolated in a very intact form.

2.3. Gel electrophoreses procedures and immunoblotting

One-dimensional Blue-native PAGE and two-dimensional Blue-native/SDS-PAGE were carried out as outlined in Heinemeyer et al. [27]. Proteins were either visualized by Coomassie blue colloidal staining [28] or blotted onto nitrocellulose filters. Blots were incubated over night with an antiserum directed against the C-terminal half of a complex I integrated carbonic anhydrase of *Arabidopsis* (encoded by locus At1g47260; [22]). Visualization of immune-positive protein spots was performed using biotinylated secondary antibodies, avidin, and horseradish peroxidase (Vectastain ABC kit, Vector laboratories, Burlingame, CA, USA).

2.4. Protein analyses by mass spectrometry

Proteins of interest were cut out of 2D Blue-native/SDS gels and pre-treated for mass spectrometry (MS) analyses as described previously in Eubel et al. [11]. Selected tryptic peptides were sequenced by Electrospray Ionization MS/MS using the Q-TOF II mass spectrometer (Micromass, Waters, Milford, MA, USA). Proteins were identified by MASCOT (<http://www.matrixscience.com/>) using the NCBI protein database.

2.5. Purification of complex I and I+III₂ supercomplex from maize by sucrose gradient ultracentrifugation

Isolated mitochondria were solubilized by digitonin (5 mg of detergent per mg of mitochondrial protein), and protein complexes were subsequently resolved by sucrose gradient ultracentrifugation as previously described by Dudkina et al. [12]. Fractions were removed from the gradient from bottom to top. Protein complexes present in individual fractions were resolved by BN PAGE and identified on the basis of their subunit compositions on second gel dimensions, which were carried out in the presence of SDS [14]. Fractions including complex I and the I+III₂ supercomplex were directly used for EM analysis.

2.6. Electron microscopy and single particle analysis

Selected fractions of the sucrose gradient including the I+III₂ supercomplex and complex I were directly used for electron microscopy. Electron microscopy was performed on a Philips CM12 electron microscope equipped with a slow-scan CCD camera. Data acquisition and single particle analyses including alignments of projections with multi-reference and non-reference procedures, multivariate statistical analysis and classification, was carried out as outlined by Dudkina et al. [12]. Resolution was determined according to Van Heel 1987 [29] by 2σ and 3σ criteria.

The trimeric X-ray structure of γ -carbonic anhydrase (PDB accession number 1QRE) from *Methanosarcina thermophila* [30] and the hydrophilic domain of complex I (PDB accession number 2FUG) from *Thermus thermophilus* [7] were used to model the carbonic anhydrase domain and the hydrophilic arm of complex I. VIS5D software (<http://www.ssec.wisc.edu/~billh/vis5d.html>) and PyMOL software were used for visualization. For the modeling of the I+III₂ supercomplex we used the X-ray structures of cytochrome *bc*₁ complex (PDB accession number 1BGY) from bovine mitochondria [31] and 3D EM model of complex I from *Yarrowia lipolytica* [6].

3. Results

3.1. Characterization of complex I and the I+III₂ supercomplex of maize

Mitochondria from green and etiolated maize seedlings were purified to investigate the structure of complex I and the I+III₂

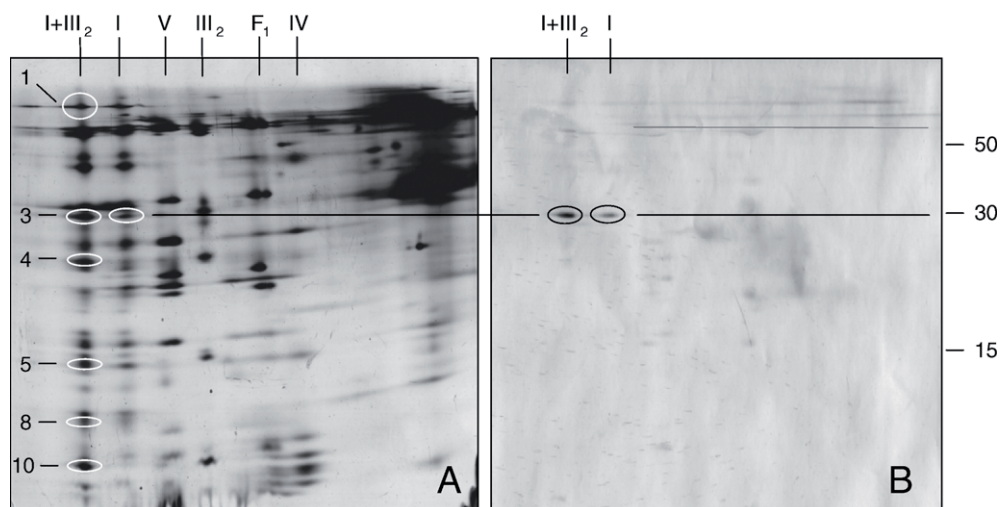


Fig. 1. Two-dimensional resolution of mitochondrial proteins from etiolated maize seedlings by Blue-native/SDS-PAGE. (A) Silver-stained gel. (B) Immunological detection of carbonic anhydrase on a corresponding Western blot. The identities of the resolved protein complexes and supercomplexes are given above the gel and the blot, the molecular masses of standard proteins to the right of the blot (in kDa). Proteins subjected to analyses by mass spectrometry are circled on the gel and numbered consecutively (for results see Table 1).

supercomplex from a C_4 plant. The OXPHOS system of maize was analyzed by 2D Blue-native/SDS-PAGE. On the first gel dimension, complex I runs at about 1000 kDa and the I+III₂ supercomplex at 1500 kDa (data not shown). Subunits of the OXPHOS complexes were resolved by SDS-PAGE. The subunit compositions of the OXPHOS complexes of mitochondria of etiolated maize seedlings (Fig. 1) resemble the ones of *Arabidopsis* [14]. On the 2D gel, complex III₂ is resolved into 9 distinct subunits, complex I into >25 and the I+III₂ supercomplex also into >25 subunits. The latter two complexes probably include several further subunits, which are invisible on the 2D gels due to overlapping positions. The subunit composition of complex I and the I+III₂ supercomplex of mitochondria of green maize seedlings was indistinguishable from the ones obtained for etiolated seedlings upon analyses by 2D Blue-native PAGE (data not shown).

The presence of carbonic anhydrases within complex I and the I+III₂ supercomplex of maize was investigated by immunoblotting using an antibody directed against a complex I integrated carbonic anhydrase of *Arabidopsis*. The antibody specifically recognizes an epitope on a protein in the 30 kDa range of both complexes (Fig. 1B). The presence of carbonic anhydrases within complex I and the I+III₂ supercomplex of maize was confirmed by mass spectrometry (MS). For this approach, the 30 kDa spot and 5 further spots of the I+III₂ supercomplex were cut out from a 2D BN/SDS gel, trypsinated and prepared for MS analysis. Overall, 13 peptide sequences were obtained (Table 1), which exactly match peptide sequences encoded by the rice genome (the complete genome sequence of maize currently is not available; rice is the closest relative of maize to be completely sequenced). The peptides are part of 8 different proteins, four of which belong to complex I (75, 23 and 11 kDa subunits and a protein homologous to a complex I integrated carbonic anhydrase of rice), and four of which belong to complex III₂ (cytochrome *c*₁, the Rieske iron–sulfur protein, 14 kDa and 8.2 kDa subunits). Sequence identities between the maize peptides and the corresponding amino acid sequences from *Arabidopsis* are in the range of 65 to 90% (data not shown).

For EM analyses, purified mitochondrial fractions from green and etiolated seedlings were loaded onto sucrose gradients and protein complexes were separated by ultracentrifugation. Afterwards, gradients were fractionated and small aliquots of all fractions were analysed by 1D Blue-native PAGE to monitor the protein complex composition of the fractions (Fig. 2). Fractions close to the bottom of the gradients included pure complex I and I+III₂ supercomplex. These fractions were selected for further analyses using single particle EM.

3.2. Electron microscopy

Negatively stained electron microscopy specimens of fractions 3 and 4 for the green seedlings and fractions 4 and 5 for the etiolated seedlings indicated large numbers of projections of complex I and I+III₂ supercomplex suitable for single particle image analysis. We analyzed a selected data set of about 28,000 projections from green maize, which was grown in the light, and a data set of about 12,000 projections from etiolated maize, which was grown in the dark. An initial analysis by multi-reference alignment, multivariate statistical analysis and classification of the projections indicated that both sets comprised the same classes of projections with similar numbers of particles. Hence, the two data sets were also combined in one large data set and analysed together, to get better resolution in the final projection maps.

After classification of the separate data sets and combined set of projections, a gallery of different projection maps of singular complex I and the I+III₂ supercomplex was obtained (Fig. 3). The I+III₂ supercomplex has one preferable orientation in a specific top-view position (Fig. 3A). Only 75 views could be assigned to side view positions; the sum of the best 32 projections is shown in Fig. 3B. Due to the very low numbers of particles, the resolution of this side view projection is very limited. The classes shown in parts D–K of Fig. 3 represent side views of complex I. All these projections show the membrane-embedded arm in horizontal position and the hydrophilic arm in about vertical position. The classes D/H and G/I represent

Table 1

Spot no. ^a (peptide)	Identified peptide sequence ^b	Protein identity ^c	Accession no. ^d (organism)
1 (b)	GSGEEIGTYVEK	75 kDa subunit, complex I	gi 115454943 (rice)
(c)	SNYLMNTSIAGLEK	75 kDa subunit, complex I	gi 125545494 (rice)
3 (b)	LGSTIQGGLR	Carbonic anhydrase, complex I	gi 115473681 (rice)
(c)	IPSGEVWVGNPAK	Carbonic anhydrase, complex I	gi 115473681 (rice)
(d)	DLVGVAYTEEETK	cyt <i>c</i> ₁ , complex III	gi 115442085 (rice)
(f)	DVVSFLSWAAEPEMEER	cyt <i>c</i> ₁ , complex III	gi 34907202 (rice)
4 (b)	LANSVDVASLR	Rieske iron-sulfur protein, complex III	P49727 (maize)
(c)	NVTINYPFEK	23 kDa TYKY subunit, complex I	gi 115455639 (rice)
(d)	SINTLFLTEMVVR	23 kDa TYKY subunit, complex I	gi 115455639 (rice)
(e)	NQDAGLADLPATVAVK	Rieske iron-sulfur protein, complex III	P49727 (maize)
5 (b)	QSLGALPLYQR	14 kDa protein, complex III	gi 115471095 (rice)
8 (b)	GFVMEFAENLILR	11 kDa subunit of complex I (At1g67350)	gi 115454659 (rice)
10 (b)	AVVYAIAPFQQK	8.2 kDa protein, complex III	gi 115466706 (rice)

^a The spot numbers correspond to the numbers given on Fig. 1.

^b Peptides were identified by ESI-MS/MS as outlined in the Material and methods section.

^c Proteins were identified by MASCOT (<http://www.matrixscience.com/>) using the NCBI protein database.

^d NCBI protein accession codes of the most similar annotated proteins.

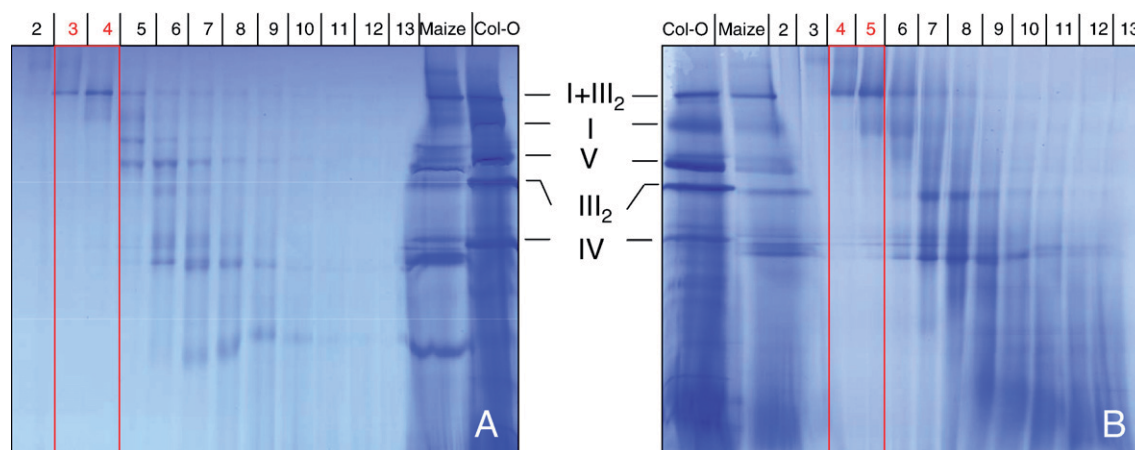


Fig. 2. Documentation of the purification of complex I and the I+III₂ supercomplex from maize by 1D Blue-native PAGE. Mitochondrial fractions from green (A) and etiolated (B) maize seedlings were solubilized using 5% digitonin and protein complexes were separated by sucrose gradient ultracentrifugation as outlined in the Materials and methods section. Gradients were fractionated into 13 fractions from bottom to top and resolved by Blue-native PAGE. As a control, digitonin solubilized total mitochondrial proteins from maize and *Arabidopsis* (Col-O) were directly resolved on the 1D Blue-native gels. Identities of the resolved protein complexes are given between the gels. Fractions 3 and 4 for the green seedlings and fractions 4 and 5 for the etiolated seedlings were used for EM analyses (Figs. 3 and 4).

identical particles which differ in their handedness caused by a different orientation on the carbon support film. There are small numbers of particles which have a shorter peripheral arm caused by the absence of the NADH-oxidizing domain (classes G, I). About 600 projections could be assigned to a top view of complex I (Fig. 3C). In this view the membrane arm is bent, as previously reported for *Arabidopsis* and *Polytomella* complex I [12,15]. The density at the left of the bend membrane arm of complex I probably represents the projected subunits of the peripheral arm. The panels J and K of Fig. 3 demonstrate identical structures of complex I from green and etiolated maize, respectively. This is in line with the identical subunit compositions obtained for complex I of etiolated and green maize seedlings upon analysis by 2D Blue-native PAGE. The best projection map of the I+III₂ supercomplex (Fig. 3A) has a resolution of 12 Å, the best one of complex I (Fig. 3D) has a resolution of 11 Å, both with the 2σ criterion [29].

Careful analyses of the classification results revealed the presence of two types of complex I particles in maize, which were designated type I and type II. The length of the membrane arm of the type I (Fig. 3D) is about 230 Å (including detergent), which is similar to the one of complex I from *Arabidopsis* [12], while the membrane arm of type II (Fig. 3E) has a length of 215 Å. Furthermore, the membrane arm of the type II complex I exhibits some extra density on its intermembrane-space exposed side (Fig. 3, marked by a white arrow). Another micro-variation concerns the angle between the hydrophobic membrane arm and the hydrophilic peripheral arm, which in most particles is 115° but in a small subset of particles is 125° (Fig. 3F). This variation only was observed for type I complex I. It is not clear if this is a matter of a different orientation of complex I on the carbon support film, intrinsic flexibility or a real structural difference.

The presence of two different structural classes of complex I from maize prompted us to re-analyze the complex I structure of *Arabidopsis*. Complex I was isolated from non-green suspension

cell cultures as described before [12] but additionally from green *Arabidopsis* plants. Structural analysis of 10,000 projections from the cell culture and 13,500 from green plants did not reveal significant differences in complex I structures (not shown). Therefore, the two data sets were combined to calculate an average projection of most optimal resolution (Fig. 3L). The structure of complex I from *Arabidopsis* very much resembles the type I structure of complex I from maize (Fig. 3D).

Maize complex I comprises the plant-specific carbonic anhydrase domain which previously was reported for *Arabidopsis* [12] and *Polytomella* [15]. This spherical extra-domain has a diameter of about 60 Å (marked by white arrowheads in Fig. 3). Furthermore, in comparison to other organisms, a small intermembrane-space-exposed protrusion of unknown function is attached to the membrane arm of complex I from *Arabidopsis*, *Polytomella* and maize (marked by black arrows in Fig. 3).

We were able to reach a resolution of 11 Å for a complex I projection map from maize. This allows us to compare it with the X-ray structure of trimeric carbonic anhydrase from *Methanosarcina thermophila* [30], the only known X-ray structure of a γ-type carbonic anhydrase (Fig. 4A, B). The truncated X-ray structure has a rather similar overall shape and a size of approximately 60 Å, and nicely fits to the matrix-exposed extra-domain of the side view projection of maize complex I (Fig. 4A). The fit appears to give a good match between the truncated carbonic anhydrase model and the EM data. For instance, a prominent groove running from the upper left to the middle right position in the truncated carbonic anhydrase model is also visible in the EM projection maps as a negative stain-filled region in the same position (Fig. 4A). We also tried to assign the position of the carbonic anhydrase on the top view of the I+III₂ supercomplex by comparison with the side view and the most likely position is presented in Fig. 4B.

In order to assign the positions of complex I and complex III₂ within the I+III₂ supercomplex we used the X-ray structures of cytochrome *c* reductase from beef [31], the peripheral arm of complex I from *Thermus thermophilus* [7] and a low-resolution

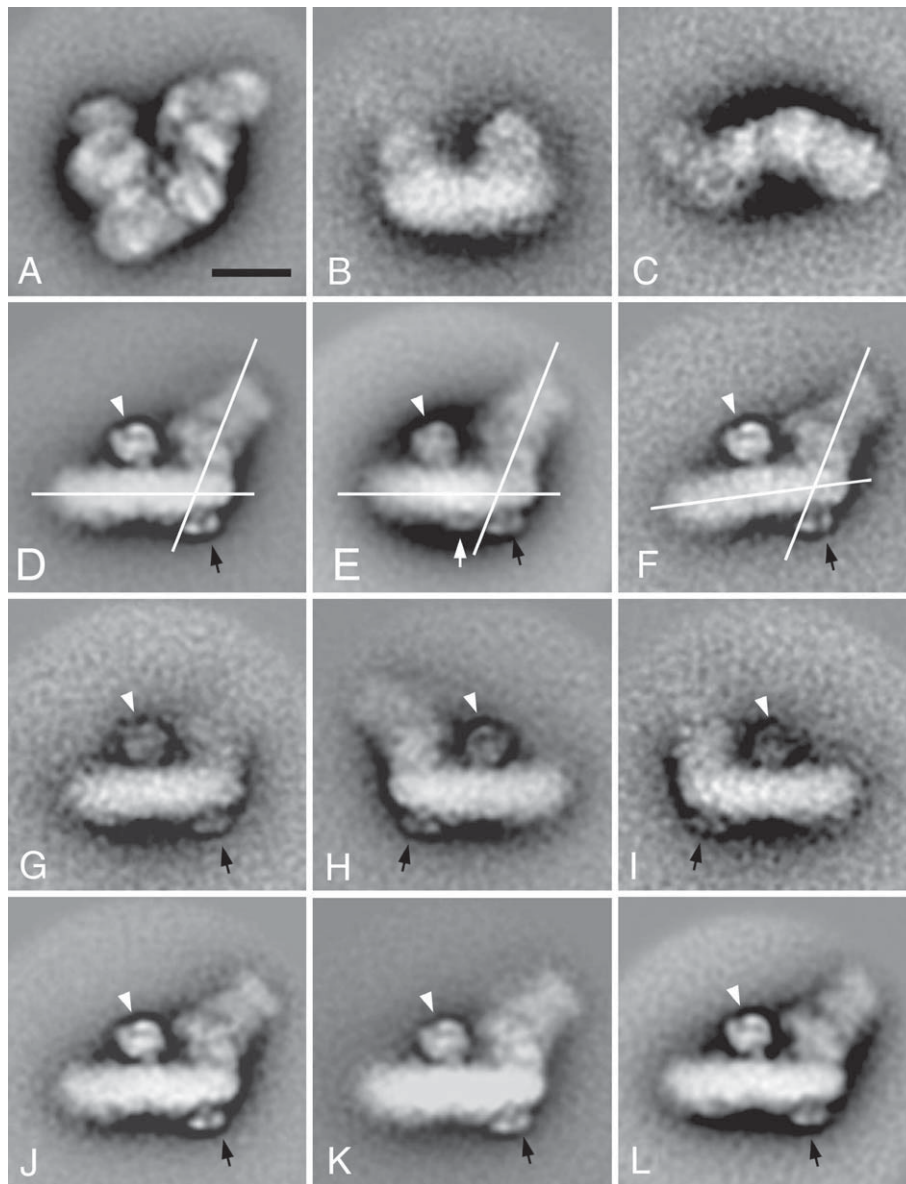


Fig. 3. Gallery of complex I and I+III₂ supercomplex projection maps from *Zea mays*. A: Average of 1024 projections of the I+III₂ supercomplex (top-view). B: Average of 32 projections of the I+III₂ supercomplex (side view). C: Average of 512 projections representing a top-view of complex I. D–K: average side view projection maps of complex I in different orientations. D: average of 4096 projections of the most prominent form of side view particles (type I), E: average of 1024 projections of a minor form of complex I (type II), F: average of 512 projections of another minor form of complex I with an altered angle between the membrane and the peripheral arm (type I), G: average of 512 projections of complex I particles lacking the NADH-oxidizing domain, H: average of 1024 projections of type I complex I in an orientation opposite to the one shown in D, I: average of 512 projections of complex I particles lacking the NADH-oxidizing domain in an orientation opposite to the one shown in G, J: type I complex I particles from green maize plants (average of 1024 projections), K: type I complex I particles from etiolated maize plants (average of 1024 projections). L: Average of 4096 projections of complex I from *Arabidopsis thaliana*. The white arrowhead marks the carbonic anhydrase domain of complex I and the black arrow another plant-specific domain localized on the intermembrane-space exposed side of the membrane arm of complex I. The white arrow indicates an extra density on the intermembrane-space exposed side of type II complex I particles.

3D EM model of *Yarrowia lipolytica* [6] to do a manual fitting in the *Zea mays* EM projections (Fig. 4). For each of the components there is only one possible way to obtain a good fit, which means that the components match the EM maps within the positions indicated, although small rotational displacements (up to 10°) would still be possible. The fittings indicate that the top-view map of the supercomplex cannot be precisely parallel to the membrane plane because the projected structure of complex III₂ does not show the expected two-fold rotational sym-

metry, as it would do without any tilt away from the membrane view (Fig. 4C). As a consequence, formation of this supercomplex possibly causes a slight bend of the inner membrane which previously was reported for the dimeric ATP synthase supercomplex of yeast and *Polytomella* [32]. However, the side view of the I+III₂ supercomplex (Fig. 4D) rather indicates a parallel position of the long axes of the peripheral complex I arm and complex III₂ with respect to the inner membrane. Therefore, the precise orientation of complexes I and III₂ within

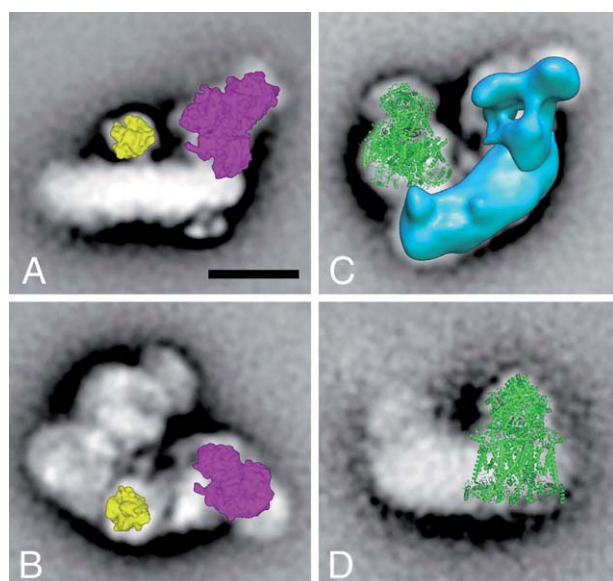


Fig. 4. Fitting of 3D structures of complex I, complex III₂, and trimeric γ -carbonic anhydrase from various sources to the single particle structures of the maize I+III₂ supercomplex and maize complex I. Fittings were carried out using truncated versions at 10 Å of the atomic structures of trimeric γ -carbonic anhydrase from *Methanosarcina thermophila* [28], the peripheral arm of complex I from *Thermus thermophilus* [7], the 3D EM structure of complex I from *Yarrowia lipolytica* (blue) [6] and the X-ray structure of complex III₂ from beef [29]. (A) Assignment of trimeric carbonic anhydrase (yellow) and the peripheral arm of complex I (purple) on maize complex I in side view position. (B) Assignment of the same structures on a top-view of the maize I+III₂ supercomplex. (C) Assignment of the complex I (blue) and complex III₂ (green) structures on the maize I+III₂ supercomplex in top-view position. (D) Assignment of the same structures on a side view of the maize I+III₂ supercomplex. The bar equals 100 Å.

the I+III₂ supercomplex currently still has to be taken with caution.

4. Discussion

The investigation of complex I and the I+III₂ supercomplex of maize by electron microscopy and single particle averaging gives several new insights into the architecture of these multi-protein particles. The overall L-shape of maize complex I is in agreement with previous studies on other species [1,2,7]. It strongly resembles complex I from *Arabidopsis* [12] and *Polytomella* [15]. In comparison to complex I from non-photosynthetic organisms there are two extra-domains on the membrane arm of complex I: a small intermembrane-space-exposed domain (Fig. 3, black arrows) and a larger matrix-exposed carbonic anhydrase domain (Fig. 3, white arrowheads). Careful analyses of average structures of various complex I subclasses in maize revealed the occurrence of two distinct micro-heterogeneities: (i) the length of the membrane arm was found to be 230 Å (“type I”) or 215 Å (“type II”). Type II complex I at the same time exhibits an additional protrusion on the intermembrane-space side of the membrane arm opposite to the carbonic anhydrase domain (Fig. 3, white arrow); (ii) the angle between the membrane and the peripheral arm of type I complex I was either 115 or 125° (for type II complex I it always was 115°).

4.1. The maize complex I

Micro-heterogeneities of complex I particles were not reported before for plant mitochondria. In general, due to the roughness of the carbon support film on which protein molecules are absorbed during sample preparation for EM analyses, slight variations in tilting out of a stable position can happen, which might artificially lead to different projection maps. However, for reasons stated below, we rather believe that the observed structural differences are biologically significant. Three different complex I side views were observed for *Zea mays* (Fig. 3D, E, F) but only one single side view was found in *Arabidopsis* (Fig. 3L). In our interpretation the differences between the projection maps of type I (Fig. 3D) and type II complex I (Fig. 3E) point to structural differences at the tip of the membrane arm of maize complex I. The discrepancy in length cannot be sufficiently explained by tilting since the features of the hydrophilic arm and the matrix-exposed domain did not change. Notably, the length of the membrane arm in the complex I projection with the different type of handedness (Fig. 3H) is the same as in Fig. 3D and longer than the one on the type II particle of Fig. 3E. A second argument for structural variation at the tip of the *Zea mays* complex I is the fact that in *Arabidopsis* only one type of side view projection was found indicating the absence of complexes resembling *Zea mays* type II particles. Nevertheless, for the smallest differences between classes, such as the extra-domain opposite to the carbonic anhydrase domain in type II particles (white arrow, Fig. 3E), different positions on the support film cannot be excluded. To establish if this extra-domain observed in Fig. 3E is absent in the type I particles 3D information would be needed. The variation in tilt parallel to the long axis of complex I, which is probably more likely than in tilt vertical to the long axis, could be responsible as well. Such tilting could also cause the observed differences concerning the angle between the membrane and the peripheral arm of type I complex I (Fig. 3D, F). If relevant under *in vivo* conditions, the variation of the angle between the two complex I arms might reflect different complex I confirmations proposed to be important for the coupling of the electron transport and proton translocation activities of complex I [6,33].

The occurrence of complex I particles with a shorter membrane arm was observed before in NDH-1, the distantly related cyanobacterial counterpart of complex I [34]. The tip of the NDH-1 membrane arm is occupied by NdhD and NdhF subunits (the counterparts of the *Arabidopsis* mitochondrial subunits NAD4 and NAD5). There are multiple copies of the *ndhD* and *ndhF* genes, and the tip can have different compositions depending on the presence of high- and low-affinity CO₂ uptake systems [35]. In two defined particles, named NDH-1I and NDH-1M, a substantially shortened membrane arm was observed [34], probably due to the absence of NdhD and/or NdhF. The subunit composition of the plant complex I membrane arm tip is, however, not yet established.

4.2. The I+III₂ supercomplex

Recently, a low-resolution structure of I+III₂ supercomplex was solved for *Arabidopsis* [12]. At that time, no top-view

projection of complex I was available, which made the assignment of single complex I and dimeric complex III within the supercomplex less precise. After that, information of complex I in top-view position was obtained for *Polytomella* [15]. It showed that the membrane arm of complex I is not straight, but slightly bent. This bending of the complex I is also very obvious in the current I+III₂ supercomplex map from maize at 12 Å resolution (Figs. 3A, 4B) and in agreement with the recently published 8 Å projection map of complex I from *E. coli* [9]. Although some side views of complex I indicated the loss of the NADH-oxidizing unit (Fig. 3G, I), we did not observe any I+III₂ supercomplex fragments lacking this unit, as described before in *Arabidopsis* [12]. Together with the relatively high-resolution (12 Å) obtained with air-dried negatively stained specimens this indicates that the maize I+III₂ supercomplex is more stable than the one of *Arabidopsis*. The higher resolution allowed us to better assign the position of the dimeric complex III within the supercomplex by fitting of the X-ray structure (Fig. 4C, D). The complex I moiety has a good fit with the low-resolution 3D model of *Yarrowia lipolytica* [6]. The beef heart complex I particle is substantially shorter [5], as noticed earlier [12], and likely different in subunit or domain composition. In comparison to the side views of the type I and II complex I particles it appears that the complex I moiety in the I+III₂ supercomplex is composed of type I particles in maize. This would mean that the type II particles are not involved in super-

complex formation and hence could have a different function. Finally, the fitting indicates that the peripheral arm of plant complex I, which has an unknown subunit composition, has a total size and shape close to the 8-subunit *Thermus thermophilus* peripheral arm (Fig. 4A, B), despite the fact that maize and prokaryotic species are only distantly related. There is, however, a lower match at two sites. The side view map indicates that the part next to the membrane interface is positioned more to the right (Fig. 4A) and the projection map in the membrane plane indicates that the upper tip of the hydrophilic domain is wider, which could indicate additional plant subunits or domains at this position (Fig. 4B).

4.3. The carbonic anhydrase extra-domain of complex I in plants

The most characteristic feature of complex I from the C₃ plant *Arabidopsis* is the large matrix-exposed extra-domain assigned to γ -carbonic anhydrase subunits [15]. This domain also is present in the C₄ plant maize. The high-resolution of the maize complex I structure obtained by single particle averaging allowed us to compare the carbonic anhydrase domain to the X-ray structure of the prototype γ -carbonic anhydrase of the archaeobacterium *Methanosarcina thermophila* [30]. Gamma-carbonic anhydrase from *M. thermophila* is homotrimeric and has a diameter of about 60 Å. The truncated X-ray structure nicely fits to the matrix-exposed extra-domain on the membrane arm of complex I

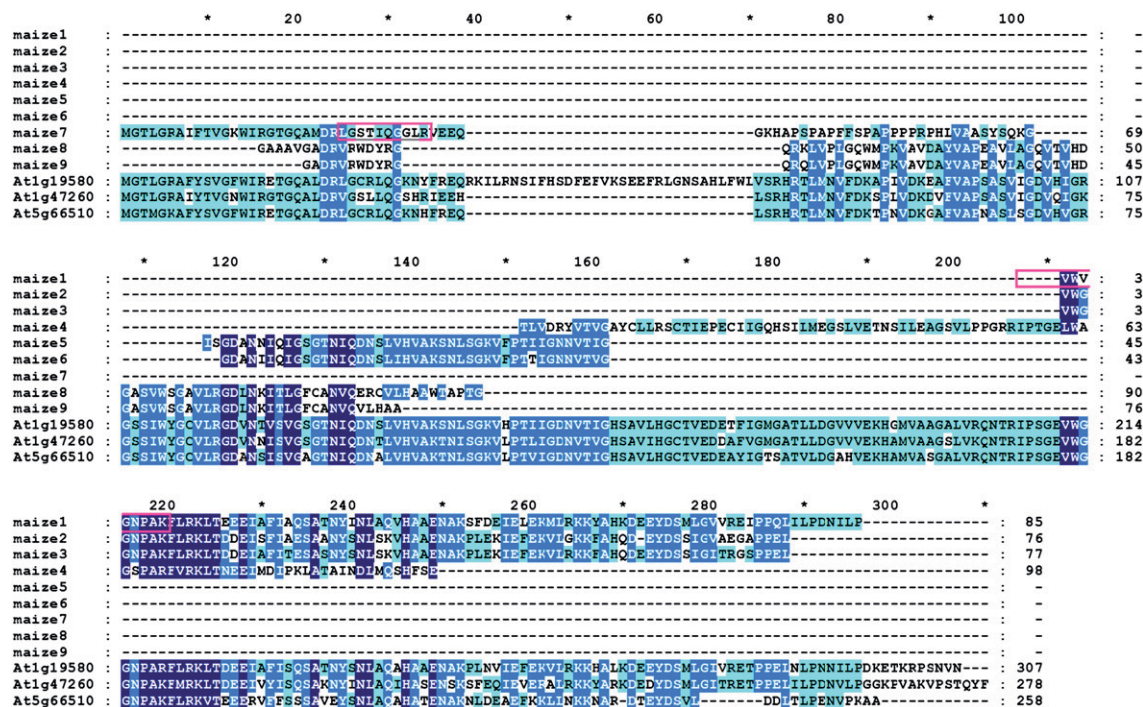


Fig. 5. Alignment of the amino acid sequences of complex I integrated carbonic anhydrases from *Arabidopsis* with putative homologues of maize. The *Arabidopsis* sequences are named according to the locus names of the *Arabidopsis thaliana* genome sequencing project at TAIR (<http://www.arabidopsis.org/>). Sequence At1g47260 was used as a probe to search the TIGR maize database (<http://maize.tigr.org/>) using the tblastn algorithm. Clones encoding nine different putative complex I integrated carbonic anhydrase subunits were identified and named “maize1” (accession: AZM4_24880), “maize2” (AZM4_51631), “maize3” (AZM4_43966), maize4 (AZM4_41212), “maize5” (AZM4_64344), “maize6” (AZM4_51632), “maize7” (AZM4_44439), “maize8” (AZM4_84283) and “maize9” (OGUBD07TV). The alignment of the sequences was carried out using clustalW at EBI (<http://www.ebi.ac.uk/clustalw/>) using standard parameters. Amino acids conserved in at least 7 sequences are underlined in dark-blue, amino acids conserved in at least 6 sequences are underlined in middle-blue and amino acids conserved in at least 3 sequences are underlined in light-blue. The two peptide sequences identified by mass spectrometry (protein 3 in Table 1) are indicated by red boxes.

from maize (Fig. 4A). This indicates that the complex I integrated γ -carbonic anhydrase domain of *Zea mays* also is a trimer. In *Arabidopsis*, five different carbonic anhydrase subunits form part of complex I. It currently is not known whether the carbonic anhydrase domains of complex I includes three copies of the same isoform or different isoforms. Probing the maize genome sequence database (<http://maize.tigr.org/>) with the sequence of one of the carbonic anhydrases of *Arabidopsis* allowed to identify partial sequences of nine different putative γ -carbonic anhydrases. Since the maize genome sequence has not been completed, further homologues might exist. The two peptide sequences obtained by MS analyses of the 30 kDa subunit of maize complex I (Fig. 1, Table 1) are identical to amino acid stretches of two of the maize carbonic anhydrase isoforms (Fig. 5). Therefore, at least two forms of γ -carbonic anhydrases occur within the maize complex I. We conclude that the carbonic anhydrase domain of plant complex I most likely is heterotrimeric.

The carbonic anhydrase domain seems to be a general feature of plant complex I, since it was now described for the C_3 plant *Arabidopsis*, the C_4 plant maize and the green alga *Polytomella* [[12,15], this study]. It was proposed that the complex I integrated carbonic anhydrases might play a role in the context of a carbon transport system between mitochondria and chloroplasts to increase the efficiency of photosynthetic carbon fixation. According to this hypothesis, mitochondrial catabolism represents an important source of CO_2 for photosynthesis. The hypothesis is supported by a recent study investigating the CO_2 uptake/ CO_2 fixation ratio in isolated protoplasts versus isolated chloroplasts [36]. The ratio was considerably lower in protoplasts, which was interpreted to be caused by CO_2 supply by mitochondria in protoplasts. The presence of carbonic anhydrases seems to be of equal importance in mitochondria of C_3 and C_4 plants but possibly for different reasons. In C_3 plants, CO_2 transport from mitochondria to plastids might be especially important during photorespiration, whereas in C_4 plants this transport should be most important in the context of the CO_2 liberation step in the bundle sheath cells. The CO_2 liberation step is known to be based on different enzymatic reactions, which take place in different cellular compartments [37]. In maize, the conversion of malate into pyruvate and CO_2 takes place in plastids by a $NADP^+$ dependant malic enzyme. In other plants, this step occurs in mitochondria by the act of a NAD^+ dependant malic enzyme. Alternatively, CO_2 liberation is carried out by a PEP carboxykinase localized in the cytosol of bundle sheath cells. However, the metabolism of C_4 subtypes seems not to be exclusively based on one or the other CO_2 liberation reaction, but rather on all of them to varying extends [38]. Possibly the complex I integrated carbonic anhydrases are especially important in C_4 plants with dominating NAD^+ malic enzyme dependant CO_2 liberation. Further investigations will be necessary to clarify the precise physiological role of the mitochondrial carbonic anhydrases in C_3 and C_4 plants.

Acknowledgements

We thank Dr. Roman Kouřil and Dr. Wilko Keegstra for their help with the processing and modelling of supercomplex

structures and Dr. Gert Oostergetel for invaluable help with electron microscopy. We also like to thank Dr. M. Radermacher for providing *Yarrowia lipolytica* complex I images. Dagmar Lewejohann is thanked for expert technical assistance. Research of our laboratories is supported by the Deutsche Forschungsgemeinschaft (grant Br 1829-7/3).

References

- [1] T. Yagi, A. Matsuno-Yagi, The proton-translocating NADH-quinone oxidoreductase in the respiratory chain: the secret unlocked, *Biochemistry* 42 (2003) 2266–2274.
- [2] T. Friedrich, B. Böttcher, The gross structure of the respiratory complex I: a lego system, *Biochim. Biophys. Acta* 1608 (2004) 1–9.
- [3] U. Brandt, Energy converting NADH: quinone oxidoreductase (complex I), *Ann. Rev. Biochem.* 75 (2006) 69–92.
- [4] V. Guenebaut, R. Vincentelli, D. Mills, H. Weiss, K.R. Leonard, Three-dimensional structure of NADH-dehydrogenase from *Neurospora crassa* by electron microscopy and conical tilt reconstruction, *J. Mol. Biol.* 265 (1997) 409–418.
- [5] N. Grigorieff, Three-dimensional structure of bovine NADH: ubiquinone oxidoreductase (complex I) at 22 Å in ice, *J. Mol. Biol.* 277 (1998) 1033–1046.
- [6] M. Radermacher, T. Ruiz, T. Clason, S. Benjamin, U. Brandt, V. Zickermann, The three-dimensional structure of complex I from *Yarrowia lipolytica*: a highly dynamic enzyme, *J. Struct. Biol.* 154 (2006) 269–279.
- [7] L.A. Sazanov, P. Hinchliffe, Structure of the hydrophilic domain of respiratory complex I from *Thermus thermophilus*, *Science* 311 (2006) 1430–1436.
- [8] U. Brandt, Proton-translocation by membrane-bound NADH: ubiquinone-oxidoreductase (complex I) through redox-gated ligand conduction, *Biochim. Biophys. Acta* 1318 (1997) 79–91.
- [9] E.A. Baranova, P.J. Holt, L.A. Sazanov, Projection structure of the membrane domain of *Escherichia coli* respiratory complex I at 8 Å resolution, *J. Mol. Biol.* 366 (2007) 140–154.
- [10] H. Schägger, K. Pfeiffer, Supercomplexes in the respiratory chains of yeast and mammalian mitochondria, *EMBO J.* 19 (2000) 1777–1783.
- [11] H. Eubel, L. Jänsch, H.-P. Braun, New insights into the respiratory chain of plant mitochondria supercomplexes and a unique composition of complex II, *Plant Physiol.* 133 (2003) 274–286.
- [12] N.V. Dudkina, H. Eubel, W. Keegstra, E.J. Boekema, H.-P. Braun, Structure of a mitochondrial supercomplex formed by respiratory-chain complexes I and III, *Proc. Natl. Acad. Sci. U.S.A.* 102 (2005) 3225–3229.
- [13] J.L. Heazlewood, K.A. Howell, A.H. Millar, Mitochondrial complex I from *Arabidopsis* and rice: orthologs of mammalian and yeast components coupled to plant-specific subunits, *Biochim. Biophys. Acta* 1604 (2003) 159–169.
- [14] P. Cardol, F. Vanrobaeys, B. Devreese, J. Van Beeumen, R. Matagne, C. Remacle, Higher plant-like subunit composition of mitochondrial complex I from: 31 conserved components among eukaryotes, *Biochim. Biophys. Acta* 1658 (2004) 212–224.
- [15] S. Sunderhaus, N.V. Dudkina, L. Jänsch, J. Klodmann, J. Heinemeyer, M. Perales, E. Zabaleta, E.J. Boekema, H.-P. Braun, Carbonic anhydrase subunits form a matrix-exposed domain attached to the membrane arm of mitochondrial complex I in plants, *J. Biol. Chem.* 281 (2006) 6482–6488.
- [16] L. Jänsch, V. Kruff, U.K. Schmitz, H.-P. Braun, Cytochrome *c* reductase from potato does not comprise three core proteins but contains an additional low molecular weight subunit, *Eur. J. Biochem.* 228 (1995) 878–885.
- [17] M.J. Runswick, I.M. Fearnley, J.M. Skehel, J.E. Walker, Presence of an acyl carrier protein in NADH:ubiquinone oxidoreductase from bovine heart mitochondria, *FEBS Lett.* 286 (1991) 121–124.
- [18] U. Sackmann, R. Zensen, D. Röhlen, U. Jahnke, H. Weiss, The acyl-carrier protein in *Neurospora crassa* mitochondria is a subunit of NADH: ubiquinone reductase (complex I), *Eur. J. Biochem.* 200 (1991) 463–469.
- [19] E.H. Meyer, J.L. Heazlewood, A.H. Millar, Mitochondrial acyl carrier proteins in *Arabidopsis thaliana* are predominantly soluble matrix proteins and none can be confirmed as subunits of respiratory Complex I, *Plant. Mol. Biol.* 64 (2007) 319–327.

- [20] A.H. Millar, V. Mittova, G. Kiddle, J.L. Heazlewood, C.G. Bartoli, F.L. Theodoulou, C.H. Foyer, Control of ascorbate synthesis by respiration and its implications for stress responses, *Plant Physiol.* 133 (2003) 443–447.
- [21] G. Parisi, M. Perales, M. Fornasari, A. Colaneri, N. Schain, D. Casati, S. Zimmermann, A. Brennicke, A. Araya, J. Ferry, J. Echave, E. Zabaleta, Gamma carbonic anhydrases in plant mitochondria, *Plant Mol. Biol.* 55 (2004) 193–207.
- [22] M. Perales, H. Eubel, J. Heinemeyer, A. Colaneri, E. Zabaleta, H.-P. Braun, Disruption of a nuclear gene encoding a mitochondrial gamma carbonic anhydrase reduces complex I and supercomplex I+III₂ levels and alters mitochondrial physiology in *Arabidopsis*, *J. Mol. Biol.* 350 (2005) 263–277.
- [23] H.-P. Braun, E. Zabaleta, Carbonic anhydrase subunits of the mitochondrial NADH dehydrogenase complex (complex I) in plants, *Physiol. Plant.* 129 (2007) 114–122.
- [24] G.D. Price, M.R. Badger, F.J. Woodger, B.M. Long, Advances in understanding the cyanobacterial CO₂-concentrating-mechanism (CCM): functional components, Ci transporters, diversity, genetic regulation and prospects for engineering into plants, *J. Exp. Bot.* (in press).
- [25] H.-P. Braun, M. Emmermann, V. Kruft, U.K. Schmitz, Cytochrome *c*₁ from potato: a protein with a presequence for targeting to the mitochondrial intermembrane space, *Mol. Gen. Genet.* 231 (1992) 217–225.
- [26] N. Hausmann, W. Werhahn, B. Huchzermeyer, H.-P. Braun, J. Papenbrock, How to document the purity of mitochondria prepared from green tissue of tobacco, pea and *Arabidopsis thaliana*, *Phyton* 43 (2003) 215–229.
- [27] J. Heinemeyer, D. Lewejohann, H.-P. Braun, Blue-native gel electrophoresis for the characterization of protein complexes in plants, *Meth. Mol. Biol.* 335 (2007) 343–352.
- [28] V. Neuhoff, R. Stamm, I. Pardowitz, N. Arold, W. Ehrhardt, D. Taube, Essential problems in quantification of proteins following colloidal staining with Coomassie Brilliant Blue dyes in polyacrylamide gels, and their solution, *Electrophoresis* 11 (1990) 101–117.
- [29] M. van Heel, Similarity measures between images, *Ultramicroscopy* 21 (1987) 95–100.
- [30] T.M. Iverson, B.E. Alber, C. Kisker, J.G. Ferry, D.C. Rees, A closer look at the active site of gamma-class carbonic anhydrases: high-resolution crystallographic studies of the carbonic anhydrase from *Methanosarcina thermophila*, *Biochemistry* 39 (2000) 9222–9231.
- [31] S. Iwata, J.W. Lee, K. Okada, J.K. Lee, M. Iwata, B. Rasmussen, T.A. Link, S. Ramaswamy, B.K. Jap, Complete structure of the 11-subunit bovine mitochondrial cytochrome *b_c1* complex, *Science* 281 (1998) 64–71.
- [32] N.V. Dudkina, S. Sunderhaus, H.-P. Braun, E.J. Boekema, Characterization of dimeric ATP synthase and cristae membrane ultrastructure from *Saccharomyces* and *Polytomella* mitochondria, *FEBS Lett.* 580 (2006) 3427–3432.
- [33] B. Böttcher, D. Scheide, M. Hesterberg, L. Nagel-Steger, T. Friedrich, A novel, enzymatically active conformation of the *Escherichia coli* NADH: ubiquinone oxidoreductase (complex I), *J. Biol. Chem.* 277 (2002) 17970–17977.
- [34] A.A. Arteni, P. Zhang, N. Battchikova, T. Ogawa, E.-M. Aro, E.J. Boekema, Structural characterization of NDH-1 complexes of *Thermosynechococcus elongatus* by single particle electron microscopy, *Biochim. Biophys. Acta* 1757 (2006) 1469–1475.
- [35] T. Ogawa, H. Mi, Cyanobacterial NADPH dehydrogenase complexes, *Photosynth. Res.* 93 (1–3) (2007) 69–77.
- [36] K. Riazunnisa, L. Padmavathi, H. Bauwe, A.S. Raghavendra, Markedly low requirement of added CO₂ for photosynthesis by mesophyll protoplasts of pea (*Pisum sativum*): possible roles of photorespiratory CO₂ and carbonic anhydrase, *Physiol. Plant.* 128 (2006) 763–772.
- [37] S.v. Caemmerer, R.T. Furbank, The C₄ pathway: an efficient CO₂ pump, *Photosynthesis Research* 77 (2003) 191–207.
- [38] G.E. Edwards, R.T. Furbank, M.D. Hatch, C.B. Osmond, What does it take to be C₄? Lessons from the evolution of C₄ photosynthesis, *Plant Physiol.* 125 (2001) 46–49.



Contents lists available at ScienceDirect

Biochimica et Biophysica Acta

journal homepage: www.elsevier.com/locate/bbabio

Review

Structure and function of mitochondrial supercomplexes

Natalya V. Dudkina^a, Roman Kouřil^a, Katrin Peters^b, Hans-Peter Braun^b, Egbert J. Boekema^{a,*}^a Electron microscopy group, Groningen Biomolecular Sciences and Biotechnology Institute, University of Groningen, Nijenborgh 4, 9747 AG Groningen, The Netherlands^b Institute for Plant Genetics, Faculty of Natural Sciences, Universität Hannover, Herrenhäuser Str. 2, D-30419 Hannover, Germany

ARTICLE INFO

Article history:

Received 27 October 2009

Received in revised form 14 December 2009

Accepted 16 December 2009

Available online 28 December 2009

Keywords:

Oxidative phosphorylation

Mitochondria

Respirasome

ATP synthase

Electron microscopy

Supercomplex

ABSTRACT

The five complexes (complexes I–V) of the oxidative phosphorylation (OXPHOS) system of mitochondria can be extracted in the form of active supercomplexes. Single-particle electron microscopy has provided 2D and 3D data describing the interaction between complexes I and III, among I, III and IV and in a dimeric form of complex V, between two ATP synthase monomers. The stable interactions are called supercomplexes which also form higher-ordered oligomers. Cryo-electron tomography provides new insights on how these supercomplexes are arranged within intact mitochondria. The structure and function of OXPHOS supercomplexes are discussed.

© 2009 Elsevier B.V. All rights reserved.

1. Introduction

Mitochondria are intracellular organelles which accommodate in their inner or cristae membrane large numbers of five oxidative phosphorylation complexes (complexes I–V). The complexes I to IV are oxidoreductases which, with the exception of complex II, couple electron transport with translocation of protons across the inner mitochondrial membrane (Fig. 1). The generated proton motive force is used by ATP synthase (complex V) for ATP synthesis from ADP and phosphate. Complex I or NADH dehydrogenase is the first and major entrance point of electrons to the respiratory chain. It transfers electrons from NADH molecules to a lipophilic quinone designated ubiquinone. Complex II or succinate dehydrogenase transmits electrons from succinate to ubiquinone and directly connects the citric acid cycle to the respiratory chain. From the reduced ubiquinone electrons can be transferred to complex III or cytochrome *c* reductase which exists in the membrane as a functional dimer. The small protein cytochrome *c* mediates electron transfer from cytochrome *c* reductase to cytochrome *c* oxidase (complex IV). Finally, electrons are transferred to molecular oxygen which is reduced to water.

The ideas about the overall organization of these five complexes, which together form the oxidative phosphorylation (OXPHOS) system, have been changing with time. A so-called “fluid-state model” is supported by the finding that all individual protein complexes of the OXPHOS system can be purified to homogeneity in an enzymatically active form and by lipid dilution experiments

(reviewed in [1,2]). It postulates that the respiratory chain complexes freely diffuse in membrane and that the electron transfer is based on random collisions of the single complexes.

The fluid-state model is challenged by a “solid-state model” which proposes stable interactions between the OXPHOS complexes within entities named supercomplexes. This model is now supported by a wide range of experimental findings: 1. Supercomplexes can be resolved by blue native polyacrylamide gel electrophoresis (BN-PAGE) [3,4]. 2. Supercomplexes are active as shown by in-gel activity measurements within blue native gels [3,5]. 3. Electron microscopy (EM) structures revealed defined interactions of OXPHOS complexes within the isolated respiratory supercomplexes [6–10]. 4. Flux control experiments [11,12] confirm that the respiratory chain operates as one functional unit. 5. Point mutations in genes encoding one of the subunits of one OXPHOS complex affect the stability of another complex. Thus, complex III is required to maintain complex I in mouse and human cultured cells mitochondria [13]. Complex IV is necessary for the assembly or stability of complex I in mouse fibroblasts [14]. 6. Oxygen uptake by isolated mitochondria of potato correlates with the abundance of supercomplexes [5]. 7. Some supercomplexes need cardiolipin for their formation [15,16]. Until some years ago, the fluid-state model was widely accepted in the field of bioenergetics. The newest edition of the Lehninger textbook is the first general textbook that presents a section on OXPHOS supercomplexes [17].

In many organisms the complexes I, III and IV were found to associate into specific supercomplexes (reviewed in [18]). Only complex II seems not to form part of any respiratory chain supercomplexes. The possible explanation for the singular state of complex II is that it is also involved in the citric acid cycle. However, a recent publication on the OXPHOS system of mouse mitochondria also

* Corresponding author.

E-mail address: e.j.boekema@rug.nl (E.J. Boekema).

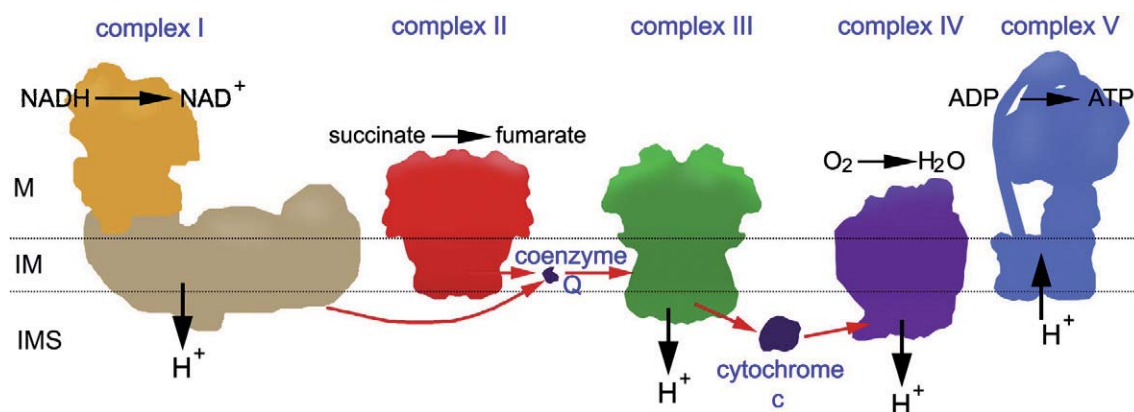


Fig. 1. A schematic representation of the OXPHOS system showing its individual components but ignoring their structural interactions. Note that complex I is depicted here almost as large as complex V. Actually, mammalian complex I is protruding as far as complex V from the membrane, but plant mitochondrial complex I is a bit smaller in size. Complex III is a functional dimer, in contrast to complex IV, although a high-resolution dimeric structure of the latter has been solved by X-ray crystallography. A full picture needs the input of the yet unsolved high-resolution structure of complex I. The position of the matrix (M), the intermembrane space (IMS) and cristae or inner membrane (IM) has been indicated.

reported detection of complex II containing supercomplexes by BN-PAGE [19]. The $I + III_2 + IV_{1-2}$ supercomplex is called respirasome because it can autonomously carry out respiration in the presence of ubiquinone and cytochrome *c*. Respiratory supercomplexes are believed to co-exist in the membrane with single OXPHOS complexes. In this review we discuss the structure and function of the various types of supercomplexes within the mitochondrial membrane. In a few cases it appears that supercomplexes further organize into larger structures called *strings*. The clearest example is the ATP synthase complex (complex V), which assembles into long oligomeric chains [20–23].

2. Respiratory supercomplexes

High-resolution crystal structures are available for most OXPHOS complexes [24]. Only complex I, which by far is the largest complex of the respiratory chain, has not been crystallized up to now. It has a unique L-like shape which results from the orthogonal association of its two arms, the matrix-exposed “peripheral arm” and the so-called “membrane arm” [25,26]. However, the overall shape varies in different organisms as revealed by electron microscopy. For instance, plant complex I has a second matrix-exposed domain which is attached to the membrane arm at a central position and which includes carbonic anhydrases [27–29]. Furthermore, complex I of *Yarrowia lipolytica* has an unknown protrusion at the tip of the membrane arm of complex I [26] and complex I from beef has an additional density at the membrane arm tip on its matrix-exposed side [18]. The structure of the peripheral arm of complex I from the archaeobacterium *Thermus thermophilus* was recently resolved by X-ray crystallography. Positions of eight subunits and all redox centers of the enzyme were determined, including nine iron sulphur centers [30]. There is much less known about the membrane arm. The main known function of the hydrophobic part is proton translocation [31], but the precise functions of the membrane domain and the coupling mechanism are not yet solved because of lack of high-resolution structural data. However, the projection map at 8 Å resolution of complex I from *E. coli* obtained by electron microscopy [32] indicates the presence of about 60 transmembrane α -helices within one membrane domain. A binding site and access channel for quinone is predicted to be at the interface with the peripheral arm. The location of subunits Nuol and Nuom at substantial distance from the peripheral arm, which contains all the redox centers of the complex, indicates that conformational changes likely play a role in the mechanism of coupling between electron transfer and proton pumping.

Complex I can form a stable association with the complex III dimer of the respiratory chain [3,4]. An investigation by single-particle EM revealed the lateral association of dimeric complex III with the tip of the membrane part of complex I in *Arabidopsis* [6], *Zea mays* [28]; see Fig. 2E) and potato [29]. The top-view projection maps of this plant supercomplex all are similar, although in potato it appears that the angle between complex I and III is variable [32]. In the bovine $I + III_2$ supercomplex the association of the complexes I and III_2 is about the same (Fig. 2F), but particles in the top-view position are extremely rare, in contrast to the side views (Fig. 2B).

Complex III_2 can associate with one or up to four copies of complex IV as it was described for potato [33], spinach [34], *Asparagus* [35] and beef [3]. The first detailed structure of a mitochondrial supercomplex was obtained for the $III_2 + IV_{1-2}$ supercomplex of *Saccharomyces cerevisiae* [10]. It could be determined because of its high stability in yeast and for the reason that this organism lacks complex I, which can associate to complex III as well, as described above. The supercomplex appeared in different positions and this allowed generating a pseudo-atomic 3D model which shows that monomeric cytochrome *c* oxidase complexes are attached to dimeric complex III at two alternate sides with their convex sides facing the complex III_2 . This is the opposite to the side involved in the formation of complex IV dimers as described by X-ray crystallography. Association of the complexes III and IV depends on the presence of cardiolipin within the inner mitochondrial membrane [15,16]. In bovine mitochondria complex I (Fig. 2A) binds to complexes III_2 and IV [18]. These supercomplexes represent the largest form of OXPHOS units and are also termed “respirasomes” [3]. Complex III_2 attaches to the complex I at its membrane arm in a region from middle to tip (Fig. 2B) in a similar way like previously described for the $I + III_2$ supercomplex of *Arabidopsis* [6]. Bovine complex IV seems to be attached to the tip of complex I (Fig. 2C).

To get a closer look to the composition of the respirasome we produced 2D cryo-EM data on the isolated bovine $I + III_2 + IV$ supercomplex on carbon support films (Fig. 2I). In contrast to negative stain freezing in an amorphous ice layer preserves the protein in native water-like environment and does not introduce any artifacts which can occur during chemical fixation with salts of heavy metals followed by air-drying. Additionally, cryo-EM allows to see internal details of the object whereas the negative stain reflects only a contour. Remarkably, freezing of the bovine respirasome provoked slightly different orientation of the complex on the carbon support film. The newly obtained projection map at 24 Å resolution (Fig. 2I) resembles the 2D negatively stained projection map of $I + III_2$ supercomplex from *Arabidopsis* and *Zea mays* (Fig. 2E). A low resolution 3D model of complex I [26] together with the crystal structures available for complexes III and IV are useful to understand

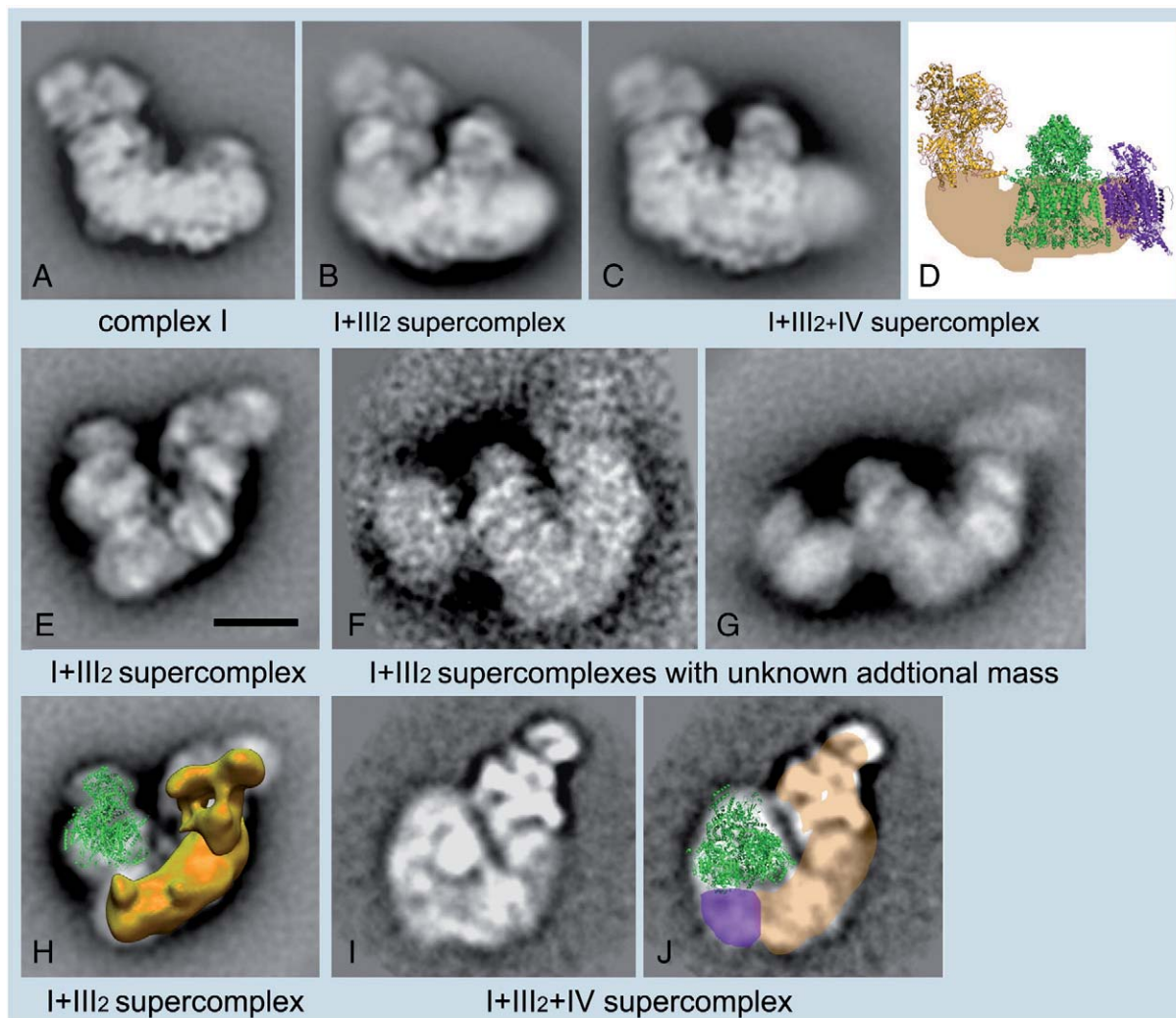


Fig. 2. Examples of EM projection maps of OXPHOS supercomplexes obtained by negative staining (A, B, C, E, F, G, H) and cryo-EM (I, J) plus modelling. (A–C) Averaged side views of bovine complex I and its supercomplexes. (D) Positions of individual complexes within the I + III₂ + IV supercomplex or respirasome from bovine mitochondria [18]. Yellow: X-ray structure of the hydrophilic domain of complex I from *Thermus thermophilus* [30], green: dimeric bovine cytochrome c reductase (complex III) [52], purple: bovine cytochrome c oxidase (complex IV) [53]. (E) Top-view of the I + III₂ supercomplex from maize [28]. (F, G) Top-views of I + III₂ supercomplexes with an unknown additional mass from bovine and potato mitochondria, respectively (N.V. Dudkina, R. Kouřil, J.B. Bultema, E.J. Boekema, unpublished data). (H) Assignment of the complexes I and III₂ within the top-view map of I + III₂ supercomplex from maize, as presented in image (E); the complex III dimer is in green in a tilted position; in yellow the 3D EM structure of complex I from *Yarrowia lipolytica* [26]. (I) Map of the bovine respirasome (N.V. Dudkina, unpublished data). (J) Modelling of the respirasome. In beige the position of the membrane arm of complex I, in green X-ray structure of the bovine dimeric complex III and in purple the position of a complex IV monomer. Scale bar, 10 nm.

the respirasome architecture. We can precisely assign the positions of complexes III₂ (Fig. 2J, in green) and I (Fig. 2J, in yellow) within the revealed structure and deduce the same overall association of complexes I and III₂ as in the plant supercomplex (Fig. 2H). The small additional density at the tip of complex I and next to the complex III₂ should represent a complex IV monomer. The rotational orientation of complex IV remains unclear and requires further investigation.

Both the 3D model of complex I [26] and the 2D cryo-EM projection map of the membrane arm of complex I [32] clearly show the curved shape of the membrane-embedded part of complex I. Our 2D projection data of *Arabidopsis*, potato, maize and bovine complex I show the same structural feature. Importantly, the curved feature of the membrane arm can be used as an indicator for a handedness determination of 3D models. Here we can apologize for a wrong handedness in Dudkina et al. [6], as at that time these data were not available. Because it now appears that there is no difference between the bovine and plant I + III₂ supercomplex, we conclude that complex III is always attached to complex I at its inner curved side. This is contradictory to the proposed 3D model at 32 Å resolution in

negative stain of the bovine respirasome [36], where complex III is attached at the outside part of the complex I. Evidently, the 3D density map was not correctly assigned. A closer look to their 3D model viewed from the inner membrane side (IMS) clearly shows the typical curvature of the membrane part of complex I, which was omitted in the assignment of the respirasome.

3. Higher organization levels of respiratory supercomplexes

It now appears that the supercomplex formation is not the highest level of OXPHOS organization. A row-like organization of OXPHOS complexes I, III and IV into respiratory strings has been proposed, based on biochemical evidence. It was suggested that respirasomes are interconnected with III₂ + IV₄ supercomplexes [37]. However, it appears that such transient strings cannot be purified after detergent solubilization which limits structural studies. Hence, the proposed respiratory string was approached by an extensive structural characterization of all its possible breakdown products, which are the various types of supercomplexes. About 400,000 molecular projections of supercomplexes from potato mitochondria were processed

by single-particle electron microscopy [29]. Two-dimensional projection maps of at least five different supercomplexes, including I + III₂, III₂ + IV₁, V₂, I + III₂ + IV₁ and I₂ + III₂ supercomplexes in different types of position, were obtained. From these maps the relative position of the individual complexes in the largest unit, the I₂ + III₂ + IV₂ supercomplex, could be determined in a coherent way. The maps also show that the I + III₂ + IV₁ supercomplex, or respirasome, differs from its counterpart in bovine mitochondria. The new structural features allow us to propose a consistent model of the respiratory string for bovine and potato mitochondria, composed of repeating I₂ + III₂ + IV₂ units (Fig. 3, [29]), which is in agreement with dimensions observed in former freeze-fracture electron microscopy data [23]. This model modifies and extends the hypothetical scheme presented in [37]. There is, however, some evidence for other types of interactions occurring at low frequencies. We found by classification of all breakdown products from cristae membranes big particles, composed of a I + III₂ supercomplex plus a large additional mass in bovine (Fig. 2F) and potato membranes (Fig. 2G), (N.V. Dudkina, R. Kouřil, J.B. Bultema, E.J. Boekema, unpublished data). The composition of the additional mass is unknown, but it appears to be larger than a single copy of complex IV, because these novel particles are larger than the respirasome (Fig. 2I, J).

Another example of a higher-level organization of supercomplexes, dealing with oligomeric ATP synthase, is discussed in the next section.

4. The dimeric ATP synthase supercomplex and its oligomeric organization

Mitochondrial F₁F₀ ATP synthase is a complex of 600 kDa formed by 15–18 subunits [38,39]. The matrix-exposed water soluble F₁ part is constituted of three α and three β subunits and connected to the membrane-embedded ring-like F₀ part via central and peripheral stalks. The F₀-part is composed of subunits a (Su 6), A6L (Su 8), e, f, g, the central stalk consists of the γ , δ and ϵ subunits and the peripheral stalk is made from subunits OSCP (Su 5), b, d, F6 (h) (different names of the yeast counterparts in brackets, reviewed in [40]). The yeast

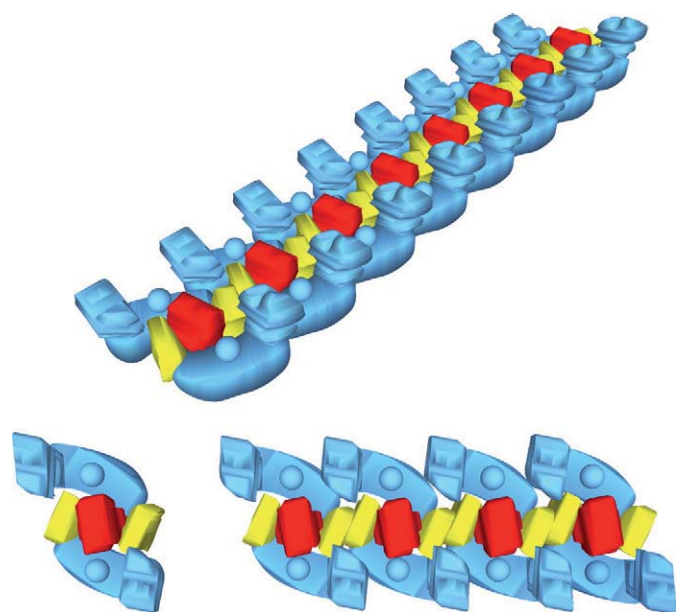


Fig. 3. A schematic model of the organization of respiratory chain complexes into a respiratory string. The basic unit (lower left) consists of two copies of complex I (blue), one copy of complex III₂ (red), and two copies of complex IV (yellow). Association of basic units into a string is mediated by complex IV, which interacts with a neighbouring complex IV through a dimeric interface found in the X-ray structure [52]; (from [29], modified).

protein has two additional, specific subunits i and k. A monomer is active in ATP catalysis and hydrolysis like its counterpart in prokaryotes, but evidence for a dimeric organization of the ATP synthase complex came as a surprise from BN-PAGE work on yeast [41]. The 1200 kDa dimeric complex includes dimer specific subunits e, g and k, which were not detected in monomers. Later, dimers were found in beef, *Arabidopsis* and several other organisms [3,4]. The dimer specific subunits e and g, as well as the subunits a, b, h and i of the monomer, stabilize the monomer–monomer interface [40]. To date, 2D maps of dimeric ATP synthase are available for bovine [8], the colorless green alga *Polytomella* [7] and *S. cerevisiae* [21] obtained by single-particle electron microscopy. In all organisms two monomers associate via the membrane F₀ parts and make an angle, which can be fixed or variable between 35 and 90°. Dimeric ATP synthase from *Polytomella* seems to be the most stable one and the monomers make one specific angle of 70°, as discussed below (Fig. 4C).

Despite the fact that the ATP synthase dimers were first described in the 1990s [41], older work even hint at a higher type of organization as oligomers. Rows of dimeric ATP synthases were demonstrated in *Paramecium* mitochondria by rapid-freeze deep-etch electron microscopy [23]. Additional BN-PAGE evidence of trimeric and tetrameric organizations of mammalian ATP synthases [20] supports the hypothesis of an oligomeric arrangement of ATP synthases in the membrane. Another BN-PAGE work on mammalian enzyme revealed only ATP synthase fragments with an even number of ATP synthases [42]. Ultrasectioning and negative staining of osmotically shocked *Polytomella* mitochondria came to the same conclusion [21]. Later, atomic force microscopy on isolated inner membranes from baker's yeast revealed rows of dimeric ATP synthases, although remarkably no curvature of the membrane was shown at all, likely due to flattening of the membrane on the substrate [43]. This is in contrast with the fact that isolated bakers' yeast ATP synthase dimers make a large angle [21]. Recently cryo-electron tomography (cryo-ET) data on bovine and rat fragmented mitochondria demonstrated long rows of dimers located at locally curved cristae membranes [22]. Averaging also revealed larger angles between monomers than reported for isolated bovine dimeric ATP synthase [8]. In another study, dimeric ATP synthase was studied in intact *Polytomella* mitochondria. Cryo-ET experiments with mitochondria embedded in amorphous ice showed the presence of oligomeric rows of ATP synthases in mitochondrial cristae [44]. Details of the rows were obtained at a resolution of 5.7 nm by averaging subvolumes of tomograms; this shows that the oligomeric chain is composed of repeating dimeric units with a spacing of 12 nm. The monomers make contact via the membrane part and the peripheral stalk (Fig. 4B) and individual dimers resemble very well the projection maps of isolated dimers in negative stain (Fig. 4C) [7] and amorphous ice (Fig. 4E) as can be seen from the connection of the stator to the F₁ headpiece (yellow arrows). The dimer–dimer interface is not yet well understood. The resolution of 5.7 nm for *Polytomella* appears in the same range as the 5 nm resolution claimed for the ATP synthase oligomers from bovine and rat liver dimers [22]. However, in contrast to the *Polytomella* data, the F₁ headpieces in the latter work merely look like feature-less spheres. In conclusion, the tomography data convincingly show the oligomeric state of the ATP synthase complex, but are far too low in resolution to reveal subunit interactions. From biochemical experiments it was predicted that subunits e, f, g, Su 8 (A6L), some transmembrane helices of the a-subunit as well as carriers for inorganic phosphate and for ADP/ATP are potential candidates for the oligomerization of ATP synthases [40].

5. Potential functions of OXPHOS supercomplexes

The occurrence of several specific supercomplexes and higher-ordered oligomers must have functional reasons. It was proposed that OXPHOS supercomplexes allow enhancement of the flow of electrons

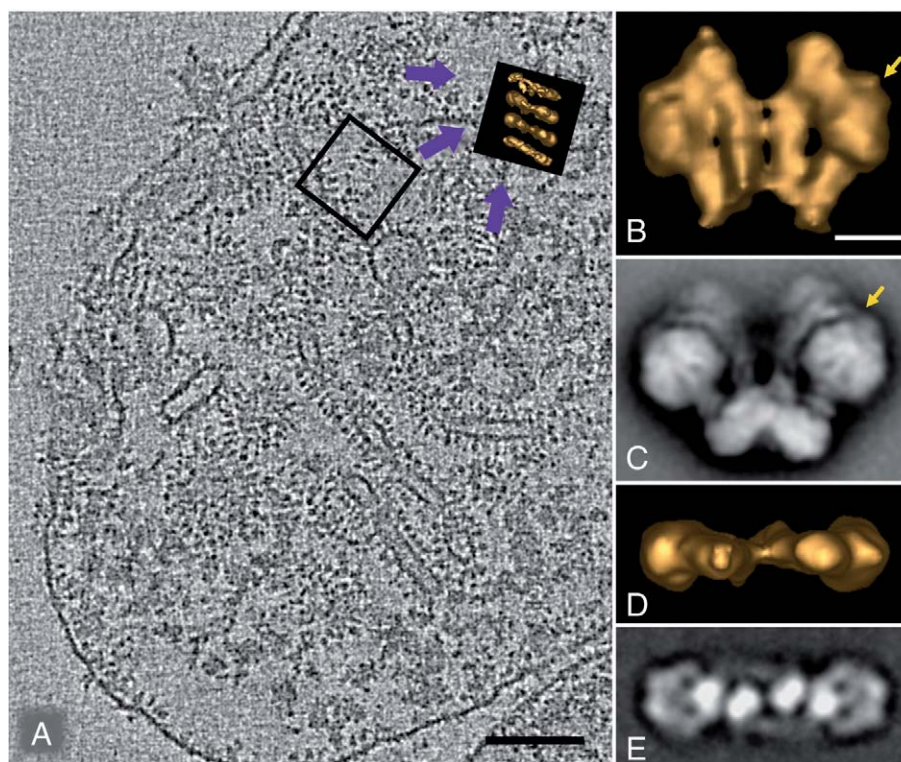


Fig. 4. Electron tomography of *Polytomella* mitochondria reveals the arrangement of oligomeric ATP synthase molecules. (A) Section of a tomogram (3D reconstruction) calculated from dual-axis electron tomography of an ice-embedded mitochondrion [44]. To reveal fine detail, hundreds of boxed subvolumes with a size as indicated were selected from several tomograms, as symbolized by purple arrows, aligned and averaged. (B) A single molecule of dimeric ATP synthase from tomography data in a side-view position, selected from the averaged subvolume from image A at a 4× larger scale. (C) Side-view of isolated ATP synthase in negative stain [7]. (D) Top-view of the same dimeric ATP synthase from tomography data as in B. (E) Top-view of isolated ATP synthase calculated by single-particle cryo-EM. Bar scale for frame A, 100 nm. Bar scale for frames B–E, 10 nm. The yellow arrows mark the connection between the F₁ headpiece and the peripheral stalk.

between the complexes by reducing the distance of diffusion of the mobile electron carriers ubiquinone and cytochrome *c* or by substrate channeling between associated OXPHOS complexes [10,45]. A direct role of the I + III₂(+ IV₁₋₂) supercomplex in ubiquinone-channeling is not clear so far, because the ubiquinone-binding domain of complex I possibly is not in close proximity to the complex I-complex III₂ interphase [6]. However, even if direct channeling does not take place, transfer of ubiquinol from complex I to complex III₂ still might be facilitated due to reduced diffusion distances. In plants the I + III₂ supercomplex might be necessary for the regulation of alternative respiration by reducing access of alternative oxidase to ubiquinol [4]. In yeast formation of the III₂+ IV₁₋₂ supercomplex seems to optimize the electron transport between complexes III and IV by a contraction of the cytochrome *c* movement between these two complexes [10]. The same can be valid for potato mitochondria based on the facts that complexes I, III and IV are rate limiting in flux control experiments and cytochrome *c* was found in the supercomplex [2]. Meantime, the same experiments did not demonstrate this for bovine heart mitochondria. Finally, supercomplex formation was suggested to be important in preventing excess oxygen radical formation [2].

Besides functional reasons, supercomplex formation is necessary for assembly and stability of its individual components. As an example, complex I is necessary for fully assembled complex III in human patients with mutations in the complex I subunits NDUFS2 and NDUFS4 [46] and the absence in complex III results in a dramatic loss of complex I in humans [47]. Furthermore, complex IV is required for the assembly of complex I in fibroblasts [14] and complex III₂ is essential for the stability of complex I in mouse cells [13]. The need for a higher organization in supercomplexes might be a more general requirement because in *Paracoccus denitrificans* assembly of respiratory complexes I, III, and IV into the respirasome stabilizes complex I [48].

The occurrence of ATP synthase dimers and oligomers has a special reason. Dimerization leads to a local curvature of the cristae membrane. Ultrastructural studies on yeast null mutants of dimer specific *e* and *g* subunits which lack the dimeric state of ATP synthases indicated that their mitochondria exhibit an unusual onion-shape morphology without any membrane foldings [49,50]. This strongly suggests that dimerization of ATP synthases is essential for cristae morphology. A recent study on mammalian mitochondria proved the organization of ATP synthases in long ribbons of dimers. The mitochondrial cristae may act as proton traps and enhance the local proton gradient necessary for ATP synthesis. In this way ATP synthases may optimize their own performance under proton-limited conditions [22].

6. Prospectives

Up to now a large amount of data on the OXPHOS system has been collected with different biochemical and biophysical techniques. Nevertheless, a complete picture of the protein organization in the cristae membrane is not yet available. Much higher resolution structural data on specific supercomplexes are necessary to give a full interpretation at the atomic level of subunit interactions and electron flow. The structural information of the dimeric ATP synthase complex, I + III₂ supercomplex and the respirasome should be improved by either X-ray crystallography or single-particle electron microscopy. The organisms discussed above, such as *Polytomella*, are obvious candidates to provide the most stable types of supercomplexes.

Despite the fact that the oligomeric organization of ATP synthases has now been proven, the position of the other OXPHOS complexes, in particular the respirasomes, within the cristae membrane is still unclear. According to [22], respirasomes and single respiratory complexes could be located in the less curved regions of the cristae membrane. Another

possibility would be a localization between the rows of ATP synthases. However, available data suggest that likely the amount of respiratory chain complexes is very limited in comparison to ATP synthases and it is difficult to detect them at this resolution. A breakthrough is expected by further application of cryo-electron tomography, as discussed for ATP synthase oligomers (Fig. 4). Electron tomography is an emerging technique, but still limited in resolution. In addition to 3D averaging and classification of individual subvolumes improvement in resolution is expected in the near future by perfecting cryo-electron microscopy hardware and software, and implementing the new generation of direct electron detectors, replacing the currently used inefficient slow-scan CCD cameras.

Finally, our understanding of supercomplex organization will also increase by studying the structural aspects of the many naturally occurring mutants of the OXPHOS system. Since the first report of a complex I deficit related to a human mitochondrial disorder in 1988, many other mitochondrial diseases have been associated to structural and functional defects at the level of this enzyme complex I (see for instance [46,51]).

Acknowledgements

We thank Mr. Jelle Bultema for discussion. This work was supported by the Netherlands organization of scientific research (NWO) and by the Deutsche Forschungsgemeinschaft (grant Br 1829-8/1).

References

- [1] C.R. Hackenbrock, B. Chazotte, S.S. Gupte, The random collision model and a critical assessment of diffusion and collision in mitochondrial electron transport, *J. Bioenerg. Biomembr.* 18 (1986) 331–368.
- [2] G. Lenaz, M.L. Genova, Structural and functional organization of the mitochondrial respiratory chain: a dynamic super-assembly, *Int. J. Biochem. Cell Biol.* 41 (2009) 1750–1772.
- [3] H. Schägger, K. Pfeiffer, Supercomplexes in the respiratory chains of yeast and mammalian mitochondria, *EMBO J.* 19 (2000) 1777–1783.
- [4] H. Eubel, L. Jänsch, H.-P. Braun, New insights into the respiratory chain of plant mitochondria supercomplexes and a unique compositions of complex II, *Plant Physiol.* 133 (2003) 274–286.
- [5] H. Eubel, J. Heinemeyer, S. Sunderhaus, H.P. Braun, Respiratory chain supercomplexes in plant mitochondria, *Plant Physiol. Biochem.* 42 (2004) 937–942.
- [6] N.V. Dudkina, H. Eubel, W. Keegstra, E.J. Boekema, H.-P. Braun, Structure of a mitochondrial supercomplex formed by respiratory-chain complexes I and III, *Proc. Natl. Acad. Sci. USA* 102 (2005) 3225–3229.
- [7] N.V. Dudkina, J. Heinemeyer, W. Keegstra, E.J. Boekema, H.P. Braun, Structure of dimeric ATP synthase from mitochondria: an angular association of monomers induces the strong curvature of the inner membrane, *FEBS Lett.* 579 (2005) 5769–5772.
- [8] F. Minauro-Sanmiguel, S. Wilkens, J.J. García, Structure of dimeric mitochondrial ATP synthase: novel F₀ bridging features and the structural basis of mitochondrial cristae biogenesis, *Proc. Natl. Acad. Sci. USA* 102 (2005) 12356–12358.
- [9] E. Schäfer, H. Seelert, N.H. Reifschneider, F. Krause, N.A. Dencher, J. Vonck, Architecture of active mammalian respiratory chain supercomplexes, *J. Biol. Chem.* 281 (2006) 15370–15375.
- [10] J. Heinemeyer, H.P. Braun, E.J. Boekema, R. Kouřil, A structural model of the cytochrome c reductase/oxidase supercomplex from yeast mitochondria, *J. Biol. Chem.* 282 (2007) 12240–12248.
- [11] H. Boumans, L.A. Grivell, J.A. Berden, The respiratory chain in yeast behaves as a single functional unit, *J. Biol. Chem.* 273 (1998) 4872–4877.
- [12] C. Bianchi, M.L. Genova, G.P. Castelli, G. Lenaz, The mitochondrial respiratory chain is partially organized in a supercomplex assembly: kinetic evidence using flux control analysis, *J. Biol. Chem.* 279 (2004) 36562–36569.
- [13] R. Acín-Pérez, M. Bayona-Bafaluy, P. Fernández-Silva, R. Moreno-Loshuertos, A. Pérez-Martos, C. Bruno, C. Moraes, J. Enriquez, Respiratory complex III is required to maintain complex I in mammalian mitochondria, *Mol. Cell* 13 (2004) 805–815.
- [14] F. Diaz, H. Fukui, S. Garcia, C.T. Moraes, Cytochrome c oxidase is required for the assembly/stability of respiratory complex I in mouse fibroblasts, *Mol. Cell Biol.* 26 (2006) 4872–4881.
- [15] M. Zhang, E. Mileevskaya, W. Dowhan, Gluing the respiratory chain together. Cardiolipin is required for supercomplex formation in the inner mitochondrial membrane, *J. Biol. Chem.* 277 (2002) 43553–43556.
- [16] K. Pfeiffer, V. Gohil, R.A. Stuart, C. Hunte, U. Brandt, M.L. Greenberg, H. Schägger, Cardiolipin stabilizes respiratory chain supercomplexes, *J. Biol. Chem.* 278 (2003) 52873–52880.
- [17] D.L. Nelson, M.M. Cox, *Lehninger Principles of Biochemistry*, Fifth edition W.H. Freeman, New York, 2008.
- [18] N.V. Dudkina, S. Sunderhaus, E.J. Boekema, H.P. Braun, The higher level of organization of the oxidative phosphorylation system: mitochondrial supercomplexes, *J. Bioenerg. Biomembr.* 40 (2008) 419–424.
- [19] R. Acín-Pérez, P. Fernández-Silva, M.L. Peleato, A. Pérez-Martos, J.A. Enriquez, Respiratory active mitochondrial supercomplexes, *Mol. Cell* 32 (2008) 529–539.
- [20] F. Krause, N.H. Reifschneider, S. Goto, N.A. Dencher, Active oligomeric ATP synthases in mammalian mitochondria, *Biochem. Biophys. Res. Commun.* 329 (2005) 583–590.
- [21] N.V. Dudkina, S. Sunderhaus, H.P. Braun, E.J. Boekema, Characterization of dimeric ATP synthase and cristae membrane ultrastructure from *Saccharomyces* and *Polytomella* mitochondria, *FEBS Lett.* 580 (2006) 3427–3432.
- [22] M. Strauss, G. Hofhaus, R.R. Schröder, W. Kühlbrandt, Dimer ribbons of ATP synthase shape the inner mitochondrial membrane, *EMBO J.* 27 (2008) 1154–1160.
- [23] R.D. Allen, C.C. Schroeder, A.K. Fok, An investigation of mitochondrial inner membranes by rapid-freeze deep-etch techniques, *J. Cell Biol.* 108 (1989) 2233–2240.
- [24] P.R. Rich, The molecular machinery of Keilin's respiratory chain, *Biochem. Soc. Trans.* 31 (2003) 1095–1105.
- [25] V. Guenebaut, R. Vincentelli, D. Mills, H. Weiss, K.R. Leonard, Three-dimensional structure of NADH-dehydrogenase from *Neurospora crassa* by electron microscopy and conical tilt reconstruction, *J. Mol. Biol.* 265 (1997) 409–418.
- [26] M. Radermacher, T. Ruiz, T. Clason, S. Benjamin, U. Brandt, V. Zickermann, The three-dimensional structure of complex I from *Yarrowia lipolytica*: a highly dynamic enzyme, *J. Struct. Biol.* 154 (2006) 269–279.
- [27] S. Sunderhaus, N.V. Dudkina, L. Jänsch, J. Klodmann, J. Heinemeyer, M. Perales, E. Zabaleta, E.J. Boekema, H.-P. Braun, Carbonic anhydrase subunits form a matrix-exposed domain attached to the membrane arm of mitochondrial complex I in plants, *J. Biol. Chem.* 281 (2006) 6482–6488.
- [28] K. Peters, N.V. Dudkina, L. Jänsch, H.P. Braun, E.J. Boekema, A structural investigation of complex I and I+III₂ supercomplex from *Zea mays* at 11–13 Å resolution: assignment of the carbonic anhydrase domain and evidence for structural heterogeneity within complex I, *Biochim. Biophys. Acta* 1777 (2008) 84–93.
- [29] J.B. Bultema, H.P. Braun, E.J. Boekema, R. Kouřil, Megastructure organization of the oxidative phosphorylation system by structural analysis of respiratory supercomplexes from potato, *Biochim. Biophys. Acta* 1767 (2009) 60–67.
- [30] L.A. Sazanov, P. Hinchliffe, Structure of the hydrophilic domain of respiratory complex I from *Thermus thermophilus*, *Science* 311 (2006) 1430–1436.
- [31] U. Brandt, Proton-translocation by membrane-bound NADH: ubiquinone-oxidoreductase (complex I) through redox-gated ligand conduction, *Biochim. Biophys. Acta* 1318 (1997) 79–91.
- [32] E.A. Baranova, P.J. Holt, L.A. Sazanov, Projection structure of the membrane domain of *Escherichia coli* respiratory complex I at 8 Å resolution, *J. Mol. Biol.* 366 (2007) 140–154.
- [33] H. Eubel, J. Heinemeyer, H.P. Braun, Identification and characterization of respirasomes in potato mitochondria, *Plant Physiol.* 134 (2004) 1450–1459.
- [34] F. Krause, N.H. Reifschneider, D. Vocke, H. Seelert, S. Rexroth, N.A. Dencher, "Respirasome"-like supercomplexes in green leaf mitochondria of spinach, *J. Biol. Chem.* 279 (2004) 48369–48375.
- [35] N.V. Dudkina, J. Heinemeyer, S. Sunderhaus, E.J. Boekema, H.P. Braun, Respiratory chain supercomplexes in the plant mitochondrial membrane, *Trends Plant Sci.* 11 (2006) 232–240.
- [36] E. Schäfer, N.A. Dencher, J. Vonck, D.N. Parcej, Three-dimensional structure of the respiratory chain supercomplex I₁III₂IV₁ from bovine heart mitochondria, *Biochemistry* 46 (2007) 2579–2585.
- [37] I. Wittig, R. Carozzo, F.M. Santorelli, H. Schägger, Supercomplexes and subcomplexes of mitochondrial oxidative phosphorylation, *Biochim. Biophys. Acta* 1757 (2006) 1066–1072.
- [38] J.P. Abrahams, A.G. Leslie, R. Lutter, J.E. Walker, Structure at 2.8 Å resolution of F₁-ATPase from bovine heart mitochondria, *Nature* 370 (1994) 621–628.
- [39] D. Stock, C. Gibbons, I. Arechaga, A.G. Leslie, J.E. Walker, The rotary mechanism of ATP synthase, *Curr. Opin. Struct. Biol.* 10 (2000) 672–679.
- [40] I. Wittig, H. Schägger, Structural organization of mitochondrial ATP synthase, *Biochim. Biophys. Acta* 1777 (2008) 592–598.
- [41] I. Arnold, K. Pfeiffer, W. Neupert, R.A. Stuart, H. Schägger, Yeast mitochondrial F₁F₀-ATP synthase exists as a dimer: identification of three dimer-specific subunits, *EMBO J.* 17 (1998) 7170–7178.
- [42] I. Wittig, H. Schägger, Advantages and limitations of clear-native PAGE, *Proteomics* 5 (2005) 4338–4346.
- [43] N. Buzhynskyy, P. Sens, V. Prima, J.N. Sturgis, S. Scheuring, Rows of ATP synthase dimers in native mitochondrial inner membranes, *Biophys. J.* 93 (2007) 2870–2876.
- [44] N.V. Dudkina, G.T. Oostergetel, D. Lewejohann, H.P. Braun, E.J. Boekema, Row-like organization of ATP synthase in intact mitochondria determined by cryo-electron tomography, *Biochim. Biophys. Acta* 1797 (2010) 272–277.
- [45] H. Schägger, Respiratory chain supercomplexes, *IUBMB Life* 52 (2001) 119–128.
- [46] C. Ugalde, R.J.R.J. Janssen, L.P. van den Heuvel, J.A. Smeitink, L.G.J. Nijtmans, Differences in assembly or stability of complex I and other mitochondrial OXPHOS complexes in inherited complex I deficiency, *Hum. Mol. Genet.* 13 (2004) 659–667.
- [47] E.L. Blakely, A.L. Mitchell, N. Fisher, B. Meunier, L.G. Nijtmans, A.M. Schaefer, M.J. Jackson, D.M. Turnbull, R.W. Taylor, A mitochondrial cytochrome b mutation causing severe respiration chain enzyme deficiency in humans and yeast, *FEBS J.* 14 (2005) 3583–3592.
- [48] A. Stroh, O. Anderka, K. Pfeiffer, T. Yagi, M. Finel, B. Ludwig, H. Schägger, Assembly of respiratory complexes I, III, and IV into NADH oxidase supercomplex stabilizes complex I in *Paracoccus denitrificans*, *J. Biol. Chem.* 279 (2004) 5000–5007.

Chapter 2 - Publications and Manuscripts

670

N.V. Dudkina et al. / Biochimica et Biophysica Acta 1797 (2010) 664–670

- [49] P. Paumard, J. Vaillier, B. Coulary, J. Schaeffer, V. Soubannier, D.M. Mueller, D. Brethes, J.P. di Rago, J. Velours, The ATP synthase is involved in generating mitochondrial cristae morphology, *EMBO J.* 21 (2002) 221–230.
- [50] M.F. Giraud, P. Paumard, V. Soubannier, J. Vaillier, G. Arselin, B. Salin, J. Schaeffer, D. Brethes, P. di Rago, J. Velours, Is there a relationship between the supramolecular organization of the mitochondrial ATP synthase and the formation of cristae? *Biochim. Biophys. Acta* 1555 (2002) 174–180.
- [51] U. Brandt, Energy converting NADH: quinone oxidoreductase (complex I), *Annu. Rev. Biochem.* 75 (2006) 69–92.
- [52] S. Iwata, J.W. Lee, K. Okada, J.K. Lee, M. Iwata, B. Rasmussen, T.A. Link, S. Ramaswamy, B.K. Jap, Complete structure of the 11-subunit bovine mitochondrial cytochrome *bc*₁ complex, *Science* 281 (1998) 64–71.
- [53] T. Tsukihara, H. Aoyama, E. Yamashita, T. Tomizaki, H. Yamaguchi, K. Shinzawa-Itoh, R. Nakashima, R. Yaono, S. Yoshikawa, The whole structure of the 13-subunit oxidized cytochrome *c* oxidase at 2.8 Å, *Science* 272 (1996) 1136–1144.

Comparative Analyses of Protein Complexes by Blue Native DIGE

Katrin Peters¹ and Hans-Peter Braun^{1*}

¹ Institute for Plant Genetics, Leibniz Universität Hannover, Herrenhäuser Str. 2, D-30419 Hannover, Germany

* Author for correspondance, braun@genetik.uni-hannover.de

Summary

Classically, DIGE is carried out on the basis of two-dimensional (2D) IEF / SDS PAGE. This allows comparative analyses of large protein sets. However, 2D IEF / SDS PAGE only poorly resolves hydrophobic proteins and is not compatible with native protein characterizations. Blue native PAGE represents a powerful alternative. Combined with CyDye labeling, blue native DIGE offers several useful applications like quantitative comparison of protein complexes of related protein fractions. Here we present a protocol for fluorophore labeling of native protein fractions for separation by blue native PAGE.

Key words: Blue native PAGE, DIGE labeling, protein complexes, membrane proteins, mitochondria

Abbreviations: 2D: two-dimensional, BN PAGE: blue native polyacrylamide gel electrophoresis, BN / SDS PAGE: blue native / sodium dodecyl sulfate polyacrylamide gel electrophoresis, DIGE: difference gel electrophoresis, DMF: dimethylformamide, IEF / SDS PAGE: isoelectric focusing / sodium dodecyl sulfate polyacrylamide gel electrophoresis, pI: isoelectric point, PMSF: phenylmethylsulfonyl fluoride.

1. Introduction

Fluorophore-based difference gel electrophoresis (DIGE) represents an ideal system for comparative proteomics. Different protein fractions can be co-electrophoresed on a single gel, thereby eliminating gel-to-gel variations. If evaluated with special software tools, fluorophore detection allows exact relative quantification of proteins present in the protein fractions to be compared.

Classically, DIGE is carried out based on the two-dimensional (2D) IEF / SDS PAGE system (1). Indeed, using this experimental system, large protein sets are efficiently resolved. However, 2D IEF / SDS PAGE also has limitations. For instance, hydrophobic proteins are not well resolved during the IEF gel dimension and proteins with very basic pIs often get lost. Additionally, 2D IEF / SDS PAGE is not compatible with native enzyme characterizations. Two-dimensional blue native (BN) / SDS PAGE represents an alternative gel system which allows overcoming these limitations. Hydrophobic as well as basic proteins are easily resolved. If applied as a one-dimensional system, BN PAGE is even compatible with in-gel enzyme activity stainings.

BN PAGE was first published by Hermann Schägger (2). The principle idea was to use Coomassie Blue not only for protein staining after gel electrophoresis, but also for the introduction of negative charges into proteins by incubating protein fractions with this compound before gel electrophoresis. Coomassie Blue is an anionic molecule but in contrast to SDS does not denature proteins. Furthermore, protein complexes remain stable. If combined with low-percentage polyacrylamide gels, protein complexes can be resolved by BN PAGE. In case sample preparation takes place in the presence of mild non-ionic detergents, even hydrophobic membrane-bound protein complexes can easily be separated. As with IEF / SDS PAGE, strips of blue native gels can be horizontally transferred onto a second gel dimension which is carried out in the presence of SDS. Using this experimental set up, protein complexes are separated into their subunits which form vertical rows of spots on the resulting 2D gels.

BN PAGE and 2D BN / SDS PAGE can be combined with the DIGE technology (3). BN DIGE allows systematic and quantitative comparison of protein complexes of related protein fractions, structural investigation of protein complexes, assignment of protein complexes to subcellular fractions like organelles, electrophoretic mapping of isoforms of subunits of protein complexes with respect to a larger proteome and topological investigations (4). So far, BN DIGE has only been applied in a few studies (4, 5, 6, 7, 8, 9). Indeed, the potential of BN

DIGE was only very recently recognized. Here we present a BN DIGE protocol suitable for the comparative analyses of protein complexes of biological fractions.

2. Materials

Buffers, solutions and reagents are given in the order of usage according to the methods protocol. Prepare all solutions freshly using analytical grade chemicals in combination with pure de-ionized water.

2.1. Preparation of a BN gel

1. Acrylamide solution: 40%, acryl / bisacryl = 32 / 1 (AppliChem, Darmstadt, Germany)
2. Gel buffer BN (6x): 1.5 M amino caproic acid, 150 mM BisTris, pH 7.0 (adjust at 4°C)
3. N,N,N',N'-tetramethylethylenediamine (TEMED), 99% (Sigma, St. Louis, Missouri, USA)
4. Ammonium persulfate solution (APS), 10% (w/v) Ammonium persulfate
5. Cathode buffer BN (5x): 250 mM Tricine, 75 mM BisTris, 0.1% (w/v) Coomassie G 250 (e.g. Merck, Darmstadt, Germany), pH 7.0 (adjust at 4°C)
6. Anode buffer BN (6x): 300 mM BisTris, pH 7.0 (adjust at 4°C)

2.2. Sample preparation for BN DIGE

1. Solubilization buffer, pH 7.4, with digitonin: 30 mM HEPES, 150 mM potassium acetate, 10% (v/v) glycerol, pH 7.4, supplemented with 5% digitonin (*see Note 1*). Solution should be briefly boiled for dissolving digitonin. Buffer is stored at 4°C.
2. Solubilization buffer, pH 10: 30 mM HEPES, 150 mM potassium acetate, 10% (v/v) glycerol, pH 10 (*see Note 2*).
3. CyDye™ fluor minimal labeling reagents. Cy2™, Cy3™ and Cy5™ (GE Healthcare, Munich, Germany). The fluorophores (400 pmol) are diluted in DMF according to the manufacturers instructions. Diluted CyDyes are stored at -20°C and should be used within 3 months (*see Note 3*).
4. Lysine stock solution: 10 mM lysine, stored at 4°C.

5. Blue loading buffer: 750 mM aminocaproic acid, 5% (w/v) Coomassie 250 G, stored at 4°C.

2.3. SDS PAGE for second gel dimension

1. Acrylamide solution: 40%, acryl / bisacryl = 32 / 1 (AppliChem, Darmstadt, Germany)
2. N,N,N',N'-tetramethylethylenediamine (TEMED), 99% (Sigma, St. Louis, Missouri, USA)
3. Ammonium persulfate solution (APS), 10% (w/v) Ammonium persulfate
4. Gel buffer SDS: 3 M Tris-HCl, 0.3% (w/v) SDS, pH 8.45
5. Gel buffer BN (6x): *see 2.1.*
6. Cathode buffer SDS: 0.1 M Tris base, 0.1 M Tricine, 0.1% (w/v) SDS, pH 8.25
7. Anode buffer SDS: 0.2 M Tris-HCl, pH 8.9
8. Overlay solution: 1 M Tris-HCl, 0.1% (w/v) SDS, pH 8.45
9. Denaturation solution: 1.0% (w/v) SDS, 1.0% (v/v) β -mercaptoethanol
10. SDS solution: 10% (w/v) SDS

3. Methods

The following protocol is suitable for the comparison of protein complexes of two related protein fractions. It is based on the usage of the CyDyeTM fluor labeling reagents (GE Healthcare, Munich, Germany). Both fractions should contain 100 μ g protein and should be labeled with different fluorophores. Afterwards, the samples are combined and loaded onto a single blue native gel. The BN gel should be prepared before sample preparation.

3.1. Preparation of a BN gel

Best resolution capacity of BN gels is achieved if the electrophoretic separation distance is greater than 12 cm. The following instructions refer to the Protean II electrophoresis unit (BioRad, Richmond, Ca, USA; gel dimensions 0.15 x 16 x 20 cm). However, units from other manufacturers are of comparable suitability for BN-PAGE, e.g. the Hoefer SE-400 or SE-600 gel systems (GE healthcare, Munich, Germany). Usage of gradient gels is recommended,

because molecular masses of protein complexes can vary between 50 kDa and several thousand of kDa (see **Note 4**).

1. Prepare a 4.5% separation gel solution by mixing 2.4 ml of Acrylamide solution with 3.5 ml of Gel buffer BN and 15.1 ml ddH₂O.
2. Prepare a 16% separation gel solution by mixing 7.4 ml of Acrylamide solution with 3 ml of Gel buffer BN, 4.6 ml ddH₂O and 3.5 ml glycerol.
3. Transfer the two gel solutions into the two chambers of a gradient former and connect the gradient former via a hose and a needle with the space in-between two glass plates which are pre-assembled in a gel casting stand. Gradient gels can either be poured from the top (16% gel solution has to enter the gel sandwich first) or from the bottom (4.5% gel solution has to enter first). Pouring the gel from the bottom, an adjustable pump (for example BioRad EconoPump) is needed.
4. Add TEMED and APS to the two gel solutions (95 µl 10% APS / 9.5 µl TEMED to the 4.5% gel solution, 61 µl APS / 6.1 µl TEMED to the 16% gel solution).
5. Pour the gradient gel, leaving space for the stacking gel, and overlay with ddH₂O. The gel should polymerize in about 60 minutes.
6. Pour off the ddH₂O.
7. Prepare the stacking gel solution by mixing 1.5 ml of Acrylamide solution, 2.5 ml of Gel buffer BN and 11 ml ddH₂O.
8. Add 65 µl APS and 6.5 µl TEMED and pour the stacking gel around an inserted comb. The stacking gel should polymerize within 30 minutes.
9. Prepare 1xAnode and 1xCathode buffers BN by diluting the corresponding stock solutions.
10. Once the polymerization of the stacking gel is finished, carefully remove the comb.
11. Add Cathode and Anode buffers BN to the upper and lower chambers of the gel unit respectively. Cool down the unit to 4°C.

3.2. Sample preparation for BN-DIGE

Starting material can either be whole cells or isolated organelles. Fractions should be treated under mild conditions in order to keep proteins in their native conformation (avoid high salt, ionic detergents, high temperatures, urea etc.). All steps of the sample preparation should be

carried out at 4°C. The BN gel should be prepared before the sample preparation is started (see **3.1.**).

1. Cell or organelle fractions, including 100 µg protein each, are centrifuged at full speed for 10 min at 4°C using an Eppendorf centrifuge.
2. Sedimented material is resuspended in 10 µL of solubilization buffer, pH 7.4, with digitonin and incubated for 20 min at 4°C (see **Note 5**).
3. Fractions are again centrifuged at full speed for 20 min at 4°C using an Eppendorf centrifuge to remove insoluble material.
4. The supernatants containing solubilised proteins and protein complexes are transferred into new 1.5mL-Eppendorf vessels and supplemented with 10 µL of solubilization buffer, pH 10, to adjust the pH value of the protein solutions to about 8.5 (see **Note 6**).
5. Labeling reaction: For CyDye™ labeling reactions, each sample is labeled with one CyDye by the addition of 1 µL of diluted CyDye solution to each protein fraction (see **Note 7**). Centrifuge the samples briefly and incubate for 30 min on ice in the dark.
6. Stop labeling reaction: Add 1 µL of lysine stock solution and incubate samples for 10 min in the dark.
7. Combine the two labeled protein fractions in one Eppendorf vessel.
8. Add 2 µL of Blue loading buffer to the combined protein fraction. Sample now is ready for loading on a BN gel.

3.3. Blue native PAGE for first gel dimension

1. Load combined CyDye-labeled protein sample (see **3.2.**) into a well of a BN gel (see **3.1.**).
2. Connect the gel unit to a power supply. Start electrophoresis at constant voltage (100V for 45 minutes) and continue at constant current (15 mA for about 11 hours). Electrophoresis should be carried out at 4°C and in the dark in order to protect the dyes.
3. (optionally:) The Cathode buffer BN, normally containing Coomassie Blue, may be replaced after half of the electrophoresis run against a Cathode buffer BN lacking Coomassie Blue (see **Note 8**).

3.4. SDS PAGE for second gel dimension

BN PAGE can be combined with a second gel dimension, which is carried out in the presence of SDS, to further separate the protein complexes into their subunits. All published protocols for SDS PAGE are suitable for combination with BN PAGE, e.g. the system published by Laemmli (**10**). However, the Tricine-SDS PAGE system developed by Schägger (**11**) generally gives the best resolution. The following instructions refer to this gel system carried out in the Protean II gel unit (BioRad, Richmond, Ca, USA). As mentioned above, gel electrophoresis units of other manufacturers are of equal suitability.

1. Cut out a strip of a BN gel and incubate it in the Denaturation solution for 30 minutes at room temperature.
2. Wash the strip with ddH₂O for 30 to 60 seconds (this step is important because β -mercaptoethanol inhibits polymerisation of acrylamide).
3. Place the strip on a glass plate of an electrophoresis unit at the position of the teeth of a normal gel comb.
4. Assemble the gel electrophoresis unit by adding 1 mm spacers, the second glass plate and clamps and transfer all into the gel casting stand (the reduced thickness of the gel of the second gel dimension (1 mm) in comparison to the strip of the first gel dimension (1.5 mm) avoids sliding down of the gel strip between the glass plates in vertical position).
5. Prepare a 16% separation gel solution by mixing 12.4 ml of Acrylamide solution, 10 ml of Gel buffer SDS, 7.6 ml ddH₂O, 100 μ l APS, 10 μ l TEMED and pour the solution into the space in-between the two glass plates below the BN gel strip. Leave space for the sample gel solution for embedding the BN gel strip. Overlay the separation gel with the Overlay solution. The gel should polymerize in about 60 minutes (*see Note 9*).
6. Prepare a 10% sample gel solution by mixing 2.5 ml of Acrylamide solution, 3.4 ml of Gel buffer BN, 1 ml glycerol, 100 μ l of SDS solution, 2.9 ml ddH₂O, 83 μ l APS and 8.3 μ l TEMED.
7. Discard the overlay solution and pour the sample gel embedding the BN gel lane. The casting stand should be held slightly diagonal to avoid air bubbles captured underneath the BN gel lane (*see Note 10*).
8. Add the Cathode and Anode buffers SDS to the upper and lower chambers of the gel unit.
9. Connect the gel unit to a power supply. Carry out electrophoresis at 30 mA per gel over night. The gel run should take place in the dark to protect the fluorophores.

3.5. Visualization of CyDyeTM -labeled protein

After completion of gel electrophoresis, fluorophores can be detected in 1D BN or 2D BN/SDS gels using a fluorescence scanner (e.g. the Typhoon fluorescence scanner from GE Healthcare) (**Figure 1**). Keep gels in the dark before starting the scanning procedure. Using the CyDye fluorophores, gels should be scanned at 50-100- μ m resolution at the appropriate excitation wavelengths (488 nm for Cy2TM, 532 nm for Cy3TM and 633 nm for Cy5TM). Digital gel images can be visualized using the Image Quant analysis software (GE Healthcare). Quantification of relative differences of individual protein abundances can be carried out using specific software such as Delta 2-D (Decodon, Greifswald, Germany) or DeCyderTM (GE Healthcare).

4. Notes

1. Digitonin is necessary for the solubilization of membrane-bound protein complexes of cellular or organellar fractions. Other non-ionic detergents (e.g. dodecylmaltoside and Triton X-100) can be used but should be applied in the presence of modified buffer systems; *see* Wittig et al. (**12**).
2. The pH value of the buffer must be >9. Normally, it is at about pH 10 without adjustment. Therefore, the buffer can be directly used.
3. Always use CyDyes from the same reaction kit diluted with dimethylformamide (DMF) of one batch to assure comparative labeling conditions. Consume diluted CyDyes within three months.
4. If very large protein complexes (>3 MDa) have to be resolved, the acrylamide gradient gel of the BN gel dimension can be substituted by a 2.5% agarose gel prepared in Gel buffer BN (**13**).
5. The resulting detergent-to-protein ratio is 5:1 (w/w).
6. A pH value of about 8.5 is a prerequisite for efficient labeling. The pH value of the protein solution can be easily controlled using pH test strips.
7. Additionally, a third fraction containing a mixture of both protein fractions (50 μ g protein each) can be labeled with a third CyDye as internal standard.
8. Coomassie Blue might quench the fluorescence signal of the CyDyes. If the cathode buffer is substituted by the same buffer lacking Coomassie Blue after half of the electrophoresis run, the background of the resulting BN gel is much clearer.

9. Concerning the Tricine-SDS PAGE system for the second gel dimension, Schägger and von Jagow (*II*) originally proposed a two-step separation gel consisting of a large 16% phase and a smaller 10% phase (called “spacer gel”). The advantage of this slightly more complicated gel system is a better resolution of large protein subunits. The two gel solutions are poured one upon the other (glycerol is added to the 16% gel solution to avoid mixing with the 10% gel solution, for details see Schägger and von Jagow (*II*)).
10. The transfer of the strip of BN gel onto a second gel dimension is proposed to be carried out by embedding the gel lane by the sample gel of the second dimension. This procedure ensures optimal physical contact between the BN gel lane and the SDS gel of the second dimension. However, BN gel strips can also be fixed onto a pre-poured SDS gel using agarose as usually carried out for 2D IEF / SDS PAGE. Physical contact of the gels might not be optimal, but the time period between the end of the first and the start of the second electrophoresis is shortened.

Acknowledgements

The authors would like to thank Christina Rode, Institute for Plant Genetics, Leibniz Universität Hannover, for critical reading of the manuscript.

References

1. O'Farrell P.Z. and Goodman H.M. (1976) Resolution of simian virus 40 proteins in whole cell extracts by two-dimensional electrophoresis: heterogeneity of the major capsid protein. *Cell*. 9: 289-298.
2. Schagger H. and von Jagow G. (1991) Blue native electrophoresis for isolation of membrane protein complexes in enzymatically active form. *Anal. Biochem.* 199: 223-231.
3. Perales M., Eubel H., Heinemeyer J., Colaneri A., Zabaleta E., Braun H.P. (2005) Disruption of a nuclear gene encoding a mitochondrial gamma carbonic anhydrase reduces complex I and supercomplex I+III₂ levels and alters mitochondrial physiology in Arabidopsis. *J Mol Biol* 350: 263-277.
4. Heinemeyer J., Scheibe B., Schmitz U.K., and Braun H.P. (2009) Blue native DIGE as a tool for comparative analyses of protein complexes. *J Prot* 72: 539-544.
5. Hedman E., Widén C., Asadi A., Dinnetz I., Schröder W.P., Gustafsson J.A., Wikström A.C. (2006) Proteomic identification of glucocorticoid receptor interacting proteins. *Proteomics* 6: 3114-3126.
6. Gillardon F., Rist W., Kussmaul L., Vogel J., Berg M., Danzer K., Kraut N., Hengerer B. (2007) Proteomic and functional alterations in brain mitochondria from Tg2576 mice occur before amyloid plaque deposition. *Proteomics* 7: 605-616.
7. Reisinger V. and Eichacker L.A. (2007) How to analyze protein complexes by 2D blue native SDS-PAGE. *Proteomics* 7: 6-16.
8. Dani D. and Dencher N.A. (2008) Native-DIGE: a new look at the mitochondrial membrane proteome. *Biotechnol J.* 3: 817-822.
9. Dani D. Shimokawa I., Komatsu T., Higami Y., Warnken U., Schokraie E., Schnölzer M., Krause F., Sugawa M.D., Dencher N.A. (2010) Modulation of oxidative

10. Laemmli, U.K. (1970) Cleavage of structural proteins during the assembly of the head of bacteriophage T4. *Nature* 227, 680-685.
11. Schägger, H. and von Jagow, G. (1987) Tricine-sodium dodecyl sulfate-polyacrylamide gel electrophoresis for the separation of proteins in the range from 1 to 100 kDa. *Anal. Biochem.* 166, 368-379.
12. Wittig I., Braun H.-P., Schägger, H. (2006) Blue-native PAGE. *Nature Protocols* 1: 418–428.
13. Henderson, N.S., Nijtmans, L.G., Lindsay, J.G., Lamantea, E., Zeviani, M. and Holt, I.J. (2000) Separation of intact pyruvate dehydrogenase complex using blue native agarose gel electrophoresis. *Electrophoresis* 21, 2925-2931.
14. Wittig I., Karas M., Schägger H. (2007) High resolution clear native electrophoresis for in-gel functional assays and fluorescence studies of membrane protein complexes. *Mol Cell Proteomics* 6: 1215–1225.

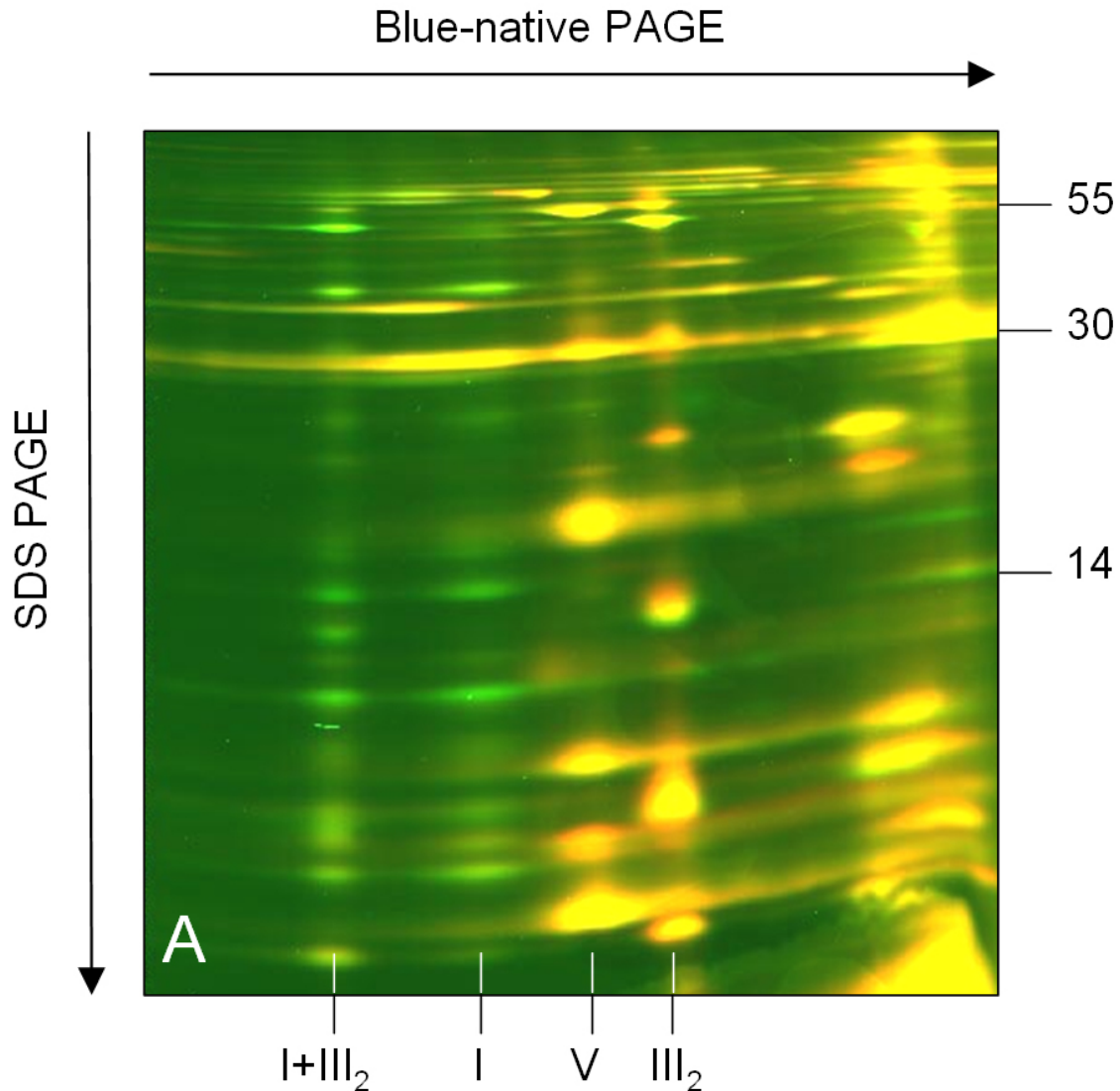


Fig. 1: Comparative analysis of the mitochondrial proteomes of a wild-type (Col-0) and a mutant (Col-0- Δ At1g47260) cell line of the model plant *Arabidopsis thaliana*. Proteins of the Col-0 fraction were labeled with Cy3, proteins of the Col-0- Δ At1g47260 fraction with Cy5. Combined protein fractions were separated by 2D BN / SDS PAGE and protein visualization was carried out by laser scanning at the respective wavelengths using the Typhoon laser scanner. On the resulting overlay image, Cy3-labeled proteins are indicated in green and Cy5-labeled proteins in red. Proteins of equal abundance in the two compared fractions are yellow. The molecular masses of standard proteins are given to the right of the figure; the identities of protein complexes are given below the gel. I: complex I; V: complex V; III₂: dimeric complex III; I+III₂: supercomplex containing complex I and dimeric complex III.

The mutant line lacks a subunit of complex I. As a consequence, amounts of complex I and the I+III₂ supercomplex are drastically reduced (from Perales et al. 2005 (3), modified).

Complex I - complex II ratio strongly differs in various organs of *Arabidopsis thaliana*.

Katrin Peters¹, Markus Nießen², Christoph Peterhänsel², Bettina Späth³, Angela Hölzle³,
Stefan Binder³, Anita Marchfelder³, Hans-Peter Braun^{1*}

¹ Institute of Plant Genetics, Faculty of Natural Sciences, Leibniz Universität Hannover,
30419 Hannover, Germany

² Institute of Botany, Faculty of Natural Sciences, Leibniz Universität Hannover, 30419
Hannover, Germany

³ Molekulare Botanik, Universität Ulm, 89081 Ulm, Germany

* Corresponding author: Tel.: +49 511 7622674; fax: +49 511 7623608

E-mail address: braun@genetik.uni-hannover.de

Abbreviations: OXPHOS, oxidative phosphorylation; BN-PAGE, blue native polyacrylamide
gel electrophoresis

Key words: oxidative phosphorylation, respiratory chain, OXPHOS complexes, mitochondria,
stoichiometry

Running title: Ratio of OXPHOS complexes in Arabidopsis

Abstract

In most studies, amounts of the protein complexes of the oxidative phosphorylation (OXPHOS) system in different organs or tissues are quantified on the basis of isolated mitochondrial fractions. However, efficiencies of mitochondrial isolations might differ with respect to tissue type due to varying efficiencies of cell disruption during organelle isolation procedures or due to tissue-specific properties of organelles. Here we report an immunological investigation on the ratio of the five OXPHOS complexes in different tissues of *Arabidopsis thaliana* which is based on total protein fractions isolated from five *Arabidopsis* organs (leaves, stems, flowers, roots and seeds) and from callus. Antibodies were generated against one surface exposed subunit of each of the five OXPHOS complexes and used for systematic immunoblotting experiments. Amounts of all complexes are highest in flowers (likewise with respect to organ fresh weight or total protein content of the flower fraction). Relative amounts of protein complexes in all other fractions were determined with respect to their amounts in flowers. Our investigation reveals high relative amounts of complex I in green organs (leaves and stems) but much lower amounts in non-green organs (roots, callus tissue). In contrast, complex II only is represented by low relative amounts in green organs but by significantly higher amounts in non-green organs, especially in seeds. In fact, the complex I – complex II ratio differs by factor 37 between callus and leaf, indicating drastic differences in electron entry into the respiratory chain in these two fractions. Results are confirmed by *in gel* activity measurements for the protein complexes of the OXPHOS system and comparative 2D blue native / SDS PAGE analyses using isolated mitochondria. We suggest that complex I has an especially important role in the context of photosynthesis which might be due to its indirect involvement in photorespiration and its numerous enzymatic side activities in plants.

Introduction

Mitochondria represent an important site for ATP production in most eukaryotic cells. Generation of ATP is carried out by the oxidative phosphorylation (OXPHOS) system, which consists of five multi-protein complexes (complex I – V) in the inner mitochondrial membrane as well as cytochrome c and ubiquinone (Hatefi 1985). Complexes I to IV form part of the electron transport chain (ETC) also termed respiratory chain. This chain catalyzes NADH oxidation by reduction of oxygen to water. The transport of electrons by complex I, III and IV is coupled to the translocation of protons from the matrix to the intermembrane space. The resulting proton gradient is used by the ATP-synthase (complex V) to produce ATP. The OXPHOS system in plants differs from the one in most mammals because some of its respiratory chain complexes have several extra protein subunits which introduce additional functions into these complexes. For example, complex I from plants includes more than 10 extra subunits (Klodmann and Braun 2011; Klodmann et al. 2010). Some of these proteins resemble known enzymes like gamma-type carbonic anhydrases (γ -CA) or L-galactone-1,4-lactone dehydrogenase (GLDH).

Furthermore, the plant OXPHOS system is especially multifaceted because it involves additional 'alternative' oxidoreductases. As a consequence, respiratory electron transport is highly branched in plants. Enzymes catalyzing these alternative pathways are type II NAD(P)H dehydrogenases and the alternative oxidase (AOX). Former ones can bypass complex I, whereas AOX bypasses complex III and IV (Rasmusson et al. 2008). The transport of electrons via these alternative pathways is not coupled with proton translocation across the inner mitochondrial membrane and therefore not directly involved in respiratory ATP production. The activity of the alternative electron pathway enzymes therefore results in a lower ATP production of the respiratory system and thus leads to a decrease of respiratory energy conservation (Rasmusson and Wallström 2010). This especially is important under high light conditions due to excess formation of reduction equivalents within chloroplasts (by photosynthesis) and mitochondria (by glycine to serine conversion in the context of photorespiration) (Rasmusson et al. 2008). In fact, expression of the genes encoding AOX and alternative NAD(P)H dehydrogenases is light regulated (Rasmusson and Escobar 2007). Thus, the alternative respiratory pathways are considered to be the basis for an overflow protection mechanism for the OXPHOS system which prevents production of reactive oxygen species (ROS) due to over-reduction of the ETC in the light. Besides the alternative

oxidoreductases also complex I is important with respect to ROS defence because mutations within complex I subunits affect the redox balance of the entire plant cell (Dutilleul et al. 2003a, 2003b)

Despite all information on components of the OXPHOS system in plants, little so far is known about the abundance and stoichiometry of the five OXPHOS complexes in this group of organisms. In contrast, several investigations on this subject were carried out for the respiratory chain complexes in mammals. It was shown that a number of genetic disorders result in defects in mitochondrial electron transfer (e.g. Alzheimer's and Parkinson's Diseases). Knowing the accurate stoichiometry of the OXPHOS complexes is necessary to develop structural models and to more extensively understand the relation of structure and function with respect to the mitochondrial OXPHOS system. Using various methods, several insights were obtained into the stoichiometry of the OXPHOS complexes in *Bos taurus* (Hatefi et al. 1985, Capaldi et al. 1988, Schägger and Pfeiffer 2001). Recently, different ratios for OXPHOS complexes were reported for various human tissues related to mutations within a mitochondrial elongation factor (Antonicka et al. 2006).

Here we report an investigation on the ratio of OXPHOS complexes in plants. To achieve reliable results, experiments were not carried out on the basis of isolated mitochondria but on the level of total protein fractions which were isolated from five different organs of *Arabidopsis* and from callus. A new set of antibodies was generated for immunological detection and quantification of the five OXPHOS complexes in plants. This study reports drastic differences in the ratio of OXPHOS complexes in different organs, especially with respect to complex I, which seems to be of special importance for photosynthesis.

Materials and Methods

Material

Organs were harvested from 7 weeks old *Arabidopsis thaliana* plants, sub-variety Columbia (Col-0). Plants were grown under long day conditions (16h light, 8h dark).

Suspension cell cultures of *Arabidopsis thaliana* (Col-0) were established as described by May and Leaver (1993). Cultures were maintained as outlined previously (Sunderhaus et al. 2006).

Phenolic extraction of proteins

Extraction of proteins from different organs of *Arabidopsis thaliana* was performed following the protocol of Hurkman and Tanaka (1986) modified by Colditz et al. (2004). Dried protein pellets were resuspended in 1x 'Sample buffer tricine' (10% (w/v) SDS, 30% (v/v) glycerol, 100 mM Tris, 4% (v/v) β -mercaptoethanol, 0.006% (w/v) bromophenol blue, pH 6.8) for Tricine-SDS-PAGE (Schägger and von Jagow 1987). Samples were either directly loaded onto a SDS-gel or stored at -80°C . Protein concentration of the fractions was determined by the use of the Bradford protein assay (Bradford 1976).

Native extraction of membrane proteins

Fresh plant material (5 g) was ground with a mortar on ice in 5 ml cold 'grinding buffer' (0.3 M mannitol, 50 mM Tris-HCl, 1 mM EDTA, 0.2 mM PMSF, pH 7.4) plus sea sand. Homogenate was filtered by the use of a gaze. Afterwards, samples were centrifuged for 1 minute at 70 xg at 4°C . Supernatants were transferred into new 2 ml-Eppendorf tubes and centrifuged again for 20 minutes at 18.300 xg at 4°C . Pellets were resuspended in 500 μl 'BN-solubilization buffer' (30 mM HEPES, 150 mM potassium acetate, 10% (v/v) glycerol, pH 7.4) plus 5% (w/v) digitonin), followed by a 20 minute incubation step on ice. Samples were centrifuged for 10 minutes at 18.300 xg at 4°C . Supernatants were transferred into new Eppendorf tubes and stored at -80°C or directly loaded onto a blue native gel (see below).

Gel electrophoresis procedures

One-dimensional blue native PAGE (1D BN-PAGE) and two-dimensional blue native / SDS PAGE (2D BN/SDS-PAGE) were performed according to Wittig et al. (2006). One-dimensional Tricine-SDS-PAGE was carried out as described by Schägger and von Jagow

(1987). Solubilization of mitochondrial protein was performed using digitonin at a concentration of 5 g/g mitochondrial protein (Eubel et al. 2003).

Western blotting

Proteins separated on polyacrylamide gels were blotted onto nitrocellulose membranes for antibody staining using the Trans Blot Cell from BioRad (Munich, Germany). Blotting was carried out as described by Krufft et al. (2001). Immunohistochemical stains were performed by using the VectaStain ABC Kit (Vector Laboratories, Burlingame, CA, USA) according to manufacturer's instructions.

For quantitative Western blotting experiments proteins were separated by SDS-PAGE using precast gels (Mini-Protean TGX™ 10% Tris-HCl, Bio-Rad, Munich, Germany). After separation, proteins were transferred on a nitrocellulose membrane using a liquid electroblotting apparatus (Mini-Protean Tetra Cell, Bio-Rad, Munich, Germany). The membrane was afterwards blocked in TTBS buffer (20 mM Tris-HCl pH 7.5, 50 mM NaCl, 0.05% Tween 20) with 1% BSA, and then incubated overnight in TTBS with an antibody directed against the 51-kDa subunit (complex I), the SDH 1-1 subunit (complex II), the alpha subunit of the mitochondrial processing peptidase (alpha MPP; complex III), the COX2 subunit (complex IV) or the beta subunit of complex V. After washing with TTBS, the membrane was incubated with a secondary monoclonal antibody directed against rabbit immunoglobulins. This secondary antibody is coupled to horseradish peroxidase (HRP) (Goat anti-Rabbit IgG HRP conjugate, Millipore, Billerica, MA, USA). HRP finally converts the 'Lumi-Light^{PLUS} Western Blotting Substrate' (Roche, Mannheim, Germany) into a fluorescence-emitting form. Light signals were recorded with the Lumi-Imager (Roche, Mannheim, Germany). Quantification of proteins was carried out using the AIDA Image Analyser Software (Raytest Isotopenmessgeräte GmbH, Straubenhardt, Germany).

Production of antibodies

Antibodies directed against the 51-kDa subunit (complex I), the SDH 1-1 subunit (complex II), the alpha subunit MPP subunit (complex III), the COX2 subunit (complex IV) and the beta subunit of complex V were produced as polyclonal peptide specific antibodies by Eurogentec (Seraing, Belgium) (for details see Supp. Tab. 1). The antibody against the 51-kDa subunit (complex I) was additionally produced as polyclonal anti-protein antibody by Eurogentec (Seraing, Belgium). For this approach, the 51-kDa subunit was over-expressed in *E. coli*, purified from inclusion bodies and separated by 1D Tricine-SDS-PAGE.

Gel staining procedures

Polyacrylamide gels were stained with Coomassie colloidal (Neuhoff et al. 1988, Neuhoff et al. 1990). *In gel* enzyme activity stains for mitochondrial respiratory chain complexes I, II and IV were carried out as described in Zerbetto et al. (1997) and Jung et al. (2000).

Results

Specificity of the IgGs directed against the OXPHOS complexes from *Arabidopsis*

This work aims to determine the ratio of the five OXPHOS complexes in different organs of *Arabidopsis thaliana*. An immunological approach was chosen for this purpose. In a first step, a new set of antibodies was generated. In order to produce antibodies with broad application spectra, surface exposed subunits were selected as targets for each complex (Supp. Fig. 1). This ensures their use under native and non-native (denaturing) conditions. For the immunization of rabbits, two surface exposed peptides of one subunit of each OXPHOS complex were selected. In the case of complex I, the over-expressed 51-kDa subunit was additionally used for immunization because the anti-peptide IgGs proved to have low quality (data not shown).

Immunoblotting experiments were carried out to test the specificity of the generated antibodies. For this approach, total protein of an *Arabidopsis* suspension culture was isolated by phenol extraction and resolved by 1D SDS-PAGE. Immunoblotting experiments revealed signals at the expected molecular mass (Fig. 1). Furthermore, all IgGs also specifically reacted with the target OXPHOS complexes resolved by native gel electrophoresis (Supp. Fig. 2).

Quantification of OXPHOS complexes in different tissues of *Arabidopsis*

After specificity had been verified for all IgGs, quantification of OXPHOS complexes was carried out by immunoblotting analyses. For this investigation, total protein fractions were isolated by phenol extraction from five *Arabidopsis* organs (leaves, stems, roots, flowers and seeds) and from callus. Gels were loaded with protein equivalent corresponding to an identical amount of fresh weight (FW). In a pre-experiment, isolated protein fractions were evaluated by 1D SDS-PAGE and Coomassie-staining (Fig. 2). As expected, the protein concentration varies depending on the analysed fraction. Protein concentration is highest in seeds and flowers. The seed storage proteins are visible in the seed fraction (20-40 kDa range) and the large subunit of RubisCO in the above 50 kDa range in the photosynthetically active fractions (leaves, stems and flowers).

Next, protein fractions from all organs were resolved by 1D SDS-PAGE and evaluated by immunoblotting. Again, defined protein amounts were loaded with respect to fresh weight of the plant material. Furthermore, defined dilutions were resolved for all fractions. Starting point of dilutions depended on the protein concentration of the tissue. Normally, dilution

series started with a total protein extract equivalent to 0.6 mg fresh weight. At least three technical replicates were performed for each sample and each complex. One representative set of Western blots for each complex and each organ is shown in Figure 3.

Results of all sets of Western blots were integrated to calculate relative quantities of the OXPHOS complexes in the different protein fractions. Quantification was based on chemiluminescence detection and evaluation was carried out using the AIDA Image Analyser Software (Raytest Isotopenmessgeräte GmbH, Straubenhardt, Germany). Since signals for all OXPHOS complexes were highest in flowers, their amounts in this fraction were defined to be 100%. Note: No statements on absolute quantities of OXPHOS complexes in Arabidopsis were obtained during this study because the intensity of the immune signals of the different antibodies most likely differs (the antibodies probably have differing specificities with respect to their target proteins).

A quantitative evaluation of the immune signals is shown in Figure 4. Results either refer to fresh weight of the analysed tissue (Fig. 4A, B) or to total protein amount (Fig. 4C, D). All complexes are present in highest amounts in flowers. However, decrease in amount with respect to flowers varies substantially for the individual complexes. Besides in flowers, abundance of complex I is especially high in leaves and very low in callus as well as root fractions. The opposite is true for complex II: It is relatively abundant in callus and seeds but of very low abundance in leaves. Complex V also is highly abundant in leaves. However, this was found to be an artefact because the IgG directed against the beta subunit of the mitochondrial ATP-synthase complex cross-reacts with the beta subunit of the chloroplast ATP-synthase (Supp. Fig. 3). Therefore, the data on complex V can not be quantitatively evaluated (chloroplast ATP synthase is even known to be present in non-green tissue (Green and Hollingsworth 1994). Variation in abundance is less severe for complexes III and IV within the investigated fractions.

Activity of OXPHOS complexes from different Arabidopsis organs

In order to investigate the activity of the OXPHOS complexes in various organs of Arabidopsis, total protein fractions were isolated under native conditions and resolved by one-dimensional blue native PAGE (Fig 5). Activity of OXPHOS complexes subsequently was visualized by *in gel* activity stains. As a control, isolated mitochondria from *Arabidopsis thaliana* cell cultures were resolved on the same gels (Fig. 5, left lane on each gel). As

expected, signals in the mitochondrial fractions were extremely high due to strong enrichment of the OXPHOS complexes.

Three bands are detectable by the activity stain for complex I (Fig. 5B). The two bands in the upper part of the gel represent complex I and the I+III₂ supercomplex. The signal in the low molecular mass range of the gel reveals activity of one of the alternative NADH-dehydrogenases. Complex I activity is detectable in all Arabidopsis organs but highest in flowers. Activity in leaves is detectable but seems not to be higher than in the other fractions. This indicates that increased amount of complex I in leaves not necessarily causes an increase in complex I activity. Interestingly, the I+III₂ supercomplex is of low abundance in flowers.

Complex II activity assay reveals two bands in the mitochondrial control fraction (Fig. 5C). The upper band represents the known 8-subunit version of complex II described before for higher plants (Eubel et al. 2003, Millar et al. 2004). The band in the lower part of the gel is a smaller form of complex II which only contains 4 subunits (Huang et al. 2010). Highest complex II activity was found in callus followed by the flower fraction. Activity in all other fractions was at the limit of detection.

Complex IV activity, apart from the control, is highest in the callus and flower fractions (Fig. 4D). Some high molecular mass complexes also are visible on the gels which represent complex IV containing respiratory supercomplexes described before (Eubel et al. 2004, Welchen et al. 2011).

We conclude that *in gel* activity of the three investigated OXPHOS complexes correlates with their relative amounts determined by immunoblotting. However, there are a few exceptions which indicate presence of unknown post-translational regulation mechanisms.

Abundance of OXPHOS complexes from mitochondria isolated from different Arabidopsis organs

Quantification of OXPHOS complexes was performed on the basis of total protein fractions and not on isolated mitochondria in order to avoid misinterpretations due to varying properties of mitochondria in the analysed tissues (e.g. variable densities which might result in differential isolation efficiencies). However, in a final experiment, quantity of OXPHOS complexes was compared by 2D BN/SDS-PAGE in two mitochondrial fractions isolated from (i) cell cultures and (ii) green leaves of Arabidopsis plants (Fig. 6). Although quantity of the resolved protein complexes were not evaluated by software tools, higher complex I abundance in the mitochondria from leaves is very obvious.

Correlation between protein abundance and gene expression

Does protein amount in different Arabidopsis tissues correlate with expression of the corresponding genes? To answer this question, the protein abundance data shown in Figure 3 were compared to expression data downloaded from the Arabidopsis eFP Browser (<http://bar.utoronto.ca/efp/cgi-bin/efpWeb.cgi>). In case isogenes are present for a subunit, mean values for expression were calculated for the analysis. The COX2 subunit was not included into the investigation because its transcription is not precisely known (COX2 is encoded by the mitochondrial genome). Since protein abundance in flowers was set as a standard, no conclusions can be drawn for this organ. The protein-transcript comparison reveals a striking correlation for the complex II subunit SDH1 (Fig. 7). In contrast, correlation for the other three subunits is low. We conclude that gene expression data not necessarily reflect abundance of proteins, which again indicates further levels of regulation during protein biosynthesis besides regulation of transcription.

Discussion

This study aims to investigate the ratio of OXPHOS complexes in various organs of *Arabidopsis thaliana*. Three different lines of evidence indicate drastic changes in complex I - complex II ratio: (i) quantitative immunoblotting using total protein fractions (ii) *in gel* activity stains using total protein fractions and (iii) analyses by 2D BN/SDS-PAGE using isolated mitochondria. Since highest amounts for all OXPHOS complexes were detected in flowers, their quantity within this fraction was set to be 100%. Complex I is especially abundant in green organs (leaves and stems) and shows a decrease in abundance in non-green fractions (roots and callus). In contrast, complex II is relatively abundant in callus and seeds but displays low amounts in leaves and stems. Figure 8 summarizes the differences in abundances of complexes I and II as obtained by quantitative immunoblotting. Also, abundances of complexes III and IV vary in different organs but variation is less extreme (Fig. 4). The complex I - complex II ratio is of special interest because these two complexes represent the main entrance points of electrons into the mitochondrial electron transport chain. However, electrons also enter the respiratory chain via the alternative oxidoreductases in plants. Dynamic changes in abundances of these enzymes were not part of the current investigation but are known to occur, e.g. due to light-regulated expression of their genes (Rasmusson et al. 2008).

The ratio of mitochondrial OXPHOS complexes extensively was analysed for other groups of organisms, especially in mammals (Hatefi 1985, Capaldi et al. 1988, Schägger and Pfeiffer 2001, Antonicka et al. 2006, Bernard et al. 2006). Initial investigations based on spectrophotometric quantification of prosthetic groups of the OXPHOS complexes revealed ratios for the complexes I, II, III, IV and V in the range of 1 : 2 : 3 : 6-7 : 3-5 in beef (Hatefi 1985). In a careful investigation, which employed spectrophotometric and electrophoretic-densitometric methods, Schägger and Pfeiffer (2001) basically confirmed these data and presented even more precise values on the ratios of the OXPHOS complexes in beef, which are 1.1 : 2.1 : 3 : 6.7 : 3.5. Benard et al. (2006) investigated the ratio of OXPHOS complexes in different rat tissues using various biochemical methods like immunological techniques as well as spectrophotometry. Ratios for complexes II, III and IV were found to be 1-1.5 : 3 : 6.5-7.5, which are consistent with the previous values published for beef. Using quantitative immunoblotting, strong differences with respect to the ratio of OXPHOS complexes were reported for human mitochondria from various tissues (Antonicka et al. 2006). All complexes

are highly abundant in muscle and heart, whereas complexes I, III, IV and V only show low abundance in liver and fibroblasts. The amount of complex II is almost the same for all tissues.

Until today, little is known about the ratio of OXPHOS complexes in plants. In contrast to results obtained for mammals, the abundances of complexes I, III, IV and V were estimated to be in a similar range in potato (Jänsch et al. 1996). Our current investigation, which is based on quantitative immunoblotting, reveals strong differences in the ratio of the protein complexes of the OXPHOS system in different organs of the model plant *Arabidopsis*. Although no data on the absolute ratios of the complexes were obtained (the antibodies used for this study most likely differ in specificity), relative differences are very clear, especially with respect to complexes I and II. Most strikingly, complex I is of high relative abundance in photosynthetically active organs (leaves, stems, flowers). It so far only was known that the alternative NAD(P)H dehydrogenases are up-regulated in the light.

Why complex I is especially important in the context of photosynthesis? There possibly are several reasons. The main function of complex I, re-oxidation of NADH in the mitochondrial matrix, is particularly essential in the light because additional NADH is formed by glycine to serine conversion during photorespiration. Indeed, NADH formed by photorespiration is the main substrate of the respiratory chain under high light, and not the NADH formed by the citric acid cycle like in mammalian systems (Tcherkez et al. 2008). Previous investigations on complex I mutants already revealed the importance of mitochondrial complex I for maintenance of the redox balance in leaves (Dutilleul et al. 2003a, 2003b). In addition, complex I of plant mitochondria is known to include side functions. Most notably, it includes five subunits very much resembling bacterial gamma-type carbonic anhydrases (reviewed in Braun and Zabaleta, 2007 and Klodmann and Braun, 2011). It was suggested that these enzymes form part of a pathway to recycle photorespiratory CO₂ for photosynthesis (Braun and Zabaleta 2007). This side function of complex I, although not experimentally proven, could well explain the special importance of complex I during photosynthesis. Finally, L-galactone-1,4 lactone dehydrogenase (GLDH), which catalyses the terminal step of ascorbate biosynthesis in plants, is associated with mitochondrial complex I. Ascorbate especially is needed in the chloroplast during photosynthesis for photoprotection (Apel and Hirt 2004). However, it so far was not shown that GLDH forms part of the fully assembled complex I in plants, but rather of its assembly intermediates (Millar et al. 2003, Pineau et al. 2008).

Therefore, the importance of complex I for ascorbate biosynthesis so far remains elusive. Further investigations will be necessary to fully understand the special importance of complex I in the context of photosynthesis.

Acknowledgements

This project was supported by the Deutsche Forschungsgemeinschaft (DFG), grant BR 1829/7-3.

References

- Antonicka, H., Sasarman, F., Kennaway, N.G., and Shoubridge, E.A. (2006). The molecular basis for tissue specificity of the oxidative phosphorylation deficiencies in patients with mutations in the mitochondrial translation factor EFG1. *Hum. Mol. Genet.* 15: 1835-1846.
- Apel, K., and Hirt, H. (2004). Reactive oxygen species: metabolism, oxidative stress, and signal transduction. *Annu. Rev. Plant Biol.* 55, 373-399.
- Benard, G., Faustin, B., Passerieux, E., Galinier, A., Rocher, C., Bellance, N., Delage, J.P., Casteilla, L., Letellier, T., and Rossignol, R. (2006). Physiological diversity of mitochondrial oxidative phosphorylation. *Am J Physiol Cell Physiol.* 291:1172-1182.
- Bradford, M.M. (1976). A rapid and sensitive method for the quantitation of microgram quantities of protein utilizing the principle of protein-dye binding. *Anal Biochem.* 72: 248-54.
- Braun, H.P. and Zabaleta, E. (2007). Carbonic anhydrase subunits of the mitochondrial NADH dehydrogenase complex (complex I) in plants. *Physiologia Plantarum* 129: 114-122.
- Capaldi, R.A., Halphen, D.G., Zhang, Y.Z., and Yanamura, W. (1988). Complexity and tissue specificity of the mitochondrial respiratory chain. *J. Bioenerg. Biomembr.* 20: 291-311.
- Colditz, F., Nyamsuren, O., Niehaus, H., Eubel, H., Braun, H.-P. and Krajinski, F. 2004. Proteomic approach: Identification of *Medicago truncatula* proteins induced in roots after infection with the pathogenic oomycete *Aphanomyces euteiches*. *Plant. Mol. Biol.* 55: 109-120.
- Dutilleul, C., Driscoll, S., Cornic, G., de Paepe, R., Foyer, C.H., and Noctor, G. (2003a). Functional mitochondrial complex I is required by tobacco leaves for optimal photosynthetic performance in photorespiratory conditions and during transients. *Plant Physiol.* 131: 264–275.
- Dutilleul, C., Garmier, M., Noctor, G., Mathieu, C., Chétrit, P., Foyer, C.H., and de Paepe, R. (2003b). Leaf mitochondria modulate whole cell redox homeostasis, set antioxidant capacity, and determine stress resistance through altered signaling and diurnal regulation. *Plant Cell.* 15: 1212-1226.
- Eubel, H., Jansch, L., and Braun, H.P. (2003). New insights into the respiratory chain of plant mitochondria. Supercomplexes and unique composition of complex II. *Plant Physiol.* 133: 274-286.
- Eubel, H., Heinemeyer, J., and Braun, H.P. (2004). Identification and characterization of respirasomes in potato mitochondria. *Plant Physiol.* 134: 1450-1459.
- Green, C.D. and Hollingsworth, M.J. (1994). Tissue-specific expression of the large ATP synthase gene cluster in spinach plastids. *Plant Mol. Biol.* 25: 369-376.
- Hatefi, Y. (1985). The mitochondrial electron transport and oxidative phosphorylation system. *Ann. Rev. Biochem.* 54: 1015-1069.
- Huang, S., Taylor, N.L., Narsai, R., Eubel, H., Whelan, J., and Millar, A.H. (2010). Functional and composition differences between mitochondrial complex II in *Arabidopsis* and

rice are correlated with the complex genetic history of the enzyme. *Plant Mol Biol.* 72: 331-342.

Hurkman, W. J. and Tanaka C. K. 1986. Solubilization of plant membrane proteins for analysis by two-dimensional gel electrophoresis. *Plant Physiol.* 81: 802-806.

Jänsch, L., Kruft, V., Schmitz, U.K., and Braun, H.P. (1996). New insights into the composition, molecular mass and stoichiometry of the protein complexes of plant mitochondria. *Plant J.* 9(3): 357-68.

Jung, C., Higgins, C.M., and Xu, Z. (2000). Measuring the quantity and activity of mitochondrial electron transport chain complexes in tissues of central nervous system using blue native polyacrylamide gel electrophoresis. *Anal Biochem.* 15: 214-223.

Klodmann, J., and Braun, H.P. (2011). Proteomic approach to characterize mitochondrial complex I from plants. *Phytochemistry* 72: 1071-1080.

Klodmann, J., Sunderhaus, S., Nimtz, M., Jänsch, L., and Braun, H.P. (2010). Internal architecture on mitochondrial complex I from *Arabidopsis thaliana*. *Plant Cell* 22: 797-810.

Krause, F., Reifschneider, N.H., Vocke, D., Seelert, H., Rexroth, S., and Dencher, N.A. (2004). "Respirasome"-like supercomplexes in green leaf mitochondria of spinach. *J Biol Chem.* 279: 48369-48375.

Kruft, V., Eubel, H., Jänsch, L., Werhahn, W., and Braun, H.P. (2001). Proteomic approach to identify novel mitochondrial proteins in *Arabidopsis*. *Plant Physiol.* 127:1694-710.

May, M.J., and Leaver, C.J. (1993). Oxidative stimulation of glutathione synthesis in *Arabidopsis thaliana* suspension cultures. *Plant Physiol.* 103: 621-627.

Neuhoff, V., Stamm, R., and Eibl, H. (1988). Clear background and highly sensitive protein staining with Coomassie Blue dyes in polyacrylamide gels: A systematic analysis. *Electrophoresis* 6: 427-448.

Millar, A., Mittova, V., Kiddle, G., Heazlewood, J., Bartoli, C., Theodoulou, F., and Foyer, C. (2003) Control of ascorbate synthesis by respiration and its implications for stress responses. *Plant Physiol* 133: 443-447.

Millar, A.H., Eubel, H., Jänsch, L., Kruft, V., Heazlewood, J.L., and Braun, H.P. (2004). Mitochondrial cytochrome c oxidase and succinate dehydrogenase complexes contain plant specific subunits. *Plant Mol Biol.* 56: 77-90.

Neuhoff, V., Stamm, R., Pardowitz, I., Arold, N., Ehrhardt, W., and Taube, D. (1990). Essential problems in quantification of proteins following colloidal staining with coomassie brilliant blue dyes in polyacrylamide gels, and their solution. *Electrophoresis* 11: 101-117.

Perales, M., Eubel, H., Heinemeyer, J., Colaneri, A., Zabaleta, E. (2005). Disruption of a Nuclear Gene Encoding a Mitochondrial Gamma Carbonic Anhydrase Reduces Complex I and Supercomplex I+III₂ Levels and Alters Mitochondrial Physiology in *Arabidopsis*. *J. Mol. Biol.* 350: 263-277.

- Pineau, B., Layoune, O., Danon, A., and De, P. (2008) L-galactono-1,4-lactone dehydrogenase is required for the accumulation of plant respiratory complex I. *J Biol Chem* 283: 32500–32505.
- Rasmusson, A.G., and Escobar, M.A. (2007). Light and diurnal regulation of plant respiratory gene expression. *Physiol. Plant.* 129: 57-67.
- Rasmusson, A.G., Geisler, D.A., and Møller, I.M. (2008). The multiplicity of dehydrogenases in the electron transport chain of plant mitochondria. *Mitochondrion* 8: 47-60.
- Rasmusson, A.G., and Wallström, S.V. (2010). Involvement of mitochondria in the control of plant cell NAD(P)H reduction levels. *Biochem. Soc. Trans.* 38: 661-666.
- Schägger, H. and von Jagow, G. (1987) Tricine-sodium dodecyl sulfate-polyacrylamide gel electrophoresis for the separation of proteins in the range from 1 to 100 kDa. *Anal. Biochem.* 166, 368-379.
- Schägger, H. and Pfeiffer, K. (2000). Supercomplexes in the respiratory chains of yeast and mammalian mitochondria. *EMBO J.* 19: 1777-1783.
- Schägger, H., and Pfeiffer, K. (2001). The ratio of oxidative phosphorylation complexes I-V in bovine heart mitochondria and the composition of respiratory chain supercomplexes. *J Biol Chem.* 276: 37861-37867.
- Sunderhaus, S., Dudkina, N., Jansch, L., Klodmann, J., Heinemeyer, J., Perales, M., Zabaleta, E., Boekema, E., and Braun, H.P. (2006). Carbonic anhydrases subunits form a matrix-exposed domain attached to the membrane arm of complex I in plants. *J. Biol. Chem.* 281: 6482-6488.
- Tcherkez, G., Bligny, R., Gout, E., Mathé, M., and Cornic, G. (2008). Respiratory metabolism of illuminated leaves depends on CO₂ and O₂ conditions. *Proc. Natl. Acad. Sci.* 105: 797-802.
- Welchen, E., Klodmann, J., and Braun, H.P. (2011). Biogenesis and Supramolecular Organization of the Oxidative Phosphorylation System in Plants. *Plant Mitochondria, Advances in Plant Biology* 1: 327-355.
- Wittig, I., Braun, H.P., and Schägger, H. (2006). Blue native PAGE. *Nat. Protoc.* 1: 418-428.
- Zerbetto, E., Vergani, L., and Dabbeni-Sala, F. (1997). Quantification of muscle mitochondrial oxidative phosphorylation enzymes via histochemical staining of blue native polyacrylamide gels. *Electrophoresis* 18: 2059-2064.

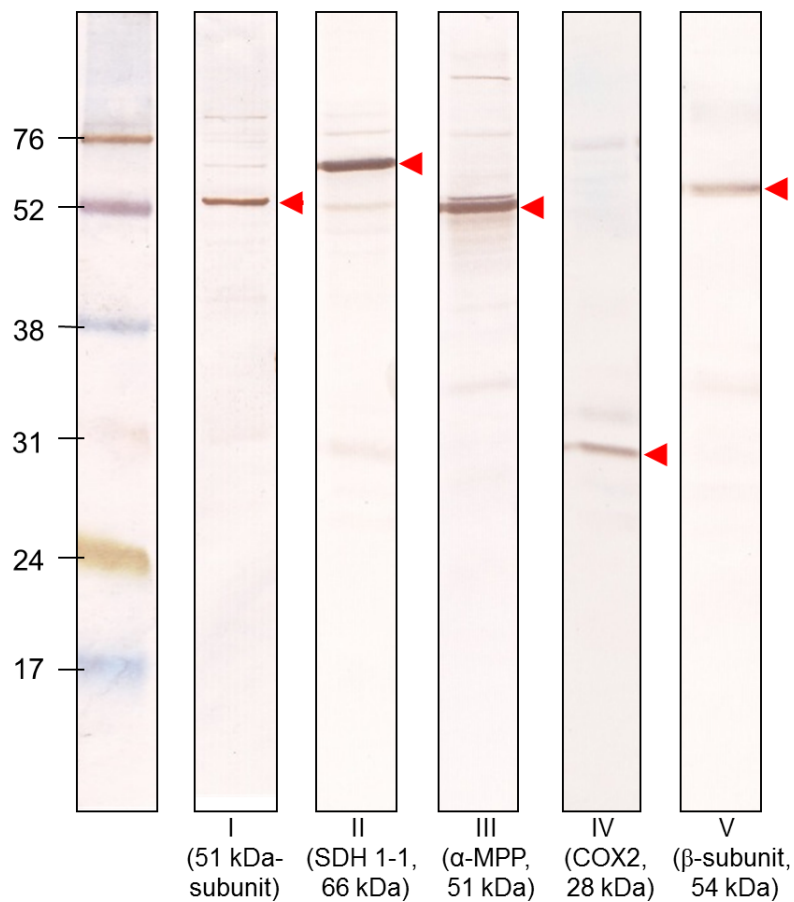
Figure 1:

Figure 1: IgG specificity. Total protein (extracted from 5 mg FW) of *Arabidopsis thaliana* Col-0 suspension cell culture was separated by SDS-PAGE and blotted onto nitrocellulose. Each Blot was incubated with an IgG (dil. 1:1000) directed against one subunit of one of the five OXPHOS complexes. Detection of immune signals was carried out by immunohistochemical staining using the Vectastain ABC kit (Vector Laboratories, Burlingame, CA, USA). The molecular masses of standard proteins (High-range Molecular Weight Rainbow Marker, GE Healthcare, Munich, Germany) are given on the left (in kDa), the target proteins of the antibodies and their molecular masses (without presequences) are given at the bottom of the blots (I, complex I; II, complex II; III, complex III, IV, complex IV; V, complex V). Red arrows indicate the expected immune signals.

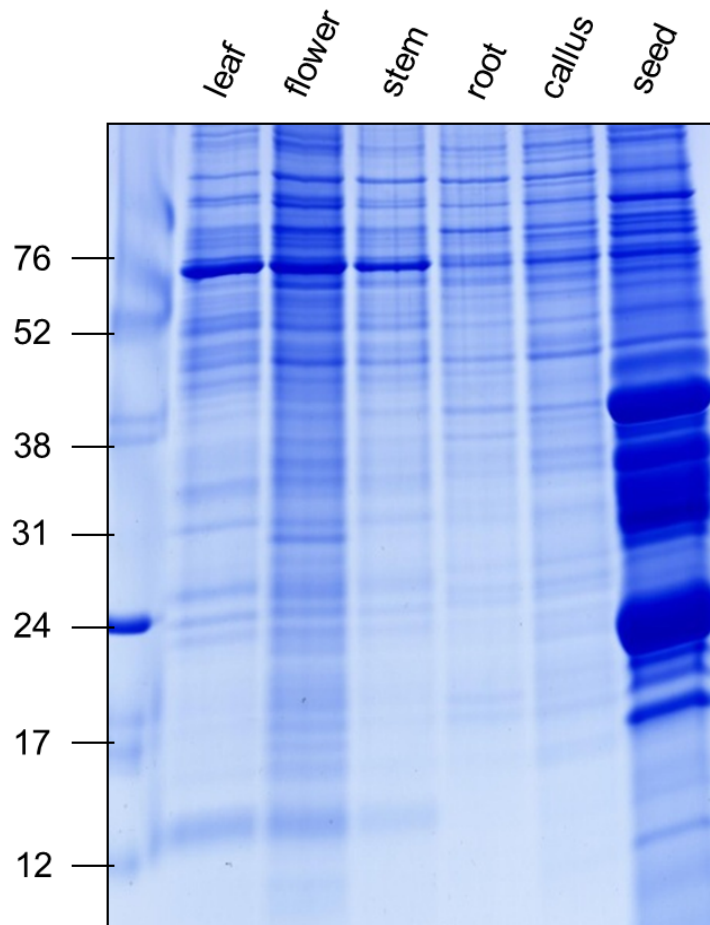
Figure 2:

Figure 2: Separation of total protein of different *Arabidopsis* organs. Total protein (extracted from 5 mg FW) of different tissues of *Arabidopsis thaliana* Col-0 was separated by SDS-PAGE and stained with Coomassie colloidal. The molecular masses of standard proteins (High-range Molecular Weight Rainbow Marker, GE Healthcare, Munich, Germany) are given on the left (in kDa), the different tissues are indicated above the gel.

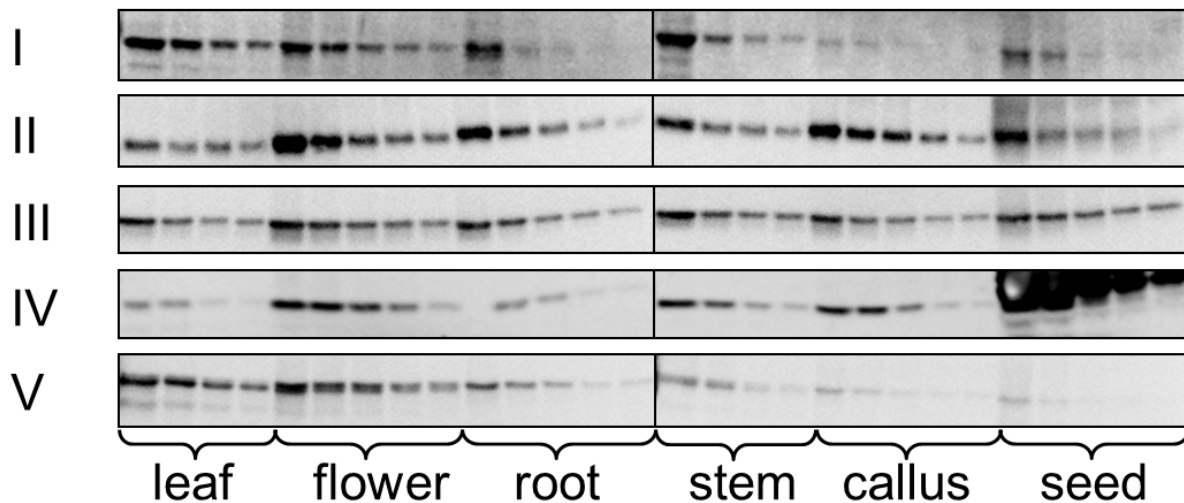
Figure 3:

Figure 3: Western blot analysis for quantification of OXPHOS complexes. Total protein from six different tissues of *Arabidopsis thaliana* Col-0 (extracted from 0.6 mg FW, respectively) was separated by 1D SDS-PAGE and subsequently transferred onto nitrocellulose membrane. Blots were incubated with specific IgGs directed against one subunit of each OXPHOS complex. The following dilutions of the extracted protein fractions were loaded onto the gel: leaf: 1/1, 1/2, 1/4, 1/8; flower: 1/2, 1/4, 1/8, 1/16, 1/32; root: 1/1, 1/2, 1/4, 1/8, 1/16; stem: 1/1, 1/2, 1/4, 1/8; callus: 1/2, 1/4, 1/8, 1/16, 1/32; seed: 1/2, 1/4, 1/8, 1/16, 1/32. Immune signals were detected by chemiluminescence using the Lumi-Imager (Roche, Mannheim, Germany). Subsequent quantification of signals was carried out using the AIDA Image Analyser Software (Raytest Isotopenmessgeräte GmbH, Straubenhardt, Germany). The identities of the OXPHOS complexes recognized by the five IgGs are given on the left, the identities of the analyzed protein fractions at the bottom of the blots. The very strong signal close to complex IV in seeds in some cases was visible on our blots and is due to a cross reaction of the COX2 antibody with one of the seed storage proteins.

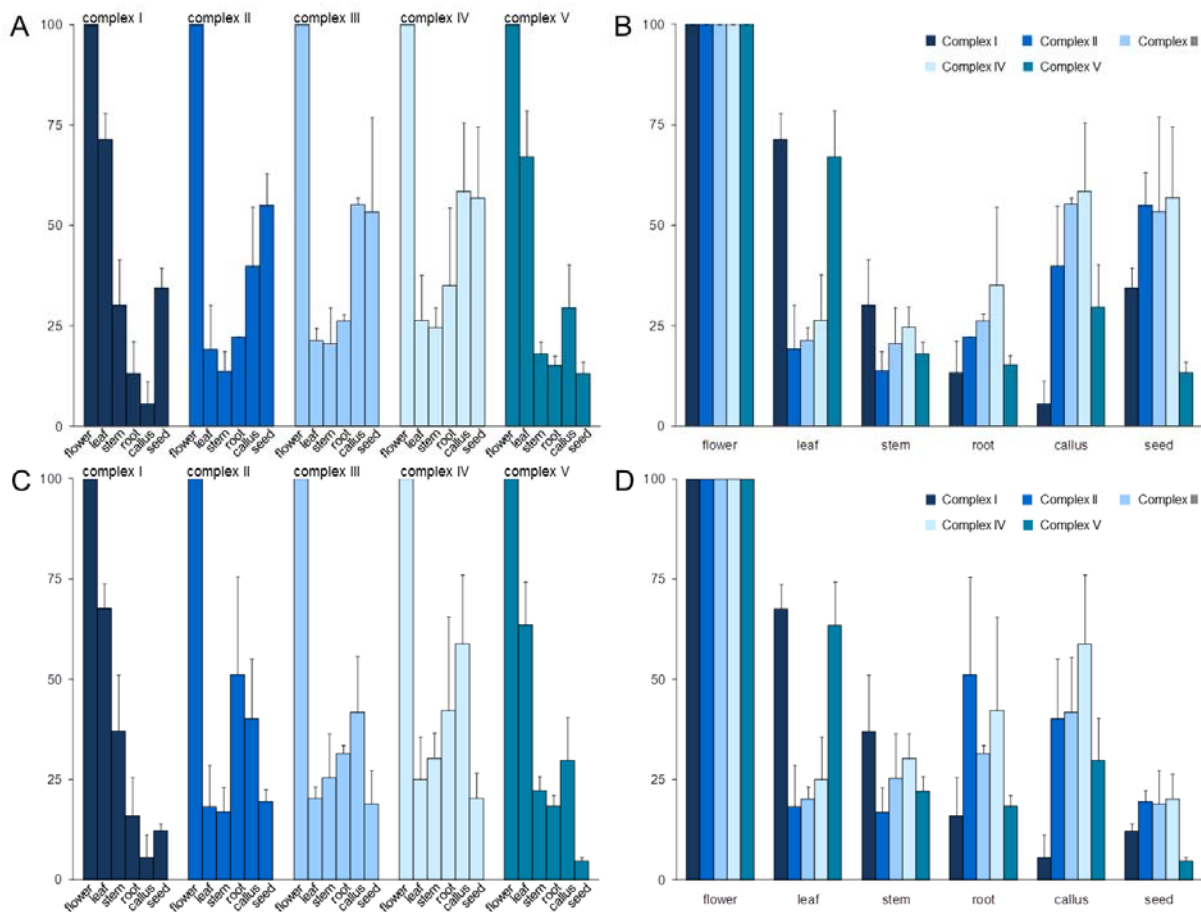
Figure 4:

Figure 4: Quantification of OXPPOS complexes in different tissues of *Arabidopsis thaliana*. Data are based on immune signals obtained by Western blotting (Fig. 3). Quantification of immune signals was carried out using the AIDA software (Raytest Isotopenmessgeräte GmbH, Straubenhardt, Germany). Results refer to three replicates for each tissue and each complex. Since all five OXPPOS complexes were most abundant in flowers, this tissue was set as a standard (100%). A: relative amounts of OXPPOS complex per FW (y-axis), analyzed tissue (x-axis). Identities of the complexes are given above the graph and by colors (complex I: dark-blue, complex II: middle-blue, complex III: light-blue, complex IV: very-light-blue, complex V: turquoise). B: Same as A, but data sorted according to tissues. The color code for the five complexes is the same as in part A of the figure. C and D: Same as A and B but quantification of OXPPOS complexes is related to total protein amount of the fractions.

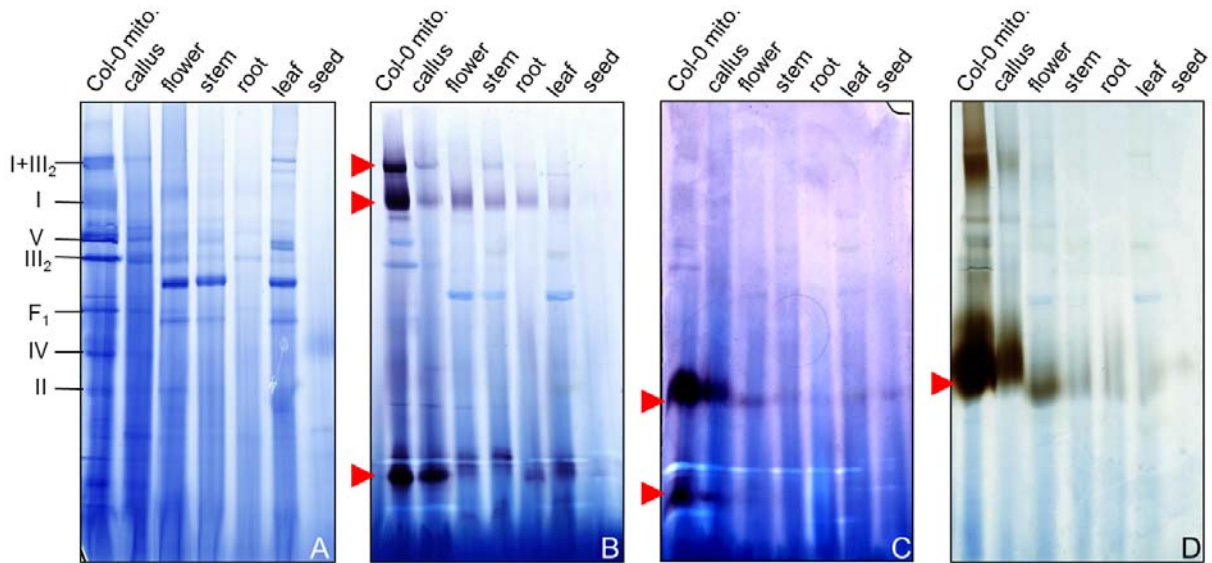
Figure 5:

Figure 5: In-gel activity of the OXPHOS complexes I, II and IV. Total membrane protein from different tissues of *Arabidopsis thaliana* Col-0 was extracted under native conditions (starting material: 285 mg FW, respectively) and separated by 1D BN-PAGE. Isolated mitochondria from *Arabidopsis thaliana* Col-0 suspension cell culture were taken as control (0.5 mg). Identities of resolved OXPHOS complexes are given on the left of the gels: I, complex I; V, complex V; III₂, dimeric complex III; F₁, F₁ part of complex V; IV, complex IV; II, complex II; I+III₂, supercomplex composed of complex I and dimeric complex III. Tissues are indicated above the gels. (A) Coomassie colloidal stain, (B) complex I activity stain, (C) complex II activity stain, (D) complex IV activity stain. Red arrows indicate activity signals.

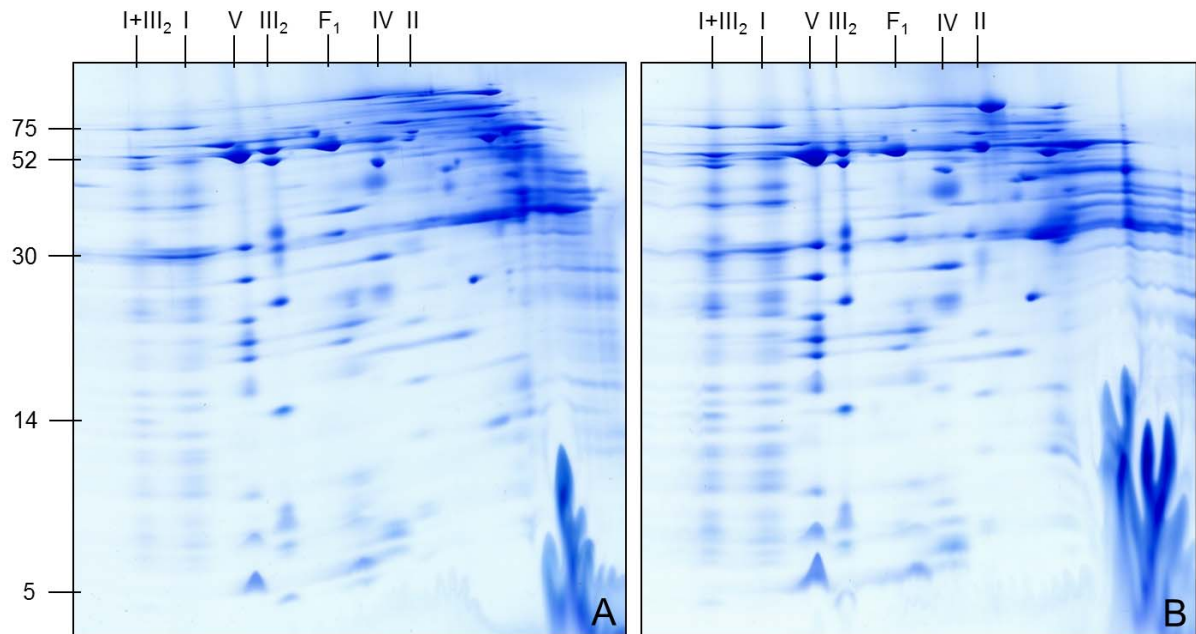
Figure 6:

Figure 6: Quantitative comparison of OXPHOS complexes in isolated mitochondria from suspension cell culture and green leaves. Total mitochondrial membrane protein (0.5 mg) from *Arabidopsis thaliana* Col-0 suspension cell culture (A) and *Arabidopsis thaliana* Col-0 green leaves (B) was separated by 2D BN/SDS-PAGE and stained with Coomassie colloidal. Identities of resolved protein complexes and supercomplexes are given above the gel (for nomenclature see Figure 5). The molecular masses of standard proteins (in kDa) are given on the left of the gel.

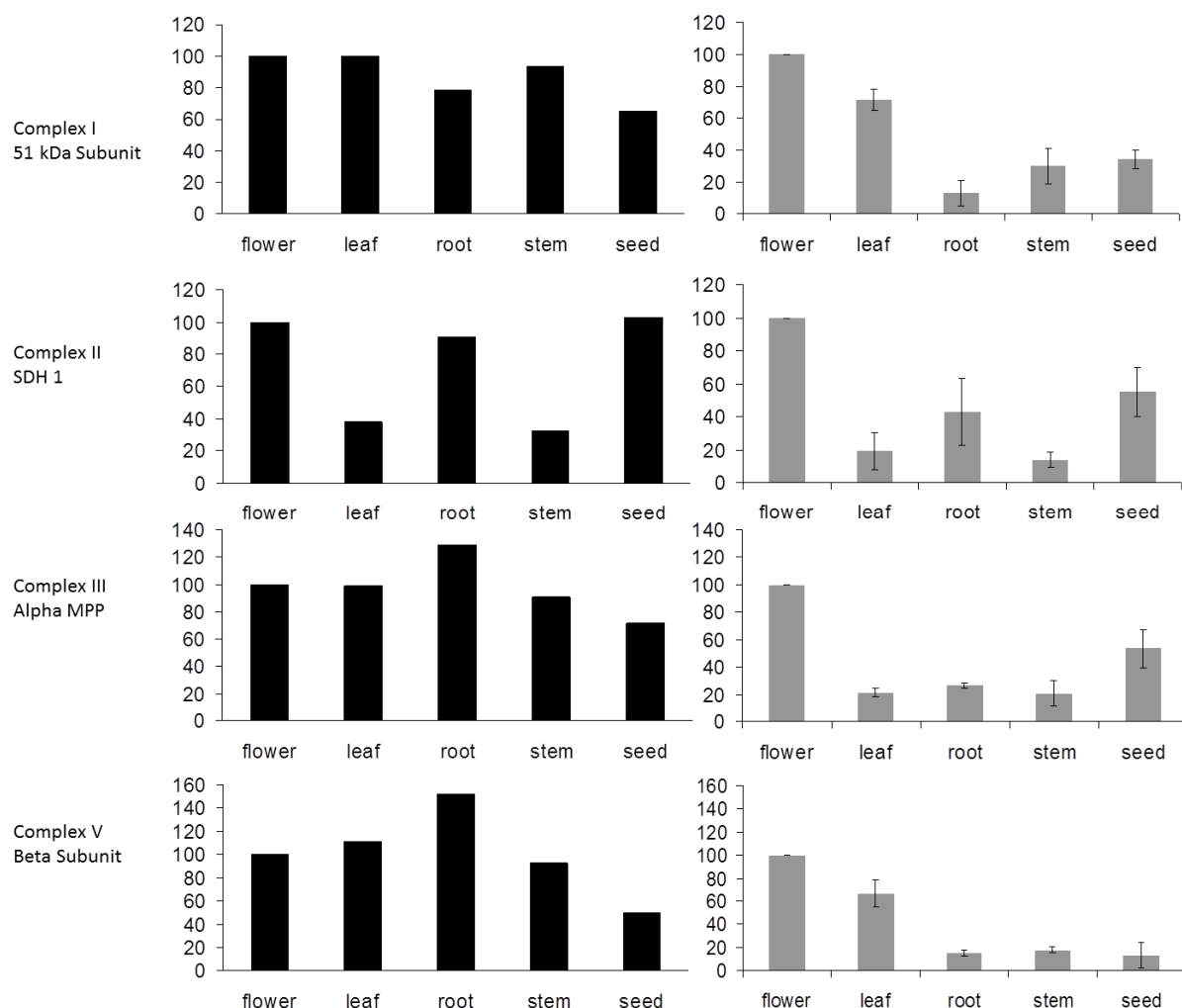
Figure 7:

Figure 7: Correlation of protein amount and expression of corresponding genes in different tissues of *Arabidopsis thaliana*. Relative amounts of four subunits of four different OXPHOS complexes per total protein were taken from Figure 4C. Corresponding gene expression data were downloaded from the Arabidopsis eFP Browser (<http://bar.utoronto.ca/efp/cgi-bin/efpWeb.cgi>). Expression data are given on the left (black bars), protein quantification data on the right (gray bars). For better comparability, expression data also are given as relative amounts of transcripts with respect to amounts in flowers. Identities of tissues are given below the bars, identities of the analyzed OXPHOS subunits on the left. Data for complex IV are not shown because expression of the gene encoding the COX2 subunit is not available from the database (COX2 is encoded on the mitochondrial genome).

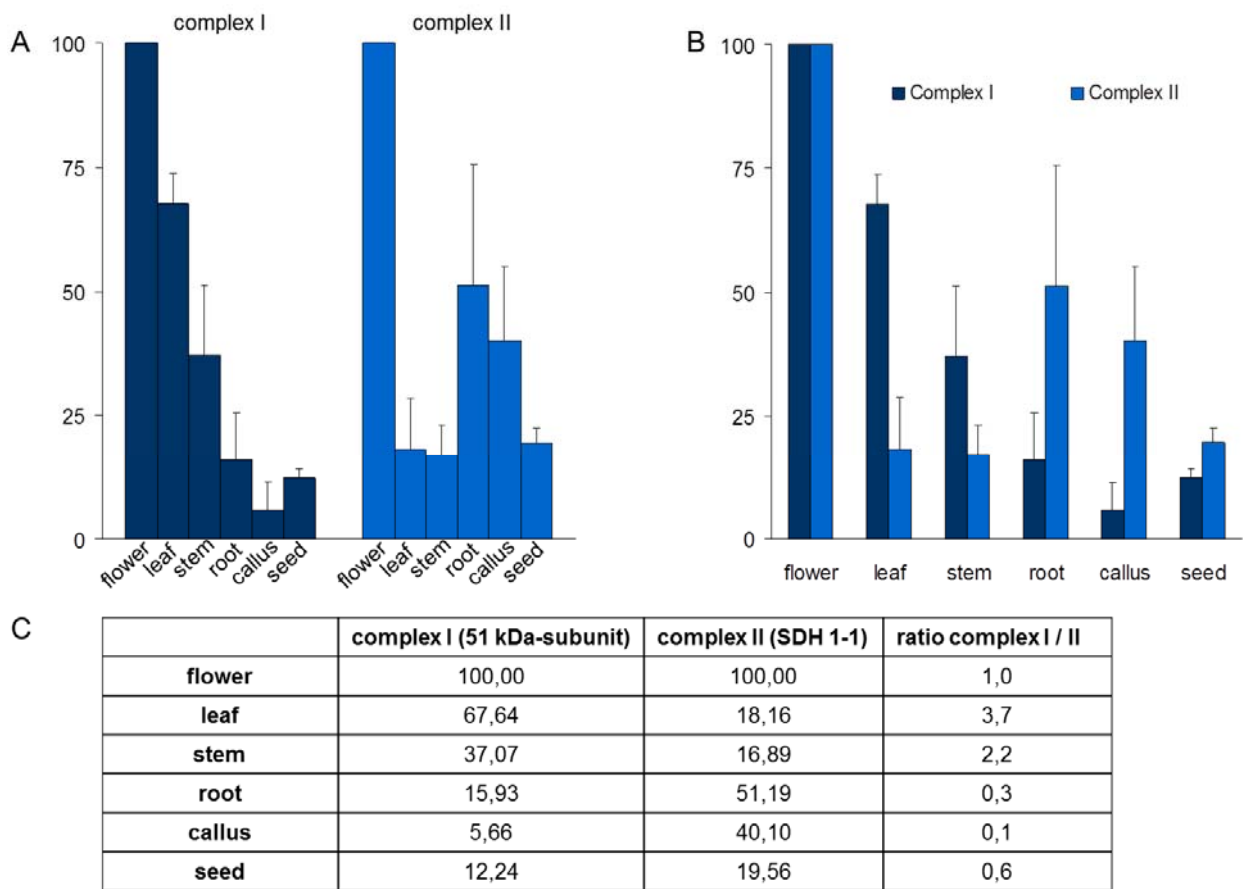
Figure 8:

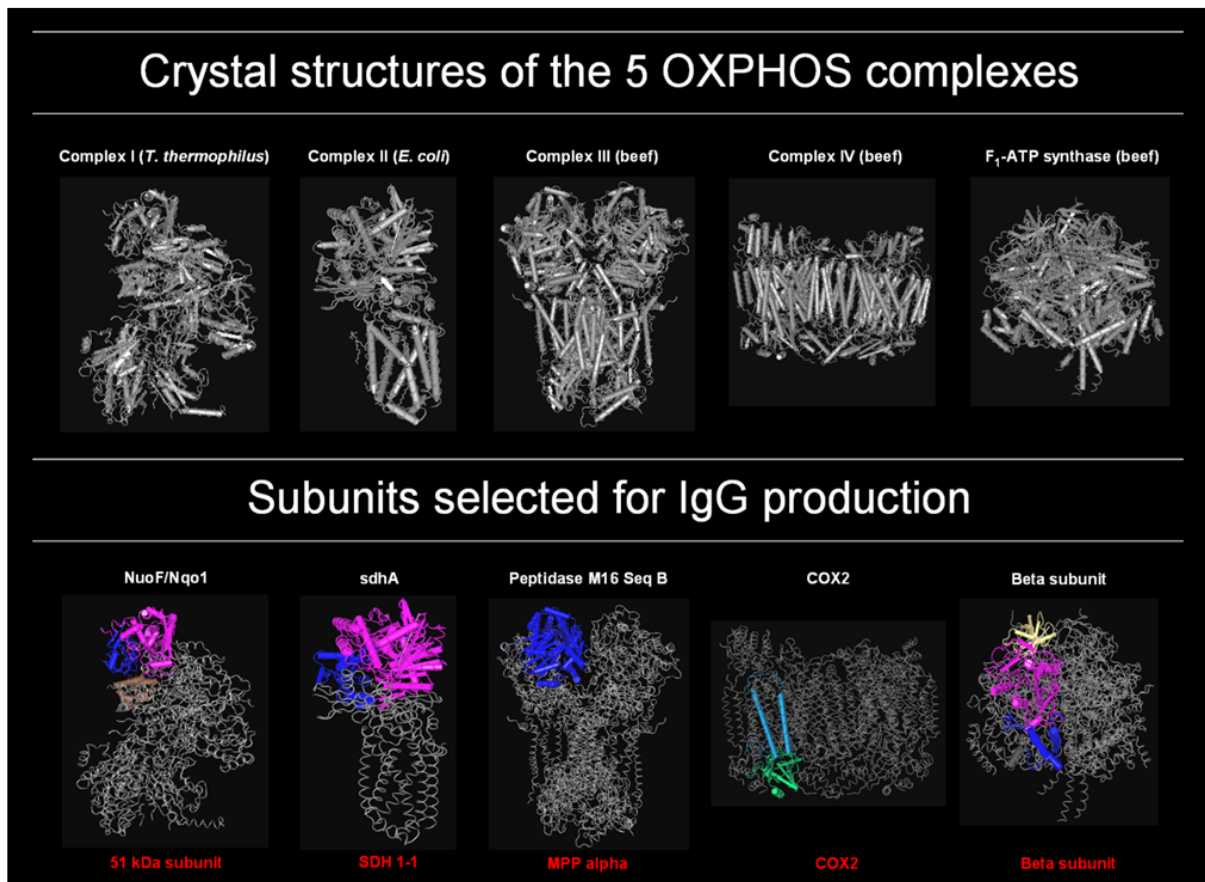
Figure 8: Complex I - complex II ratios in different tissues of *Arabidopsis thaliana* Col-0. Data represent a subset of results presented in Figure 4. A: relative amounts of complex I and II (reference: amounts in flowers) per total protein of the fraction. The analyzed tissues are given below the graphs. B: same as A, but data sorted by tissues. C: Complex I - complex II ratio in numbers.

Supp. Table 1

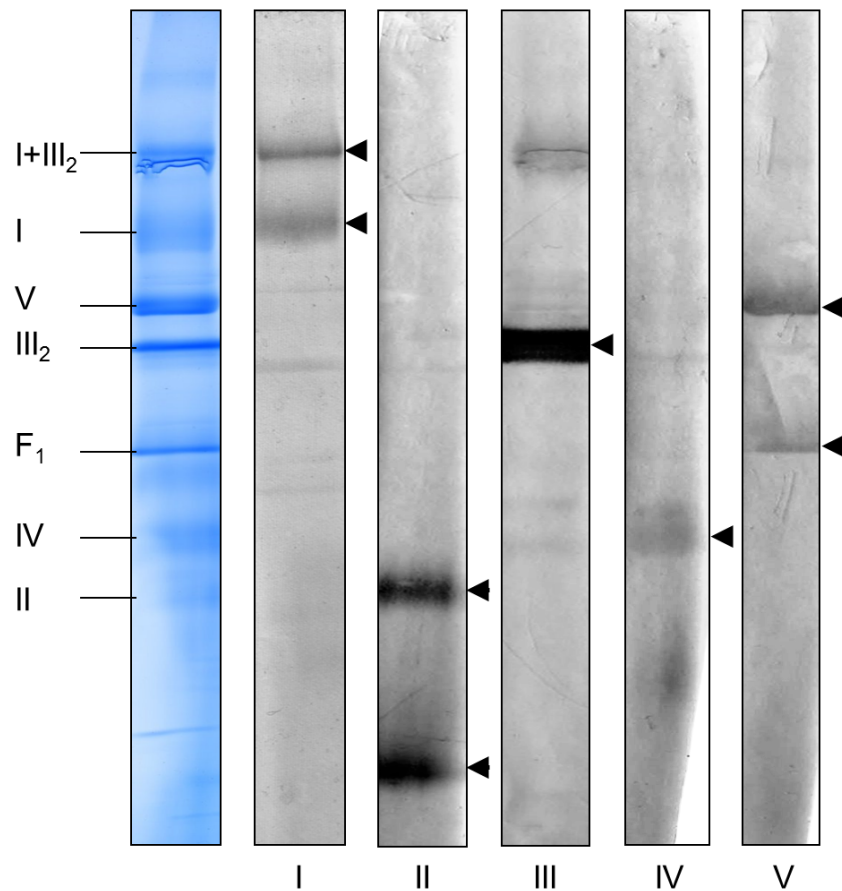
Complex (subunit)	Peptide 1	Peptide 2
Complex I (51-kDa subunit)	EMKKSGLRGRGGAGF	GAMKRGDWHRTKDLV
Complex II (SDH 1-1)	CANRVAEISKPGEKQK	LDDIEDTFPPKARVY
Complex III (alpha-MPP)	TYGERKPVQFLKSV	VLAVPSYDTISSKFR
Complex IV (COX2)	YGSRVSNQLIPQTGEA	VEAVPRKDYGSRVS
Complex V (beta-subunit)	GVGERTREGNDLYRE	EVVAKAEKIAKESAA

Supp. Table 1: Peptide sequences for the generation of IgGs. Surface exposed peptides were chosen. Synthesis of peptides was performed by Eurogentec (Seraing, Belgium). Peptides were coupled to KLH and a mix of both peptides for each complex subunit was used for the immunization of rabbits. The immunization protocol includes three boosts with the peptide-mix.

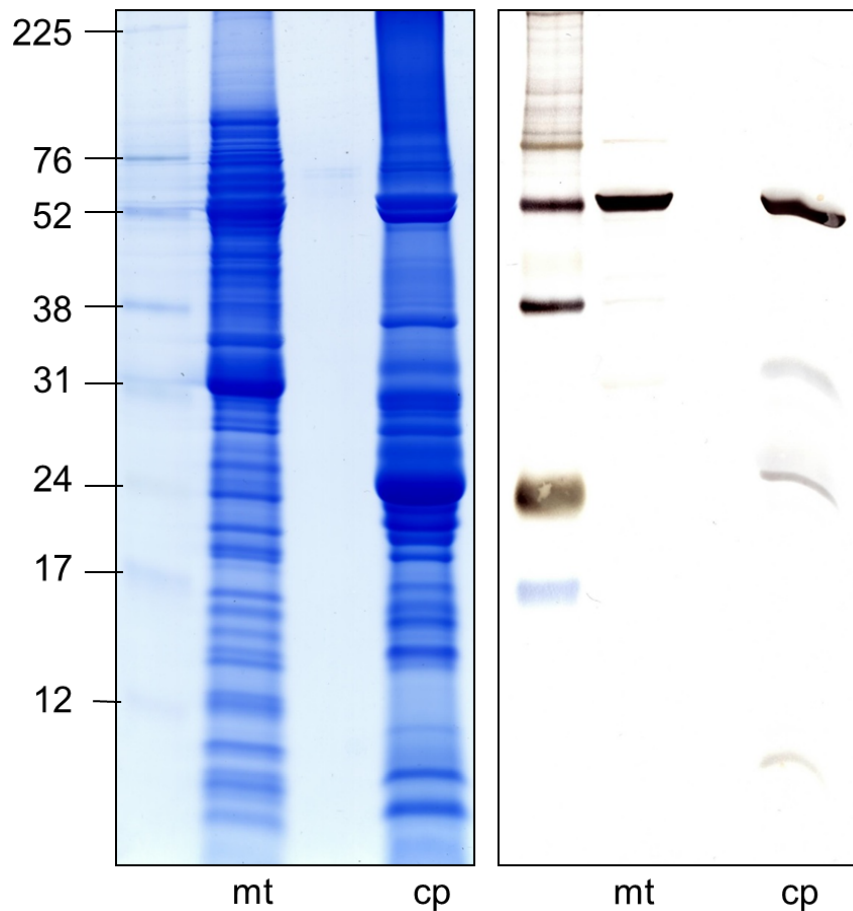
Supp. Figure 1:



Supp. Figure. 1: Crystal structures of the five OXPHOS complexes and the selected subunits for IgG production. The upper part of the figure shows the crystal structures of the 5 OXPHOS complexes from different species (data taken from the crystal structure database at <http://www.ncbi.nlm.nih.gov/sites/entrez?db=structure>. Accessions: NuoF/Nqo1: 2FUG; sdhA: 1NEK; peptidase M16 Seq B: 1PP9; COX2: 2OCC; beta subunit ATP-synthase: 1BMF). In the structures below the selected subunits for IgG production are colored. These subunits were over- expressed in *E. coli*. Peptides for the production of peptide specific antibodies were chosen with regard to their surface exposure to increase prospects of antigen-IgG interactions under native conditions. The names of the corresponding subunits in *Arabidopsis thaliana* are given in red at the bottom of the figure.

Supp. Figure 2:

Supp. Figure. 2: Specificity of the generated OXPHOS IgGs under native conditions. Total membrane protein (330 μ g) of isolated mitochondria from *Arabidopsis thaliana* Col-0 suspension cell cultures was separated by one-dimensional blue native PAGE. Western blots were incubated with IgGs (dil. 1:1000) directed against one subunit of each OXPHOS complex (for identities of subunits see supp. Fig. 1). Detection of immune signals was carried out by immunohistochemical staining using the Vectastain ABC kit (Vector Laboratories, Burlingame, CA, USA). Identities of the OXPHOS complexes are given on the left on the Coomassie stained reference gel (for nomenclature see figure 5). The target OXPHOS complexes of the five immune reactions are given below the blots, respectively. Furthermore, immune signals are indicated by arrows.

Supp. Figure 3:

Supp. Figure. 3: The IgG directed against the beta subunit of the mitochondrial ATP-synthase (complex V) cross-reacts with ATP-synthase from chloroplasts. Total protein of isolated mitochondria ('mt', 5 mg) from *Arabidopsis thaliana* Col-0 suspension cell cultures and isolated chloroplasts ('cp', 50 mg) from *Arabidopsis thaliana* Col-0 plants were separated by one-dimensional SDS-PAGE. The reference gel on the left was stained with Coomassie colloidal. The Western blot on the right was incubated with the IgG directed against the beta subunit of mitochondrial ATP-synthase (dil. 1:1000). Detection of immune signals was carried out by immunohistochemical staining using the Vectastain ABC kit (Vector Laboratories, Burlingame, CA, USA). The molecular masses (in kDa) of standard proteins (High-range Molecular Weight Rainbow Marker, GE Healthcare, Munich, Germany) are given on the left.

Chapter 3

3 Supplementary discussion and outlook

In this supplementary discussion, the structure as well as possible functions of OXPHOS complexes and supercomplexes will be discussed against the background of a highly branched electron transport chain in plants. In the very end of this thesis, the outlook will present promising approaches, which were beyond of the scope of this thesis and which might contribute towards a more profound understanding of the plant OXPHOS system.

3.1 The highly branched electron transport chain of plant mitochondria

A deeper knowledge of the mitochondrial respiratory chain is of crucial importance since it is known from mammals that disorders concerning this part are leading to severe diseases, e.g. Alzheimer's and Parkinson's disease in humans. Also for plants, the recent state of knowledge shows that the mitochondrial OXPHOS system has more functions besides electron transfer and oxidative phosphorylation. From this point of view, it is very important to get a complete characterization of the OXPHOS system with all its structural and functional specialties in plants, because this will result in a more detailed understanding of the interaction patterns of different pathways in plants under defined conditions. In contrast to other organisms, the electron transport chain in plants is highly branched, due to the existence of alternative oxidoreductases (type II NAD(P)H dehydrogenases, AOX) and other enzymes (GLDH, ETFQ-OR, G3P) acting as additional electron entry points into the respiratory chain.

In their investigation of supercomplexes in plant mitochondria, Eubel et al. (2003) were able to show that neither AOX nor the alternative NAD(P)H dehydrogenases form part of any supercomplex. However, they hypothesized that formation of the I+III₂ supercomplex might play a role in regulation of alternative respiration in a way that the I+III₂ supercomplex reduces access of AOX to its substrate ubiquinol by channelling electrons directly from complex I via UQ to complex III₂ within the supercomplex. Following the hypothesis of Eubel et al. (2003) would mean that the more I+III₂ supercomplex formation exists, the less AOX activity should occur and *vice versa*. Indeed, there are several lines of evidence indicating the existence of a direct electron channelling: (i) flux control experiments (Lenaz and Genova 2009), (ii) X-ray structure of the matrix arm of complex I (Sazanov and Hinchliffe 2006) and single-particle EM data for the I+III₂ supercomplex (Dudkina et al. 2005), which display a close proximity of the ubiquinone reduction and ubiquinol oxidation sites in the supercomplex. Even if direct electron channelling does not occur in the supercomplex, the transfer of ubiquinol from complex I to complex III₂ might be favoured because of potentially lower diffusion distances. For yeast, it

was reported by Heinemeyer et al. (2007) that formation of the III₂+IV₁₋₂ supercomplex optimizes electron transport between these two complexes. This was also shown for potato mitochondria by Lenaz and Genova (2009), who also suggested that supercomplex formation might limit the generation of ROS.

In 2010, Sunderhaus et al. initiated a study on the supramolecular structure of the OXPHOS system in the thermogenic tissue of *Arum maculatum*, which is known to produce large amounts of AOX for heat production during pollination in the spadix. Accordingly, the electron channelling assumption of Eubel et al. (2003) would predict low amounts of I+III₂ supercomplex. In contrast to this, Sunderhaus et al. (2010) reported that the respiratory chain in *Arum maculatum* differs from the one in *Arabidopsis thaliana* in a way that no monomeric complex I could be detected. Complex I is only present in the I+III₂ supercomplex. Furthermore, supercomplexes containing complex IV could be shown for *Arum maculatum*, even though only in low abundances, but not for *Arabidopsis*. As already reported by Eubel et al. (2003), also Sunderhaus et al. (2010) were able to show that AOX does not form part of any OXPHOS complex or supercomplex and no connection between the amounts of I+III₂ supercomplex and AOX activity was detected. Hence, they concluded, that supercomplex formation does not affect the activity of alternative respiration. This might also invalidate the assumption that electrons are directly channelled, via UQ, between complex I and complex III₂ within the supercomplex.

Thus, not only the occurrence of electron channelling is disputable, but the question if OXPHOS complexes and alternative respiratory enzymes are using common UQ pools also remains unsolved. Dudkina et al. (2005) reported that there might be an UQ pool in the complex III₂-containing supercomplex. On the other hand, Rasmusson et al. (2008) pointed out that the use of different UQ pools seems more reliable for the case that there is no direct channelling of electrons within supercomplex formation.

Although there is no evidence that the I+III₂ supercomplex regulates alternative respiration, it is known that complex I is involved in maintaining the redox balance during photosynthesis. Dutilleul et al. (2003a) investigated a cytoplasmic male-sterile *Nicotiana sylvestris* mutant (CMSII) which lacks functional complex I. They were able to show that the CMSII mutant has an increased alternative respiration via NADH dehydrogenases and AOX as well as modified abundances and activities of several antioxidant enzymes. This study led the authors to the statement that the loss of functional complex I induces antioxidant crosstalk within the cell and readjustment of organelle metabolism in order to maintain the cellular redox balance. Hence, it can be deduced that complex I plays an important role for the redox balance under regular

photosynthetic conditions and that the absence of complex I forces the cell to modulate enzymatic activity in order to keep the redox balance stable.

Such an effect could also be demonstrated by Dutilleul et al. (2003b). By investigating the role of mitochondrial complex I in leaves using the same CMSII mutant the following conclusions were drawn: (i) Complex I plays an important role in photorespiratory metabolism *in vivo*. (ii) Mitochondrial complex I is required for optimal photosynthetic performance. (iii) Complex I is necessary to avoid redox disruption of photosynthesis when leaf mitochondria have to oxidize simultaneously respiratory and photorespiratory substrates. Both studies (Dutilleul et al. 2003a, Dutilleul et al. 2003b) revealed a necessity of mitochondrial complex I for the maintenance of an appropriate redox balance in leaves. This is especially true during phases of adjustment of the photosynthetic system like transitions or decreased intercellular CO₂ that occur during the onset of drought.

These findings are in line with the data reported in section 2.4, in which the ratio of OXPHOS complexes was investigated in different tissues of *Arabidopsis thaliana*. Complex I was found to be highly abundant in green organs (leaves and stems) but less abundant in non-green tissue (callus and seeds). This led to the suggestion that complex I might have further light-dependent side functions besides its participation in electron transport and proton translocation. This is supported by the findings of Dutilleul et al. (2003a, 2003b) on the importance of complex I in processes of photosynthesis, photorespiration and maintenance of cell redox balance.

Since evidence was adduced for complex I being involved in maintaining the cell redox balance, the upcoming question again is: What about the potential role of the I+III₂ supercomplex in this regulatory mechanism? The hypothesized function of this supercomplex, the regulation of alternative respiration, could not be proven so far, but there are several hints which indicate a role of this supercomplex in redox balance.

(i) First, the I+III₂ supercomplex is very abundant in higher plants like *Arabidopsis thaliana* (Dudkina et al. 2005), *Zea mays* (Peters et al. 2008), *Solanum tuberosum* (Bultema et al. 2009) and *Arum maculatum* (Sunderhaus et al. 2010) but of lower abundance in mammalian mitochondria (Eubel et al. 2004b). In mammals and yeast supercomplexes containing complex IV (I+III+IV in various amounts of the individual complexes) are mainly existent (Dudkina et al. 2008), whereas in plants these larger supercomplexes are rarely detectable (Eubel et al. 2004a, Eubel et al. 2004b, Krause et al. 2004, Dudkina et al. 2006a, Sunderhaus et al. 2010). The fact that the I+III₂ supercomplex mainly exists in plants, together with the knowledge that the alternative oxidoreductases (alternative NAD(P)H dehydrogenases and AOX) are plant specific lead to the assumption that, indeed, the I+III₂ supercomplex might play a role in the

context of alternative respiration. Although it could not be proven so far that the supercomplex regulates alternative respiration, an interaction of alternative oxidoreductases and the I+III₂ supercomplex would be perfectly in line with the study of Sunderhaus et al. (2010). The authors were able to show that in *Arum maculatum* spadix mitochondria, which are known to have an extremely high rate of alternative respiration, complex I is completely absent in its monomeric form but is existent in the I+III₂ supercomplex.

(ii) Furthermore, photosynthesis always comes along with photorespiration. Especially under high light conditions, there is excess formation of reduction equivalents within chloroplasts (by photosynthesis) and mitochondria (by glycine to serine conversion in the context of photorespiration). If the previous hypothesized direct electron channelling between complex I and complex III₂ within the supercomplex exists, this would result in a higher respiration rate due to a faster electron transfer because of the reduced diffusion distance between both complexes (Dudkina et al. 2005). This would explain the high amounts of I+III₂ supercomplex formation in plant mitochondria in contrast to other organisms which do not carry out photosynthesis. Additionally, this assumption is supported by the finding that mitochondria from green leaves, where most of the photosynthesis in plants takes place and therefore high amounts of reduction equivalents are present, contain clearly more I+III₂ supercomplex than mitochondria isolated from non-green callus tissue (section 2.4).

(iii) Further evidence was given by Lenaz and Genova (2009), who suggested a possible role of supercomplexes in limiting ROS formation. Complex I is known to be one of the major sources for ROS formation in mitochondria. There is evidence that ROS are generated due to the reaction of complex I bound FMN with oxygen (Galkin and Brandt 2005). Hence, Lenaz and Genova (2009) hypothesized that FMN only becomes exposed to oxygen when complex I is dissociated from complex III₂. In their study they also suggest that complex I might undergo conformational changes when associated with other complexes and thereby avoid FMN to react with oxygen.

Taking this knowledge into account, conclusions can be drawn which are going beyond the statements of Dutilleul et al. (2003a, 2003b). The investigated CMSII mutant not only lacks functional complex I but also the I+III₂ supercomplex (Pineau et al. 2005). Since complex I in its monomeric form is a major source of ROS formation, as mentioned above, it makes sense that up to 90% of complex I is associated with dimeric complex III forming a supercomplex structure, which is known to limit ROS generation. However, in the CMSII mutant complex I is absent and hence, one major source of ROS is discarded. The higher abundance of alternative oxidoreductases, which was determined by Dutilleul et al. (2003a) in the CMSII mutant, is due

to an increase of NADH, which occurs because of the lack of complex I and the I+III₂ supercomplex, which normally oxidises the NADH. Concerning NADH oxidation, again the I+III₂ supercomplex seems to be more important than complex I because oxidation of NADH within the supercomplex structure is supposed to be enhanced due to reduced diffusion distances between the single complexes (Dudkina et al. 2005). Therefore, it is questionable if the contribution to optimized photosynthesis (including photorespiratory metabolism) and cell redox balance really depends on complex I or if it is more likely the I+III₂ supercomplex which is responsible for these regulatory mechanisms.

(iv) As a last point, further evidence is given by a study of Perales et al. (2005) in which a complex I mutant lacking CA2 (Δ At1g47260) was investigated. As already mentioned in section 1.4, CAs are suggested to be involved in CO₂ distribution between mitochondria and chloroplasts. This process is especially important under conditions resulting in high photorespiration rates. Therefore, CAs can also be considered to play a role in optimizing photosynthetic processes. Perales et al. (2005) were able to show that lack of CA2 results in a serious decrease of complex I abundance. Additionally, also the I+III₂ supercomplex is extremely decreased. If this supercomplex has another important functional role besides the hypothesized ones, remaining complex I amounts in the CA2 mutant should be existent in the supercomplex in order to keep its function. Since this is obviously not the case in this mutant, it can be assumed that the I+III₂ supercomplex is most probably somehow involved in optimizing photosynthetic processes and stabilizing cell redox balance.

All this evidence indicates a functional role of the I+III₂ supercomplex in processes related to alternative respiration, optimizing photosynthetic processes, stabilizing cell redox balance and preventing ROS formation. Nevertheless, more investigations on the potential functions of this supercomplex are necessary.

However, besides the previous suggested function of supercomplex formation in the regulation of alternative respiration, the necessity of supercomplexes for the assembly and stability of individual components was determined. Evidence exist that complex I is necessary for the presence of fully assembled complex III in human mitochondria (Ugalde et al. 2004). Other studies reveal that an absence of assembled complex III results in a loss of complex I in human mitochondria confirming a structural dependence of these two complexes (Blakely et al. 2005). And also in mouse cells complex III was found to be responsible for the stability of complex I (Acín-Pérez et al. 2004). Furthermore, it was reported that complex IV is important for complex I assembly in fibroblasts (Diaz et al. 2006). These functional roles of supercomplexes

would also explain why activity of the I+III₂ supercomplex is also detectable in non-photosynthetically active tissues like callus (section 2.4).

3.2 Outlook

This thesis could reveal new insights into structure and function of the respiratory chain in plants. In order to achieve a complete characterization of the OXPHOS system, a substantial investment of additional work is required. Many questions concerning structure and function of the respiratory chain complexes still remain unanswered. Especially in plants this topic is much more complicated than in other organisms due to the plant specific extra subunits, which are present in most respiratory complexes. Individual complexes participate in electron transport and oxidative phosphorylation but additionally fulfil supplementary functions, like complex I, which was shown to be involved in whole cell redox balance. The functions of the supercomplexes are not entirely solved so far and also the formation of supercomplexes to higher oligomeric structures needs further investigation. In the following section, some approaches will be outlined, which could contribute to a deeper understanding of the OXPHOS system.

Structural investigations of respiratory chain complexes were done by X-ray crystallography. Unfortunately, this was performed only for complexes from bacteria (*Escherichia coli*, *Thermus thermophilus*), yeast (*Yarrowia lipolytica*) and mammals (*Bos taurus*, *Sus scrofa*) but not for plants. Crystallization of complex I, which by far is the largest of the respiratory complexes, required the most effort. The first crystal structure of the entire bacterial complex I from *Thermus thermophilus* was published by Efremov et al. (2010) and shortly after, the structure of the entire mitochondrial enzyme from *Yarrowia lipolytica* was presented by Hunte et al. (2010). In both studies, the resolution of the membrane arm was too low to display the assignment of subunits. Recently, Efremov and Sazanov (2011) published the structure of complex I membrane domain from *E. coli* with a higher resolution and were able to identify subunits.

X-ray crystallography produces detailed information about structure and also indirectly about function of the respiratory chain complexes. However, a cross-species transfer of these data is difficult because of the significant differences in OXPHOS systems between plants and other organisms (plant specific subunits, highly branched electron transfer system). Since crystal structures from non-plant species can only provide hints for their plant counterparts, the need for other strategies enabling the investigation of the OXPHOS system in plants is obvious.

Thanks to progress in methodology, also plant OXPHOS complexes have become accessible to structural characterization. For example, Klodmann et al. (2010) used a biochemical approach to assign subunits to plant complex I. Furthermore, the progress in EM techniques enables generation of high quality structural data, resulting in new findings about structures and possible functions of plant respiratory chain complexes and supercomplexes. By the use of methods like cryo-ET, it also became possible to reveal the overall structure of the OXPHOS system in mitochondrial membranes (section 2.2). Due to the progress in EM techniques and biochemical methods to purify organelles and individual protein complexes, it will become possible to obtain more new, very detailed, structural data of the plant OXPHOS system in the near future. Recently, Dudkina et al. (2011) were able to investigate the interaction of the complexes I, III and IV within the bovine respirasome using cryo-ET. For the analysis of supercomplexes it could be beneficial to use plant species, which are known to possess very stable supercomplexes. The colourless green alga *Polytomella*, for example, contains unusually stable dimeric ATP synthase complex and was already used for the investigation of the row-like organization of this supercomplex in intact mitochondria by cryo-ET (Dudkina et al. 2010b).

Besides the structural analysis of the OXPHOS system, it is also important to figure out the functions of the individual complexes and supercomplexes. As already discussed in section 3.1, plant OXPHOS complexes are involved in several processes of vital importance for the plant cell, like complex I which is involved in maintaining the redox balance during photosynthesis. In this thesis, the investigation of the ETC was based on proteomics. For a complete understanding of the functions of OXPHOS complexes, it might be beneficial to also undertake transcriptomic studies. Proteome and transcriptome are highly dynamic, changing with time, requirements and stresses. Integration of information from these two fields will lead to a more complete understanding of the living organism. Analysing the transcriptome under defined conditions as well as in specific tissues will reveal differences in the expression of the genes of the individual OXPHOS complexes. This in turn, on the one hand, might lead to suggestions of possible side functions of those higher expressed complexes besides electron transport. On the other hand, since it is known that the expression level of a gene does not necessarily correlate with the amount of protein, comparison of the expression profiles of the OXPHOS complexes with the proteomic data will indicate the rate of regulation of the complexes. This regulation either takes place on the level of transcripts (transcriptional processes associated with nuclear or organelle genomes, post-transcriptional processing, RNA-editing) or on the protein level (post-translational modifications, modification of proteins modifying enzymatic functions).

However, expression profiling in combination with proteomic studies can be beneficial to figure out potential differences in gene expression, protein amounts as well as regulation of the five OXPHOS complexes under defined conditions.

As already discussed in section 3.1, plant OXPHOS complexes differ in their abundances regarding different tissues. Thereby, complex I was found to be highly abundant in green organs (section 2.4), which is in line with its contribution in maintaining cell redox balance during photosynthesis (Dutilleul et al. 2003a, Dutilleul et al. 2003b). Hence, it will be very interesting to also have a look at the other complexes, since complex II behaves inversely to complex I and shows higher amounts in non-green tissue. This suggests a role of complex II in this type of tissue. Indeed, Gleason et al. (2011) reported that complex II contributes to localized ROS production in mitochondria, which regulates plant stress and defense response. This is perfectly in line with the high amounts of complex II detected in callus (section 2.4) since it is known that this tissue is heavily stress exposed (Halliwell 2003). And also for the other respiratory chain complexes, tissue specific investigations might reveal new insights into physiological functions.

Another powerful tool for physiological studies is the investigation of knock-out mutants. Plenty of information about functions of complex I is achieved by analyses of knock-out mutants (e.g. Dutilleul et al. 2003a, Dutilleul et al. 2003b, Perales et al. 2005). Today, lots of *Arabidopsis thaliana* knock-out mutants are commercially available. Therefore, this is a promising approach for future investigations of the physiological role of individual OXPHOS complexes under defined conditions. Since there is evidence that complex I is involved in photosynthetic processes, analyses of complex I mutants in combination with different CO₂ concentrations (high CO₂, low CO₂) are inevitable. In this context, also the I+III₂ supercomplex should be examined more carefully due to its suggested potential role in regulation of alternative respiration as well as the possible relation to processes which are involved in stabilizing cell redox balance (section 3.1).

References

- Acín-Pérez, R., Bayona-Bafaluy, M.P., Fernández-Silva, P., Moreno-Loshuertos, R., Pérez-Martos, A., Bruno, C., Moraes, C.T. and Enríquez, J.A. (2004) Respiratory complex III is required to maintain complex I in mammalian mitochondria. *Mol. Cell* 13: 805–815.
- Berry, E.A., Guergova-Kuras, M., Huang, L.S. and Crofts, A.R. (2000) Structure and function of cytochrome bc complexes. *Annu Rev Biochem* 69: 1005–1075.
- Blakely, E.L., Mitchell, A.L., Fisher, N., Meunier, B., Nijtmans, L.G., Schaefer, A.M., Jackson, M.J., Turnbull, D.M. and Taylor, R.W. (2005) A mitochondrial cytochrome b mutation causing severe respiratory chain enzyme deficiency in humans and yeast. *FEBS J* 272: 3583–3592.
- Brandt, U. (2006) Energy converting NADH:quinone oxidoreductase (complex I). *Annu. Rev. Biochem* 75: 69–92.
- Braun, H.-P. and Schmitz, U.K. (1999) The protein-import apparatus of plant mitochondria. *Planta* 209: 267–274.
- Braun, H.-P. and Zabaleta, E. (2007) Carbonic anhydrase subunits of the mitochondrial NADH dehydrogenase complex (complex I) in plants. *Physiol Plant* 129: 114–122.
- Braun, H.-P., Emmermann, M., Kruft, V. and Schmitz, U.K. (1992) The general mitochondrial processing peptidase from potato is an integral part of cytochrome c reductase of the respiratory chain. *EMBO J* 11: 3219–3227.
- Bultema, J., Braun, H.-P., Boekema, E. and Kouril, R. (2009) Megacomplex organization of the oxidative phosphorylation system by structural analysis of respiratory supercomplexes from potato. *Biochim Biophys Acta* 1787: 60–67.
- Carrie, C., Murcha, M.W. and Whelan, J. (2010) An in silico analysis of the mitochondrial protein import apparatus of plants. *BMC Plant Biol* 10: 249.
- Clifton, R., Millar, A.H. and Whelan, J. (2006) Alternative oxidases in Arabidopsis: a comparative analysis of differential expression in the gene family provides new insights into function of non-phosphorylating bypasses. *Biochim. Biophys. Acta* 1757: 730–741.
- Davies, K.M., Strauss, M., Daum, B., Kief, J.H., Osiewacz, H.D., Rycovska, A., Zickermann, V. and Kuhlbrandt, W. (2011) Macromolecular organization of ATP synthase and complex I in whole mitochondria. *Proceedings of the National Academy of Sciences* 108: 14121–14126.

References

- Diaz, F., Fukui, H., Garcia, S. and Moraes, C.T. (2006) Cytochrome c oxidase is required for the assembly/stability of respiratory complex I in mouse fibroblasts. *Mol. Cell. Biol* 26: 4872–4881.
- Dudkina, N.V., Eubel, H., Keegstra, W., Boekema, E.J. and Braun, H.-P. (2005) Structure of a mitochondrial supercomplex formed by respiratory-chain complexes I and III. *Proc. Natl. Acad. Sci. U.S.A* 102: 3225–3229.
- Dudkina, N.V., Heinemeyer, J., Sunderhaus, S., Boekema, E.J. and Braun, H.-P. (2006a) Respiratory chain supercomplexes in the plant mitochondrial membrane. *Trends in Plant Science* 11: 232–240.
- Dudkina, N.V., Kouril, R., Peters, K., Braun, H.-P. and Boekema, E.J. (2010a) Structure and function of mitochondrial supercomplexes. *Biochim. Biophys. Acta* 1797: 664–670.
- Dudkina, N.V., Kudryashev, M., Stahlberg, H. and Boekema, E.J. (2011) Interaction of complexes I, III, and IV within the bovine respirasome by single particle cryoelectron tomography. *Proceedings of the National Academy of Sciences*.
- Dudkina, N.V., Oostergetel, G.T., Lewejohann, D., Braun, H.-P. and Boekema, E.J. (2010b) Row-like organization of ATP synthase in intact mitochondria determined by cryo-electron tomography. *Biochimica et Biophysica Acta (BBA) - Bioenergetics* 1797: 272–277.
- Dudkina, N.V., Sunderhaus, S., Boekema, E.J. and Braun, H.-P. (2008) The higher level of organization of the oxidative phosphorylation system: mitochondrial supercomplexes. *J Bioenerg Biomembr* 40: 419–424.
- Dutilleul, C., Driscoll, S., Cornic, G., Paepe, R. de, Foyer, C.H. and Noctor, G. (2003b) Functional mitochondrial complex I is required by tobacco leaves for optimal photosynthetic performance in photorespiratory conditions and during transients. *Plant Physiol* 131: 264–275.
- Dutilleul, C., Garmier, M., Noctor, G., Mathieu, C., Chétrit, P., Foyer, C.H. and Paepe, R. de (2003a) Leaf mitochondria modulate whole cell redox homeostasis, set antioxidant capacity, and determine stress resistance through altered signaling and diurnal regulation. *Plant Cell* 15: 1212–1226.
- Efremov, R.G. and Sazanov, L.A. (2011) Structure of the membrane domain of respiratory complex I. *Nature* 476: 414–420.
- Efremov, R.G., Baradaran, R. and Sazanov, L.A. (2010) The architecture of respiratory complex I. *Nature* 465: 441–445.

References

- Eubel, H. (2004a) Identification and Characterization of Respirasomes in Potato Mitochondria. *Plant Physiol* 134: 1450–1459.
- Eubel, H., Heinemeyer, J., Sunderhaus, S. and Braun, H.-P. (2004b) Respiratory chain supercomplexes in plant mitochondria. *Plant Physiology and Biochemistry* 42: 937–942.
- Eubel, H., Jansch, L. and Braun, H.-P. (2003) New insights into the respiratory chain of plant mitochondria. Supercomplexes and a unique composition of complex II. *Plant Physiol* 133: 274–286.
- Fowler, L.R. and Hatefi, Y. (1961) Reconstitution of the electron transport system. III. Reconstitution of DPNH oxidase, succinic oxidase, and DPNH, succinic oxidase. *Biochem Biophys Res Commun* 5: 203–208.
- Fowler, L.R. and Richardson, S.H. (1963) Studies on the electron transfer system. L. On the mechanism of reconstitution of the mitochondrial electron transfer system. *J Biol Chem* 238: 456–463.
- Galkin, A. and Brandt, U. (2005) Superoxide radical formation by pure complex I (NADH:ubiquinone oxidoreductase) from *Yarrowia lipolytica*. *J. Biol. Chem* 280: 30129–30135.
- Gleason, C., Huang, S., Thatcher, L.F., Foley, R.C., Anderson, C.R., Carroll, A.J., Millar, A.H. and Singh, K.B. (2011) Mitochondrial complex II has a key role in mitochondrial-derived reactive oxygen species influence on plant stress gene regulation and defense. *Proc. Natl. Acad. Sci. U.S.A* 108: 10768–10773.
- Gray, M.W., Burger, G. and Lang, B.F. (2001) The origin and early evolution of mitochondria. *Genome Biol* 2: 1018.1 - 1018.5.
- Hackenbrock, C.R., Chazotte, B. and Gupte, S.S. (1986) The random collision model and a critical assessment of diffusion and collision in mitochondrial electron transport. *J Bioenerg Biomembr* 18: 331–368.
- Halliwell, B. (2003) Oxidative stress in cell culture: an under-appreciated problem? *FEBS Lett* 540: 3–6.
- Hatefi, Y. (1985) The Mitochondrial Electron Transport and Oxidative Phosphorylation System. *Annu. Rev. Biochem* 54: 1015–1069.

References

- Hatefi, Y., Haavik, A.G., Fowler, L.R. and Griffiths, D.E. (1962) Studies on the electron transfer system. XLII. Reconstitution of the electron transfer system. *J Biol Chem* 237: 2661–2669.
- Hatefi, Y., Jurtschuk, P. and Haavik, A.G. (1961) Studies on the electron transport system. XXXI. DPNH-cytochrome c reductase II. *Biochim Biophys Acta* 52: 119–129.
- Heazlewood, J., Howell, K. and Millar, A. (2003) Mitochondrial complex I from *Arabidopsis* and rice: orthologs of mammalian and fungal components coupled with plant-specific subunits. *Biochim Biophys Acta* 1604: 159–169.
- Heinemeyer, J., Braun, H.-P., Boekema, E.J. and Kouril, R. (2007) A structural model of the cytochrome C reductase/oxidase supercomplex from yeast mitochondria. *J. Biol. Chem* 282: 12240–12248.
- Ho, L.H.M., Giraud, E., Lister, R., Thirkettle-Watts, D., Low, J., Clifton, R., Howell, K.A., Carrie, C., Donald, T. and Whelan, J. (2007) Characterization of the regulatory and expression context of an alternative oxidase gene provides insights into cyanide-insensitive respiration during growth and development. *Plant Physiol* 143: 1519–1533.
- Huang, S., Taylor, N.L., Narsai, R., Eubel, H., Whelan, J. and Millar, A.H. (2010) Functional and composition differences between mitochondrial complex II in *Arabidopsis* and rice are correlated with the complex genetic history of the enzyme. *Plant Mol. Biol* 72: 331–342.
- Hunte, C., Zickermann, V. and Brandt, U. (2010) Functional modules and structural basis of conformational coupling in mitochondrial complex I. *Science* 329: 448–451.
- Klodmann, J. and Braun, H.-P. (2011) Proteomic approach to characterize mitochondrial complex I from plants. *Phytochemistry* 72: 1071–1080.
- Klodmann, J., Sunderhaus, S., Nimtz, M., Jansch, L. and Braun, H.-P. (2010) Internal architecture of mitochondrial complex I from *Arabidopsis thaliana*. *Plant Cell* 22: 797–810.
- Krause, F., Reifschneider, N.H., Vocke, D., Seelert, H., Rexroth, S. and Dencher, N.A. (2004) "Respirasome"-like supercomplexes in green leaf mitochondria of spinach. *J. Biol. Chem* 279: 48369–48375.
- Lenaz, G. and Genova, M.L. (2009) Structural and functional organization of the mitochondrial respiratory chain: a dynamic super-assembly. *Int. J. Biochem. Cell Biol* 41: 1750–1772.
- Logan, D.C. (2006) The mitochondrial compartment. *Journal of Experimental Botany* 57: 1225–1243.

References

- Mannella, C.A. (2006) Structure and dynamics of the mitochondrial inner membrane cristae. *Biochimica et Biophysica Acta (BBA) - Molecular Cell Research* 1763: 542–548.
- Mannella, C.A. and Tedeschi, H. (1987) Importance of the mitochondrial outer membrane channel as a model biological channel. *J. Bioenerg. Biomembr* 19: 305–308.
- Mannella, C.A., Marko, M. and Buttle, K. (1997) Reconsidering mitochondrial structure: new views of an old organelle. *Trends Biochem Sci* 22: 37–38.
- Maxwell, D.P., Wang, Y. and McIntosh, L. (1999) The alternative oxidase lowers mitochondrial reactive oxygen production in plant cells. *Proc. Natl. Acad. Sci. U.S.A* 96: 8271–8276.
- Michalecka, A.M., Svensson, A.S., Johansson, F.I., Agius, S.C., Johanson, U., Brennicke, A., Binder, S. and Rasmusson, A.G. (2003) Arabidopsis genes encoding mitochondrial type II NAD(P)H dehydrogenases have different evolutionary origin and show distinct responses to light. *Plant Physiol* 133: 642–652.
- Millar, A., Mittova, V., Kiddle, G., Heazlewood, J., Bartoli, C., Theodoulou, F. and Foyer, C. (2003) Control of ascorbate synthesis by respiration and its implications for stress responses. *Plant Physiol* 133: 443–447.
- Millar, A.H., Eubel, H., Jansch, L., Kruff, V., Heazlewood, J.L. and Braun, H.-P. (2004) Mitochondrial cytochrome c oxidase and succinate dehydrogenase complexes contain plant specific subunits. *Plant Mol. Biol* 56: 77–90.
- Mitchell, P. (1961) Coupling of phosphorylation to electron and hydrogen transfer by a chemi-osmotic type of mechanism. *Nature* 191: 144–148.
- Pangborn, M. (1942) Isolation and purification of a serologically active phospholipid from beef heart. *J Biol Chem*: 247–256.
- Perales, M., Eubel, H., Heinemeyer, J., Colaneri, A., Zabaleta, E. and Braun, H.-P. (2005) Disruption of a Nuclear Gene Encoding a Mitochondrial Gamma Carbonic Anhydrase Reduces Complex I and Supercomplex I+III₂ Levels and Alters Mitochondrial Physiology in Arabidopsis. *Journal of Molecular Biology* 350: 263–277.
- Peters, K., Dudkina, N.V., Jansch, L., Braun, H.-P. and Boekema, E.J. (2008) A structural investigation of complex I and I+III₂ supercomplex from *Zea mays* at 11-13 Å resolution: assignment of the carbonic anhydrase domain and evidence for structural heterogeneity within complex I. *Biochim. Biophys. Acta* 1777: 84–93.

References

- Pineau, B., Layoune, O., Danon, A. and De, P. (2008) L-galactono-1,4-lactone dehydrogenase is required for the accumulation of plant respiratory complex I. *J Biol Chem* 283: 32500–32505.
- Pineau, B., Mathieu, C., Gérard-Hirne, C., Paepe, R. de and Chétrit, P. (2005) Targeting the NAD7 subunit to mitochondria restores a functional complex I and a wild type phenotype in the *Nicotiana sylvestris* CMS II mutant lacking nad7. *J. Biol. Chem* 280: 25994–26001.
- Price, G., Badger, M., Woodger, F. and Long, B. (2008) Advances in understanding the cyanobacterial CO₂-concentrating-mechanism (CCM): functional components, Ci transporters, diversity, genetic regulation and prospects for engineering into plants. *J Exp Bot* 59: 1441–1461.
- Rasmusson, A.G. and Wallström, S.V. (2010) Involvement of mitochondria in the control of plant cell NAD(P)H reduction levels. *Biochem. Soc. Trans* 38: 661–666.
- Rasmusson, A.G., Fernie, A.R. and van Dongen, J.T. (2009) Alternative oxidase: a defence against metabolic fluctuations? *Physiol Plant* 137: 371–382.
- Rasmusson, A.G., Geisler, D.A. and Møller, I.M. (2008) The multiplicity of dehydrogenases in the electron transport chain of plant mitochondria. *Mitochondrion* 8: 47–60.
- Rüchel R., Steere, R.L. and Erbe, E.F. (1978) Transmission-electron microscopic observations of freeze-etched polyacrylamide gels. *J Chromatogr* 166: 563–575.
- Sagan, L. (1967) On the origin of mitosing cells. *J Theor Biol* 14: 255–274.
- Sazanov, L.A. and Hinchliffe, P. (2006) Structure of the hydrophilic domain of respiratory complex I from *Thermus thermophilus*. *Science* 311: 1430–1436.
- Schägger, H. (2002) Respiratory chain supercomplexes of mitochondria and bacteria. *Biochimica et Biophysica Acta (BBA) - Bioenergetics* 1555: 154–159.
- Schägger, H. and Jagow, G. von (1991) Blue native electrophoresis for isolation of membrane protein complexes in enzymatically active form. *Anal. Biochem* 199: 223–231.
- Scheffler, I.E. (1998) Molecular genetics of succinate:quinone oxidoreductase in eukaryotes. *Prog Nucleic Acid Res Mol Biol* 60: 267–315.
- Schlame, M., Rua, D. and Greenberg, M. (2000) The biosynthesis and functional role of cardiolipin. *Progr. Lipid Res.* 39 (2000), pp. 257–288.
- Stock, D., Gibbons, C., Arechaga, I., Leslie, A.G. and Walker, J.E. (2000) The rotary mechanism of ATP synthase. *Curr. Opin. Struct. Biol* 10: 672–679.

References

- Strauss, M., Hofhaus, G., Schröder, R.R. and Kühlbrandt, W. (2008) Dimer ribbons of ATP synthase shape the inner mitochondrial membrane. *EMBO J* 27: 1154–1160.
- Sun, F., Huo, X., Zhai, Y., Wang, A., Xu, J., Su, D., Bartlam, M. and Rao, Z. (2005) Crystal structure of mitochondrial respiratory membrane protein complex II. *Cell* 121: 1043–1057.
- Sunderhaus, S., Dudkina, N., Jansch, L., Klodmann, J., Heinemeyer, J., Perales, M., Zabaleta, E., Boekema, E. and Braun, H.-P. (2006) Carbonic anhydrase subunits form a matrix-exposed domain attached to the membrane arm of mitochondrial complex I in plants. *J Biol Chem* 281: 6482–6488.
- Sunderhaus, S., Klodmann, J., Lenz, C. and Braun, H.-P. (2010) Supramolecular structure of the OXPHOS system in highly thermogenic tissue of *Arum maculatum*. *Plant Physiol. Biochem* 48: 265–272.
- Svensson, A.S. and Rasmusson, A.G. (2001) Light-dependent gene expression for proteins in the respiratory chain of potato leaves. *Plant J* 28: 73–82.
- Thirkettle-Watts, D. (2003) Analysis of the Alternative Oxidase Promoters from Soybean. *Plant Physiol* 133: 1158–1169.
- Tsukihara, T., Aoyama, H., Yamashita, E., Tomizaki, T., Yamaguchi, H., Shinzawa-Itoh, K., Nakashima, R., Yaono, R. and Yoshikawa, S. (1996) The whole structure of the 13-subunit oxidized cytochrome c oxidase at 2.8 Å. *Science* 272: 1136–1144.
- Ugalde, C., Janssen, R.J.R.J., van den Heuvel, L.P., Smeitink, J.A.M. and Nijtmans, L.G.J. (2004) Differences in assembly or stability of complex I and other mitochondrial OXPHOS complexes in inherited complex I deficiency. *Hum. Mol. Genet* 13: 659–667.
- Vander Heiden, M.G. (2001) Bcl-xL Promotes the Open Configuration of the Voltage-dependent Anion Channel and Metabolite Passage through the Outer Mitochondrial Membrane. *Journal of Biological Chemistry* 276: 19414–19419.
- Welchen, E., Klodmann, J. and Braun, H.-P. (2011) Biogenesis and supermolecular organization of the oxidative phosphorylation system in plants. In *Plant Mitochondria*. Edited by Kempken, F. pp. 327–355. Springer Science+Business Media LLC, New York, NY.
- Wittig, I., Braun, H.-P. and Schägger, H. (2006) Blue native PAGE. *Nat Protoc* 1: 418–428.
- Yagi, T., Yano, T., Di Bernado, S. and Matsuno-Yagi, A. (1998) Procaryotic complex I (NDH-1), an overview. *Biochim. Biophys. Acta* 1364: 125–133.

References

Yankovskaya, V., Horsefield, R., Törnroth, S., Luna-Chavez, C., Miyoshi, H., Léger, C., Byrne, B., Cecchini, G. and Iwata, S. (2003) Architecture of succinate dehydrogenase and reactive oxygen species generation. *Science* 299: 700–704.

Curriculum vitae

Name: Katrin Peters
Date of Birth: 16.03.1982
Place of Birth: Uelzen, Germany
Citizenship: Citizen of Germany
Marital Status: unmarried

SCHOOL EDUCATION

1988 – 1992 Primary school in Wieren
1992 – 1994 Orientierungsstufe in Bad Bodenteich
1994 – 2001 Secondary school ‘Herzog-Ernst-Gymnasium’ in Uelzen
Qualification: ‘Abitur’

ACADEMIC EDUCATION

Oct. 2001 – Sept. 2002 Student at the Universität Hildesheim,
major: Lehramt Grund-, Haupt- und Realschule
subjects: Biology, English, Mathematics
Oct. 2002 – Oct. 2005 Student at the Leibniz Universität Hannover,
major: Plant Biotechnology
Oct. 2005 Bachelor-degree in Plant Biotechnology (B.Sc.)
Thesis: “Untersuchungen zur Apoptose in Zellkulturen von
Arabidopsis thaliana.”
(‘Investigation of apoptosis in cell cultures of *Arabidopsis thaliana*.’)
Grade: ‘excellent’
Oct. 2005 – Sept. 2007 Student at the Leibniz Universität Hannover,
major: Plant Biotechnology
Sept. 2007 Master-degree in Plant Biotechnology (M.Sc.)

Thesis: “Untersuchungen zum mitochondrialen NADH-Dehydrogenase-Komplex aus Mais“

(‘Investigation of the mitochondrial NADH-dehydrogenase-complex in maize.’)

Grade: ‘with honours’

Since Oct. 2007

PhD student at the Leibniz Universität Hannover, Institute of Plant Genetics, Department Plant Proteomics, Prof. Dr. Hans-Peter Braun

Publications

Journal research papers and manuscripts:

Peters, K., Dukina, N.V., Jansch, L., Braun, H.-P. and Boekema, E.J. (2008): A structural investigation of complex I and I+III₂ supercomplex from *Zea mays* at 11-13 Å resolution: assignment of the carbonic anhydrase domain and evidence for structural heterogeneity within complex I. *Biochim. Biophys. Acta (Bioenergetics)* 1777: 84-93.

Dudkina, N.V., Kouřil, R., Peters, K., Braun, H.-P. and Boekema, E.J. (2010): Structure and function of mitochondrial supercomplexes. *Biochim. Biophys. Acta (Bioenergetics)* 1797: 664-670.

Peters, K. and Braun, H.-P. (2011): Comparative analyses of protein complexes by blue native DIGE. *Methods Mol. Biol. In press.*

Peters, K., Nießen, M., Peterhänsel, C., Späth, B., Marchfelder, A., Hölzle, A., Binder, S. and Braun, H.-P.: Complex I - complex II ratio strongly differs in various organs of *Arabidopsis thaliana*. *In preparation.*

Conference Contributions:

Posters

Peters, K., Dudkina, N.V., Boekema, E.J. and Braun, H.-P.: Characterization of mitochondrial complex I and supercomplex I+III₂ from *Zea mays*.
International Conference for Plant Mitochondrial Biology (ICPMB), 2007, Nara, Japan.

Peters, K., Späth, B., Hölzle, A., Binder, S., Marchfelder, A. and Braun, H.-P.: Immune depletion approach for in depth analysis of the plant mitochondrial proteome.
International Conference for Plant Mitochondrial Biology (ICPMB), 2009, Lake Tahoe, USA.

Peters, K., Klodmann, J., Sunderhaus, S. and Braun, H.-P.: Physiological role of mitochondrial gamma carbonic anhydrases in the CO₂ metabolism of plant cells.
24th New Phytologist Symposium: Plant respiration and climate change: scaling from mitochondria to the globe, 2010, Oxford, UK.

Peters, K., Nießen, M., Peterhänsel, C. and Braun, H.-P.: Quantification of OXPHOS complexes in different tissues of *Arabidopsis thaliana*.
International Conference for Plant Mitochondrial Biology (ICPMB), 2011, Hohenroda, Germany.

Danksagung

Lieber Hans-Peter, an dieser Stelle möchte ich mich als erstes bei dir dafür bedanken, dass du mir die Möglichkeit gegeben hast in deiner Abteilung zu promovieren. Vielen Dank für die großartige Betreuung und Unterstützung und danke auch dafür, dass du dir immer Zeit für mich genommen hast und mich motiviert hast, wenn es mal nicht so gut lief. Vielen Dank auch dafür, dass du mir die Teilnahme an internationalen Konferenzen ermöglicht hast, die mich nicht nur wissenschaftlich voran gebracht haben, sondern die mir auch privat sehr viel Freude bereitet haben und an die ich mich noch lange und gerne zurück erinnern werde.

Der gesamten AG Braun möchte ich ganz herzlich für die schöne Zeit danken. Ohne das freundschaftliche Arbeitsklima und eure stete Hilfsbereitschaft hätte die Arbeit hier mit Sicherheit nicht so viel Spaß gemacht.

Bei meinen **lieben Bürokollegen Christina, Jenni und Christof** möchte ich mich für die schöne Zeit in unserem „Doktoranden-Kinderzimmer“ bedanken. Ich kann mir kaum vorstellen, dass es da draußen noch irgendwo eine Bürogemeinschaft gibt, die auf so engem Raum so viel Spaß hat.

Liebe Steffi, liebe Jenni, bei euch möchte ich mich vor allem für eure Freundschaft und eure Unterstützung bedanken und dafür, dass ihr bei Problemen jedweder Art immer für mich da gewesen seid.

Liebe Dagmar, vielen Dank für deine stetige Unterstützung im Labor, für die vielen wertvollen Tipps und für alles, was du mir in all den Jahren im Labor beigebracht hast. Ohne deine Hilfe und deine souveräne Art wäre der ein oder andere Versuch mit Sicherheit schief gegangen.

Bedanken möchte ich mich auch bei **Christoph Peterhänsel** sowie bei der gesamten **CP-Arbeitsgruppe** dafür, dass ihr mich so freundlich bei euch im Labor aufgenommen habt und für die vielen Tipps und Diskussionen.

Lieber Markus, vielen Dank für deine Freundschaft und vor allem für deine unermüdliche Bereitschaft mir jederzeit mit Rat und Tat zur Seite zu stehen und mich immer wieder aufs Neue zu motivieren. Die Welt hat nicht genug Lakritz um das wieder gut zu machen!

Liebe Steffi, lieber Holger, lieber Markus, vielen Dank für die vielen Tipps und die Unterstützung während der Schlussphase dieser Arbeit.

Liebe Mama, lieber Papa, lieber Mirko, vielen Dank für eure Liebe und euer Vertrauen in mich. Ihr habt mich zu dem gemacht, was ich bin und ohne euch hätte ich das hier wohl nicht geschafft! Ihr seid die Besten!

Liebe Omek, vielen Dank für deine Unterstützung und dafür, dass heute alle diese Seiten lesen können. Du bist die weltbeste Omi, die man sich wünschen kann!

Lieber Kurt, ich bin glücklich, dass du da bist und freue mich auf alles was jetzt kommt!

Erklärung

Hierdurch erkläre ich, dass ich meine Dissertation mit dem Titel „Characterization of the OXPHOS system in plant mitochondria“ selbständig verfasst und die benutzten Hilfsmittel und Quellen sowie gegebenenfalls die zu Hilfeleistungen herangezogenen Institutionen vollständig angegeben habe.

Die Dissertation wurde nicht schon als Masterarbeit, Diplomarbeit oder andere Prüfungsarbeit verwendet.

Hannover, den 14.10.2011